



doi:10.7289/V5M32SS9

**ASSESSMENT AND APPLICATIONS OF DISTRIBUTED HYDROLOGIC MODEL
RUSSIAN-NAPA RIVER BASINS, CA**

Lynn E. Johnson
Chengmin Hsu
Robert Zamora
Robert Cifelli

With contributions by:

Tim Coleman
Christopher Fields
James Halgren
John Labadie
Gi-Hyeon Park
Angela Pelle

Earth System Research Laboratory
Physical Sciences Division
Boulder, Colorado
January 2016

noaa

NATIONAL OCEANIC AND
ATMOSPHERIC ADMINISTRATION



Office of Oceanic and
Atmospheric Research

NOAA Technical Memorandum OAR PSD – 316

**ASSESSMENT AND APPLICATIONS OF DISTRIBUTED HYDROLOGIC MODEL
RUSSIAN-NAPA RIVER BASINS, CA**

Lynn E. Johnson
NOAA Earth System Research Laboratory, Boulder, CO
CIRA, Colorado State University, Ft. Collins, CO

Chengmin Hsu
NOAA Earth System Research Laboratory, Boulder, CO
CIRES, University of Colorado Boulder, Boulder, CO

Robert Zamora
NOAA Earth System Research Laboratory, Boulder, CO

Robert Cifelli
NOAA Earth System Research Laboratory, Boulder, CO

With contributions by:
Tim Coleman, NOAA Earth System Research Laboratory
Christopher Fields, CIRA, Colorado State University
James Halgren, Riverside Technology, Inc.
John Labadie, CIRA, Colorado State University
Gi-Hyeon Park, Riverside Technology, Inc.
Angela Pelle, University of Alabama

Earth System Research Laboratory
Physical Sciences Division
Boulder, Colorado
January 2016



UNITED STATES
DEPARTMENT OF COMMERCE

Secretary Penny Pritzker
Department of Commerce

NATIONAL OCEANIC AND
ATMOSPHERIC ADMINISTRATION

Dr. Kathryn Sullivan
Under Secretary for Oceans and
Atmosphere / Administrator

Office of Oceanic and
Atmospheric Research

Craig McLean
Assistant Administrator for
Oceanic and Atmospheric
Research

NOTICE

Mention of a commercial company or product does not constitute an endorsement by NOAA/Earth System Research Laboratory. Use of information from this publication concerning proprietary products or the test of such products for publicity or advertising purposes is not authorized.

The findings and conclusions on this report are those of the authors and do not necessarily represent the views of the funding agency.

CITATION

Johnson, L.E., C. Hsu, R. Zamora, and R. Cifelli, 2016. Assessment and Applications of Distributed Hydrologic Model - Russian-Napa River Basins, CA. NOAA Technical Memorandum PSD-316, NOAA Printing Office, Silver Spring, MD, 101 pp. doi:10.7289/V5M32SS9

TABLE OF CONTENTS

SUMMARY	x
1. INTRODUCTION	
1.1 Overview	1
1.2 Collaborations	1
1.3 Objectives	3
1.4 Outline of Report	3
2. RUSSIAN-NAPA RIVER BASINS	
2.1 Basins Description	5
2.2 Terrain and Hydrography	5
2.3 Land Use / Land Cover	6
2.4 Hydrogeology and Soils	6
2.5 Reservoirs and Diversions	7
2.6 Precipitation	10
2.7 Surface Runoff	13
2.8 Evapotranspiration	16
2.9 Soil and Bedrock Moisture	17
2.10 Groundwater	19
2.11 Water Budget	20
3. RUSSIAN-NAPA RIVERS DISTRIBUTED HYDROLOGIC MODEL	
3.1 Description of Model	21
3.2 Base Data	25
3.3 Precipitation	32
3.4 Soil Moisture	37
3.5 Evapotranspiration	42
4. ASSESSMENT OF THE DISTRIBUTED HYDROLOGIC MODEL	
4.1 RDHM Simulations of Surface Runoff	44
4.2 Calibration Procedure	44
4.3 Calibration and Verification Results	50
4.4 Assessment of Multi-Radar Multi-Sensor Precipitation (MRMS) Products	59
4.5 Comparison of 4 km and 1 km RDHM simulations	61
4.6 Comparison of Observed and Simulated Soil Moisture	61
5. RDHM APPLICATIONS	
5.1 Threshold Frequency Application	66
5.2 Fisheries Habitat Assessment	67
5.3 Integration with Water Management Model	70
5.4 Implementation in CHPS-FEWS	73
6. CONCLUSIONS AND RECOMMENDATIONS	
6.1 Conclusions	75
6.2 Recommendations	78

6. REFERENCES	80
ABBREVIATIONS AND ACRONYMS	88
APPENDIX A – FLOOD FLOW ASSESSMENT STATISTICS	90
APPENDIX B – LOW FLOW ASSESSMENT STATISTICS	92
APPENDIX C. INTRINSIC POTENTIAL FISHERIES HABITAT MAPPING	101

LIST OF FIGURES

Figure 1. Russian River, California.	5
Figure 2. National Land Cover Database 2006 – the Russian and Napa River watersheds.	7
Figure 3. Generalized geology of the Russian River basin, CA.	8
Figure 4. Irrigated agriculture in the basin.	9
Figure 5. Atmospheric rivers are a primary source of floods and water supply for California.	10
Figure 6. Thirty-year (1981 – 2010) annual precipitation normal from PRISM.	11
Figure 7. Santa Rosa (a) Precipitation frequency, (b) Seasonal distribution of precipitation.	12
Figure 8. Russian River flows for water year 2011-2012.	13
Figure 9. Annual peak flows – Russian River at Guerneville, CA.	15
Figure 10. Lake Mendocino flood frequency summary (1962 – 2012).	15
Figure 11. Flow duration curves for 5 watersheds in Russian-Napa basins.	16
Figure 12. HMT soil moisture and rain gauge stations.	17
Figure 13. Soil composition for Russian River basin.	18
Figure 14. a) Saturated hydraulic conductivity 0-20 cm depth, b) Depth to restrictive layer.	19
Figure 15. Example of soil moisture and related data available at the HMT web site.	19
Figure 16. Annual average water budget for the Alexander Valley.	20
Figure 17. Components of the RDHM model.	21
Figure 18. Schematic diagram of the Sacramento Soil Moisture Accounting (SAC-SMA) model.	22
Figure 19. Schematic diagram of RDHM computational schemes for (a) watershed processes and, (b) channel and hill-slope routing.	22
Figure 20 Comparison of the HRAP and 1/16 HRAP resolution illustrates the impacts of stream connectivity.	25
Figure 21. Santa Rosa Creek impervious area.	27
Figure 22. Spatial variability of a priori parameters for:	
(a) Lower zone primary free water maximum,	29
(b) Lower zone supplemental free water maximum,	29
(c) Lower zone primary free water storage depletion rate, and	29
(d) Lower zone supplemental free water storage depletion rate.	29
Figure 23. Spatial variability of a priori parameters for:	
(a) Lower zone tension water maximum,	30

(b) Upper zone tension water maximum,	30
(c) Ratio of maximum and minimum percolation rates, and	30
(d) Exponent of the percolation equation (Shape Parameter).	30
Figure 24. Spatial variability of a priori parameters for:	
(a) Upper zone free water storage interflow depletion rate,	31
(b) Permanent impervious area fraction of the watershed,	31
(c) Upper zone free water maximum, and	31
(d) Percolation fraction that goes directly to the lower zone free water storage.	31
Figure 25. CNRFC QPE data for 2012/03/17/0000z.	33
Figure 26. Scatter plots of the CNRFC 6 hourly QPEs against HMT 6 hourly gauge accumulations.	34
Figure 27. HMT 6-hr total precipitation and CNRFC 6-h gridded RDHM precipitation at nearest HRAP cell for WLS, HBG, HLD, and CZC.	34
Figure 28. Three-day rainfall accumulation in northern California.	35
Figure 29. MRMS processing system.	36
Figure 30. Radar QPE at 2012/03/16/20z generated from the MRMS.	37
Figure 31. Derived soil moisture calibration vs. CSI supplied calibration.	39
Figure 32. Response of well water table depths to precipitation at different locations underscores the influence of the deeper subsurface conditions in groundwater recharge.	41
Figure. 33. NOAA PSD Surface Flux Observatory.	42
Figure 34. Comparison between observed and simulated ET - June, September, and December, 2012.	43
Figure 35. Location of calibration sites in Russian-Napa rivers.	44
Figure 36. Hydrograph calibration procedure.	45
Figure 37. Sequence of steps to calibrate SAC-SMA module of RDHM.	48
Figure 38. Total period flow statistics. a) %Bias for volume (- sign is $Q_{sim} > Q_{obs}$), b) Nash-Sutcliff Coefficient.	51
Figure 39. Austin Cr. simulation. a) 2011 calibration period, b) 2012 verification period.	52
Figure 40. Comparison of observed and simulated cumulative runoff indicates divergence for first rainfall event after prolonged dry period.	52
Figure 41. Comparison of observed and simulated flood events in terms of %Bias (volume) a) by event and station, and b) by frequency histogram.	53
Figure 42. Comparison of observed and simulated flood events in terms of Nash-Sutcliff Coeff. a) N-S by events, and b) N-S Coef frequency (%).	53
Figure 43. Comparison of observed and simulated flood events in terms of flood peak differences (%), a) all events, and b) frequency histogram of peak flow differences.	54
Figure 44. Comparison of observed and simulated flood events in terms of time-to-peak differences.	54
Figure 45 Locations of NMFS low flow gaging sites used for independent RDHM verification.	55
Figure 46. Illustration of procedures for verification of RDHM versus observed flows – W.Br. Russian River.	56

Figure 47. (a) Low flow bias for the NMFS gages; (b) Comparison of low flow recession for Austin Cr nr Cazadero.	57
Figure 48. Comparison of RDHM and BCM simulations of daily flows with USGS observed flows at the W.Br. Russian River nr Ukiah gage.	58
Figure 49. RDHM low flow biases cumulative distribution functions.	59
Figure 50. MRMS system was used to generate four alternate QPE mappings over the Russian-Napa River basins.	60
Figure 51. Distributed hydrologic model simulations obtained using the MRMS QPE mappings.	61
Figure 52. Comparison of observed and simulated runoff for 1-km and 4-km RDHMs.	61
Figure 53. a) Soil wetness fraction observed at HLD and simulated by RDHM for the period 2 February, 2011 – 12 March 2012, b) Regression analysis for the HMT HLD observations and RDHM simulated soil wetness fractions for the period 2 February, 2011 – 12 March 2012.	63
Figure 54. HMT observed soil wetness fractions (solid black line), and soil wetness fractions simulated by RDHM (solid red line) for the period 2 February, 2011 – 12 March 2012.	64
Figure 55. Total drainable storage capacities estimated for each catchment (from Vannier et al 2014).	65
Figure 56. (a) 100-year threshold frequency flows (cfs); (b) Peak flow TF levels for Dec. 2 -3 2012 flood event.	67
Figure 57. W. Br. Russian River stream trace.	68
Figure 58. Profile of elevation and drainage area extracted from the RDHM 1-km grids which lie on the stream path.	68
Figure 59. Profile of 23 August 2011 stream flows extracted from the RDHM 1-km grids which lie on the stream path.	69
Figure 60. Profile of Fisheries Habitat Intrinsic Potential Index and elevation.	70
Figure 61. (a) Prototype tributary model in GeoMODSIM coupled with the RDHM. (b) Prototype tributary GeoMODSIM model showing four agricultural demand nodes.	71
Figure 62. (a) GeoMODSIM output showing the effects of simulated frost demands. (b) GeoMODSIM results demonstrating the benefits of improved pond operation.	72
Figure 63. Flow diagram of stand-alone RDHM within FEWS.	73
Figure 64. (a) Precipitation fields including HRRR forecasts retrieved and converted to RDHM forcing, (b) Time series of stream flows are generated in CHPS-FEWS at selected grid points in the basin.	74
Figure 65. Animated visualizations of spatial distributions of precipitation, surface runoff, and soil moisture are available using web-oriented displays.	74
Appendix B. Low flow verification illustrations of procedures for verification of RDHM versus observed flows – all sites.	92
Appendix C. Figure C-1. Fisheries habitat assessment for W.Br. Russian River based on Intrinsic Potential mapping for steelhead.	101
LIST OF TABLES	
Table 1. PRISM Basin Average Precipitation [in] (1981 - 2010).	11
Table 2. Russian-Napa Rivers USGS Surface Water Gage Sites.	14

Table 3. Flood frequency (from FEMA Flood Insurance Study - for Sonoma County, CA).	15
Table 4 HMT Soil Moisture Monitoring Stations.	17
Table 5. SAC-SMA model parameters and states with their realistic ranges or default values.	23
Table 6. HRAP cell size on the earth's surface.	26
Table 7. Percentage impervious area for watersheds.	27
Table 8. Soil moisture station data summary.	38
Table 9. Soil sensor calibration parameters.	40
Table 10. Dominant parameters of the various periods and their effects.	46
Table 11. Streamflow gaging stations used for low flow verification.	56
Table 12. Low flow verification statistics.	58
Table 13. USGS regional regression equations for California North Coast Region flood frequencies.	66
Table A-1. Accuracy statistics at the seven stations for the calibration period.	90
Table A-2. Accuracy statistics at the seven stations for the verification period.	91

SUMMARY

Distributed hydrologic models (DHMs) take account of the spatial variability of rainfall, as well as the variability of watershed terrain, soils, soil moisture, and land use. Given predictions of surface flows at any grid location, DHMs also provide an enhanced basis for flash flood warnings and are supportive to a variety of water management applications. DHMs also provide an ancillary means to assess the accuracy of multi sensor-based precipitation mappings.

The overall objective of this report is to assess the accuracy of the distributed hydrologic modeling approach in representing surface hydrologic processes, including flood events and low flows. It is also intended to examine how the DHM approach may be applied in support of NWS hydrologic forecasting services, as well as related water management purposes.

The NWS-OHD Research Distributed Hydrologic Model (RDHM) was used. Activities for RDHM setup, parameterization, sensitivity, calibration, and performance assessment are described. The modeling effort has sought to determine advantages which may accrue with the distributed approach. These advantages are associated with the spatial detail of flow predictions at any location throughout the basin which can inform efforts for flood mitigation, water supply, irrigation and ecosystem management. RDHM represents the general functionality of the class of distributed hydrologic models (DHMs) operating on a gridded data structure.

A case study conducted on the Russian-Napa River basins in California has involved forcing a distributed hydrologic model with CNRFC gridded precipitation fields. The Russian River watershed encompasses 1,485 sq. mi. within Sonoma and Mendocino Counties, California. The Napa River basin, located just east of the Russian River basin, encompasses approximately 426 square miles. Total population in the study area is approximately 700,000. Primary water uses are for domestic supply and irrigation of (predominately) vineyards. There are efforts to re-establish endangered fisheries habitat in the basins. Together these are two of the most flood-prone rivers in the State of California because of the watershed's unique geography and its proximity to the coast, which together produce climatologically heavy wintertime rainfall.

The RDHM is a conceptual hydrologic prediction model which can be used to account for runoff, streamflow, soil moisture, snowmelt, evapotranspiration, and various hydrologic states during storm events and inter-storm periods. RDHM routes both surface and subsurface water flow based on conceptual representations of terrain, soils, vegetation, and the influences of these on infiltration and evapotranspiration. The required inputs are precipitation and temperature. The OHD provided base data sets on terrain and channel networks, soils, and the default parameters for the RDHM model.

The modeling effort involved a variety of atmospheric and ground observations. Surface meteorological stations operated by the NWS and the HMT provided data on precipitation, temperature and evapotranspiration energy dynamics. Soil moisture observations were provided by the HMT. Streamflow data provided by the USGS was particularly valuable for RDHM calibration and verification purposes. The CNRFC provided the primary datasets on precipitation fields. Ancillary precipitation data was obtained from weather radars operated by the NWS and the KPIX TV weather radar.

After setting up the RDHM for the two basins, precipitation and temperature data sets for a multi-year period 2010 to 2012 were applied, and the subsequent surface runoff and soil moisture dynamics were simulated. The simulation period was divided into three parts for a) model warmup, b) model calibration, and c) model verification. Model warmup was required to establish initial model states that reflect the basin conditions. A manual calibration approach was used which involved model parameter adjustments guided by a collection of statistical performance metrics for a) total simulation period, b) flood events, and c) low flows. Verification involved simulation without adjustment of parameters. An independent verification of low flows was obtained using data collected by the NMFS on selected tributaries to the Russian River.

Results of the RDHM modeling activities are summarized in general terms here.

- The default data sets for defining the RDHM grid structure and model parameter values provide a workable foundation for the simulation model. Manual calibration procedures employed demonstrate improved simulations, but are time consuming and non-reproducible by other analysts.
- RDHM has been shown to provide so-called “natural” surface flow estimates that are reasonably accurate when the precipitation forcings are accurate (e.g. location, timing and intensity), the land surface and subsurface parameters portray the hydrologic response (e.g. soil moisture and evapotranspiration dynamics), and water management influences are minimal.
- In general, the CNRC QPE data was reasonably accurate and provided a good basis for assessing accuracy of the RDHM. However, comparison of the CNRFC QPE rainfall fields to independent rain gage readings indicated general underestimation of actual rainfall amounts.
- For the MRMS application, rainfall fields generated by both radar with gauge correction and radar with VPR & gauge correction products are well estimated in terms of magnitude and timing. Denser rain gage networks can improve estimations of rainfall patterns and magnitude, including bias corrections of mixed radar and gage networks.
- The accuracy of flood flow predictions is considered reasonable in general, but there can be significant inaccuracies associated with three factors, 1) precipitation, 2) initial soil and bedrock moisture conditions, and 3) water management actions. Initial soil and bedrock moisture conditions seem to negatively affect simulation accuracies for flood events occurring after prolonged dry periods. Water management factors of reservoir capture of flood flows and diversions for water supply and irrigation can negatively influence RDHM simulation accuracies. Low flow simulation accuracy is strongly influenced by water diversions.
- Results shown here indicate that “out of the box” RDHM can simulate soil moisture values in the upper soil layers of the Russian river basin with moderate skill. Model skill varies seasonally. The weakest performance was found during the winter season. Overall the model soil moisture values are 2.0% to 6.0% higher than the observations.
- Distributed modeling provides higher resolution detail on hydrologic response at ungaged locations which is needed by water managers and the general public. Users should be wary of simulation results for small drainage areas which may be missed by the precipitation mappings.

Several demonstration applications of the RDHM were developed for a) threshold frequency concept to support flash flood warning operations, b) fisheries habitat assessment to support salmon restoration management, c) water management model integration to account for water storage and diversion operations, and d) real-time implementation to support RFC and WFO flash flood warning operations. Activities are continuing on these prototypes.

1. INTRODUCTION

1.1 Overview

Application of distributed hydrologic models is motivated by the prospect that higher resolution forcing data, such as gridded precipitation fields, should be matched by equivalent resolution mapping of hydrologic responses for surface runoff, soil moisture and evapotranspiration. Distributed hydrologic models have potential for improving hydrologic forecasting given the capability to represent spatially-varying land characteristics and precipitation that has historically been lumped into watershed average characteristics. Provided that the distributed model is forced with accurate inputs (i.e., precipitation) at sufficient time and spatial resolution, it stands to reason that the model could provide high resolution information on surface runoff characteristics that is currently not available with the lumped model approach.

Applied research activities on hydrologic processes in the Russian-Napa river basins in California seek to determine if the distributed modeling approach can produce accurate hydrologic simulations using high resolution space and time scales (~ 4 km, 6 hr; ~1 km, 1 hr). We are using the NWS OHD Research Distributed Hydrologic Model (RDHM) which is a gridded version of the NWS-River Forecast System model used by the NWS River Forecast Centers. In a general sense, the RDHM can be considered a Distributed Hydrologic Model (DHM) as it represents the functionality of distributed models in general.

The Russian-Napa Rivers watersheds are a good location for the case study because they have a full array of physical hydrologic and water resource management issues (flooding, municipal and agricultural water supply, fisheries, recreation).

1.2 Collaborations

The project has been aided by various collaborations and coordination with other agencies, summarized herewith. However, the results and conclusions of this project are attributable to authors only, and do not reflect policies of the NOAA National Weather Service or other agencies.

NOAA Hydrometeorology Testbed (HMT)

The Hydrometeorology Testbed program (<http://hmt.noaa.gov/>) conducts research on precipitation and weather conditions that can lead to flooding, and fosters transition of scientific advances and new tools into forecasting operations. HMT's outputs support efforts to balance water resource demands and flood mitigation in a changing climate. HMT's regional implementations started in California, and have been extended to the Pacific Northwest, and the Southeast. HMT is led by the Physical Sciences Division of NOAA/ESRL's Physical Sciences Division with partners across NOAA, other agencies and universities.

California Department of Water Resources (DWR)

The DWR operates and maintains the State Water Project, provides dam safety and flood control and inspection services, assists local water districts in water management and water conservation planning, and plans for future statewide water needs. This project is part of DWR's Enhanced Flood Response and Emergency Preparedness (EFREP) Program. The HMT has had a cooperative partnership with DWR's EFREP program to develop and install a 21st century observing system for extreme precipitation in California. Research identified a major gap in existing hydrometeorological monitoring and precipitation forecasting; the limited ability to track and quantify water vapor transport across the Pacific Ocean and into California. New methodologies and monitoring technologies have been developed to fill this gap. This hydrological modeling project is directed to assessing the role that distributed modeling can provide for flood mitigation and water management applications in California.

California-Nevada River Forecast Center

The NWS California – Nevada River Forecast Center (CNRFC; <http://www.cnrfc.noaa.gov/>) provides river flow forecasts for locations in the Russian River basin as well as inflow to the two major reservoirs. The NWS California – Nevada River Forecast Center (CNRFC; <http://www.cnrfc.noaa.gov/>) is one of 13 National Weather Service (NWS) River Forecast Centers in the United States. In support of fulfilling the NWS hydrologic mission of protecting lives and property, the CNRFC provides river and flood forecasts for approximately 220 flood, non-flood, and reservoir locations in California, Nevada, and a portion of Southern Oregon (Figure 1). These forecasts include those for flood and routine flow conditions, ensemble streamflow predictions, spring snowmelt and water supply. The CNRFC coordinates with eleven NWS Weather Forecast Offices (WFOs) to provide a conduit for the public warning process and an interface for local customers and partners. Precipitation products at ~4-km grid and 6-hr time step from CNRFC archives were used for this project.

There is also coordination with the major federal water agencies including the US Army Corps of Engineers and the US Bureau of Reclamation. The CNRFC operates a joint forecasting service with the California Department of Water Resources, Division of Flood Management as well as with the Weather Forecast Offices (e.g. WFO San Francisco / Monterrey, <http://www.wrh.noaa.gov/mtr/>) who issue the flood advisories, watches and warnings to local emergency response agencies and the public. These river and reservoir forecasts are provided directly to the USACE (<http://www.spk.usace.army.mil/>) and California DWR State-Federal Flood Operations Center in Sacramento, CA (<http://www.water.ca.gov/floodmgmt/>).

National Marine Fisheries Service

The NOAA Fisheries Office of Habitat Conservation protects, restores, and promotes stewardship of coastal and marine habitat to support our nation's fisheries for future generations. The Russian River watershed has been selected as the first Habitat Focus Area under NOAA's Habitat Blueprint (<http://www.habitat.noaa.gov/habitatblueprint/index.html>). This is an important step to increase the effectiveness of NOAA's habitat conservation science and management efforts by identifying places where NOAA offices work to meet multiple habitat conservation objectives on a watershed scale. The objectives we have identified in the Russian River include:

- Rebuilding endangered Coho and threatened steelhead stocks to sustainable levels through habitat protection and restoration.
- Improving frost, rainfall, and river forecasts in the Russian River watershed through improved data collection and modeling.
- Increasing community resiliency to flooding damage through improved planning and water management strategies.

US Geological Survey – California Water Science Center

The project has been aided greatly by the streamflow data collected by USGS hydrologists who operate, maintain and process records for stream flows at a number of gaging stations in the region. Highly quality, long-term records for instantaneous flood peak and daily flows provided the basis for comparison to RDHM simulated flows. Other USGS data collections and reports provided useful background on streamflow statistical patterns (e.g. flood frequency), groundwater resources and other watershed studies.

Sonoma County Water Agency

The Russian River basin serves multiple water supply needs for domestic, agricultural, fisheries and recreation users. And there is always the threat of flooding. A primary water management authority is the Sonoma County Water Agency (SCWA; <http://www.scwa.ca.gov/>). The SCWA supplies 600,000 residents with potable water and is responsible for maintaining over 75 miles of streams, numerous facilities and a flood warning system to help reduce the risk of flooding. The SCWA is a primary sponsor of the USGS flow gaging program in the basin. The SCWA has developed the RRIFR for endangered

fisheries restoration (<http://www.scwa.ca.gov/rriifr/>), and operates some of the wastewater treatment and recycling programs. Headwaters of the Russian River lie in the jurisdiction of Mendocino County and the Russian River Flood Control and Water Conservation Improvement District who have comparable responsibilities for water supply and fisheries habitat.

Russian River IWRSS Case Study

The Russian River basin has been identified as a pilot for demonstration of a national program for Integrated Water Resources Science and Services (IWRSS). The IWRSS seeks to apply advanced water resources monitoring, data management and modeling technologies to obtain a comprehensive common operating picture usable by the various governmental agencies and stakeholders to identify optimal plans and actions for mitigating adverse impacts and enhancement of environmental quality and sustainability. Federal agencies involved include NOAA, the USGS and US Army Corps of Engineers. Addressing these problems in the context of the Russian River basin has potential for advancing the state-of-practice for holistic integrated water management; results and products realized from this case can be leveraged to other areas and can inform nationwide IWRSS efforts.

1.3 Objectives

This HMT research-to-operations (R2O) activity is aimed at assessing the distributed modeling approach for forecast and water management applications. It is supportive to the DWR Enhanced Flood Response and Emergency Preparedness (EFREP) project objectives and may provide guidance for operational adoption by the CNRFC, WFO-MTR, SCWA and the NWS National Water Center.

The project relates strongly to the goals of the NWS Weather Ready Nation (NWS 2012):

- Goal 1 - Improve weather decision services for events that threaten lives and livelihoods
- Goal 2 - Deliver a broad suite of improved water forecasting services to support management of the Nation's water supply
- Goal 3 - Enhance climate services to help communities, businesses, and governments understand and adapt to climate-related risks
- Goal 4 - Improve sector-relevant information in support of economic productivity
- Goal 5 - Enable integrated environmental forecast services supporting healthy communities and ecosystems

The overall objective of this report is to assess the accuracy of the distributed hydrologic modeling approach in representing surface hydrologic processes, including flood events and low flows. It is also intended to examine how the DHM approach may be applied in support of NWS hydrologic forecasting services, as well as related water management purposes. Specific objectives to be addressed are guided by the NWS Office of Hydrologic Development Science Plan (2009):

- Can distributed hydrologic models be used with current observational networks to provide accurate river simulations and forecasts?
- What measurements and observational network density are most critical for accurate hydrological modeling?
- What level of hydrologic model complexity is appropriate for hydrologic forecasts?
- What is the level of uncertainty of hydrologic forecasts?
- What is the performance of the distributed model given various inputs derived from as many sources as possible?
- How can a distributed modeling approach be implemented to support CNRFC, WFO, NMFS, SCWA and other agencies' forecast operations and water management?

1.4 Outline of Report

Sections of this report following include:

-
- Section 2 - Basin Description
 - Section 3 – Russian-Napa Rivers Distributed Hydrologic Model (RDHM)
 - Section 4 - Assessment of the Distributed Hydrologic Model
 - Section 5 - Applications of Distributed Hydrologic Modeling
 - Section 6 – Conclusions and Recommendations
 - Section 7 – References
 - Abbreviations and Acronyms
 - Appendices

2. RUSSIAN-NAPA RIVER BASINS

2.1 Basins Description

The Russian River watershed encompasses 1,485 sq. mi. (3846 sq. km., 950,000 acres) within Sonoma and Mendocino Counties, California (Figure 1). It is one of the most flood-prone rivers in the State of California because of the watershed's unique geography and its proximity to the coast, which together produce climatologically heavy wintertime rainfall. The Russian River faces challenges related to flood threats and mitigation, water supply, maintaining endangered species habitats, water quality, and recreation. Mitigating the flood threat, maintaining flow levels and habitats for fisheries, and multiple water supply demands compound the water management complexities.

The Russian River drains much of central and northern Sonoma County and southern Mendocino County. The river rises in the coastal mountains of Mendocino County, north of the city of Ukiah, and flows into Lake Mendocino, a major flood control reservoir. The Russian flows south from the lake through Mendocino to Sonoma County, paralleled by Highway 101. It turns west at Healdsburg, receiving water from Lake Sonoma via Dry Creek, and empties into the Pacific Ocean at Jenner.



Figure 1. Russian River, California

The Napa River basin (not shown), located just east of the Russian River basin, encompasses approximately 426 square miles (1,103 km²). It is almost entirely within Napa County (a small portion is also in Solano County). In the valley, it flows 55 miles (89 km) southeast past Calistoga, St Helena, Rutherford, Oakville and through Napa, its head of navigation. Downstream from Napa, it forms a tidal estuary, entering Mare Island Strait, a narrow channel on the north end of San Pablo Bay. It discharges into San Pablo Bay through the Napa Sonoma Marsh.

Sonoma County, located on the northern coast of the U.S. state of California, is the largest (in area) and northernmost of the nine San Francisco Bay Area counties. Its population at the 2010 census was 483,878. Its largest city and county seat is Santa Rosa. Mendocino County had a population of 87,841 in the 2010 Census. Napa County has a population in 2010 was 136,484.

Sonoma, Mendocino and Napa Counties are large producers in California's Wine Country region, which also includes Lake County. Sonoma County has over 250 wineries and in 2002 ranked as the 32nd county in the United States in agricultural production, largely due to the extent of available, fertile agricultural land, in addition to the abundance of high quality irrigation water. More than 7.4 million tourists visit each year, spending more than \$1 billion in 2006.

2.2 Terrain and Hydrography

The Russian River begins at 1960 ft (597 m) MSL about 5 mi (8 km) east of Willits in Mendocino County. It flows generally southward to Redwood Valley, then parallels U.S. Route 101 past Calpella, to join the East Fork Russian River just below Lake Mendocino. A portion of the Eel River is diverted to headwaters of the E. Fk. Russian River in Potter Valley upstream of Lake Mendocino. From there the

river flows south, past Ukiah and Hopland, and crosses into Sonoma County just north of Cloverdale. Closely paralleled by U.S. Route 101, it descends into the Alexander Valley, where it is joined by Big Sulphur Creek.

East of Healdsburg, Maacama Creek joins the Russian River. After a series of sweeping bends, the river flows under the Healdsburg Memorial Bridge and U.S. Route 101 and receives water from Lake Sonoma via Dry Creek. The river then turns westward and joins Mark West Creek north of Forestville followed by Green Valley Creek to the south. The river passes Rio Nido and Guerneville where it is paralleled by State Route 116. Austin Creek enters from the north before passing through Duncans Mills then the Russian River flows under State Route 1 and empties into the Pacific Ocean between Jenner and Goat Rock Beach.

The tributaries generally have drainage less than 100 sq. mi. and are quite steep as they drain off the mountains from the east and west to join the main stem. The principal tributaries of the Russian River in the Study Area include Big Sulphur Creek, Maacama Creek, Dry Creek, and Mark West Creek. The principal tributary of Mark West Creek is Laguna, which drains a large flat marshy area and enters Mark West Creek about 5 miles upstream from its mouth. In addition, numerous smaller creeks empty into the Russian River. These creeks typically have smaller watersheds in the surrounding hills. The creeks exit the hills and flow across the alluvial valleys before emptying into the Russian River if enough flow remains after infiltration into the alluvial deposits.

The Napa River, which lies to the east of the Russian, rises in northwestern Napa County just south of the summit of Mt. St. Helena in the Mayacamas Mountains of the California Coast Ranges. The source begins as seasonal Kimball Canyon Creek in Robert Louis Stevenson State Park at an elevation of 3,745 feet (1,141 m) which descends the southern slope of Mt. St. Helena to Kimball Canyon Dam. Reservoirs in the watershed include Lake Hennessey, Lake Milliken, and Bell Canyon Reservoir. All of these dams are located on the tributary streams along the eastern side of the watershed, and effectively block every major east side tributary between St. Helena and Napa, except Soda Creek. In 1986, the worst of 23 floods recorded since 1865 on the Napa River occurred. 5,000 people were evacuated, 250 homes were destroyed, and three people lost their lives.

2.3 Land Use / Land Cover

The study site has a complex terrain with the land cover dominated by “Evergreen Forest”, “Scrub/Shrub”, and “Grass Land”. Among these dominant land covers are the clusters of the lands classified as “Cultivated Crops (Vineyard)” and “Developed”. Figure 2 shows the National Land Cover Dataset (NLCD 2006) showing the land cover distribution of in the Russian and Napa watersheds. Land cover can influence streamflow and soil moisture fluctuation through the functions of evapotranspiration and direct runoff.

2.4 Hydrogeology and Soils

The Russian-Napa River watersheds are underlain predominantly by the Franciscan formation, which is a highly erodible mélangé that formed during the Jurassic-Cretaceous age and has become highly fractured due to seismic and volcanic activity. The watershed features a series of wide valleys separated by narrow bedrock channels. Numerous streams within the basins, including the upper main stem Russian River, follow the northwest to southeast orientation of the geologic faults.

As summarized by Walls (2013), the geological history of the Russian River basin has involved active plate tectonics, seismic and volcanic activity. Collision between the Pacific and the North American tectonic plates caused uplift and formed the northwestern portion of the California Coast Range geomorphic province (Jennings 1938). Much of the mountainous terrain in the Basin is steep and highly erodible, which produces relatively high quantities of coarse sediment that have filled alluvial valleys. Hills and mountains comprise approximately 80% of the Basin, with alluvial valleys filling the remaining 20% (Figure 3) (Haydon 2007). Streams have carved through uplifted bedrock in the mountainous

portions of the watershed, where upon leaving their canyon bound reaches they deposit sediment and flow across alluvial valleys before joining the main stems Russian-Napa River or other streams.

Approximately 60% of the Basin is shallowly underlain by Franciscan complex, the oldest formation in the Basin (Haydon 2007). Franciscan rocks are a heterogeneous assemblage of metamorphosed sedimentary, volcanic, and metaphoric rocks which are highly fractured, especially along fault zones. The southeastern portion of the watershed is home to active geothermal vents and a formation known as the Sonoma Volcanics; a large geothermal power generation facility is located there.

The main stem Russian River valley consists of a series of northwest trending wide alluvial valleys separated by bedrock canyons. The alluvial valleys formed by lateral fault blocks of the San Andreas Fault system moving at different rate relative to each other, creating local depressions known as pull-apart basins. Rocks from the surrounding terrain are eroded, transported by streams, and deposited in these depressions. Alluvial valleys compose approximately 20% of the Basin in a variety of formations including terraces, alluvial fans, and flat valley floors. Major alluvial valleys along the main stem are the Ukiah, Hopland, and Alexander Valleys, the Middle Reach, and Santa Rosa Plain. These areas have significant groundwater aquifers.

2.5 Reservoirs and Diversions

Water control and diversion facilities in the Russian River were summarized by Kennedy/Jenks (2007). Two dams have been built to control water flow in the watershed; the Coyote Valley Dam on the East Fork forms Lake Mendocino and the Warm Springs Dam on Dry Creek forms Lake Sonoma. Inflows to Lake Mendocino come from the E. Fk. Russian River basin. Total drainage area at Coyote Dam is 105 sq. mi. This drainage area comprises 7.1% of the total Russian River drainage (1485 sq. mi.), 7.8% above Guerneville (1338 sq. mi.), 13% above Healdsburg (793 sq. mi.), and 29% of the drainage above Hopland (362 sq. mi.). The nearest stream gage is USGS 11461500 EF Russian R nr Calpella, Ca. which has a drainage area of 92.2 sq. mi. This gage has been in continuous operation since 1962 and has an average daily flow for the 50-year period 1963-2012 of 311 cfs (or 3.8 ft/yr), a peak flow of 12,500 cfs and a minimum flow of 2 cfs.

River flows in the E. Fk. Russian River basin have historically been augmented by trans-basin diversions from the upper Eel River basin through the Potter Valley project. The Eel River flows are sustained by releases from the Lake Pillsbury Reservoir. After passing through the Pacific Gas and Electric powerhouse, part of the flow is used for irrigation in Potter Valley and the remainder flows into

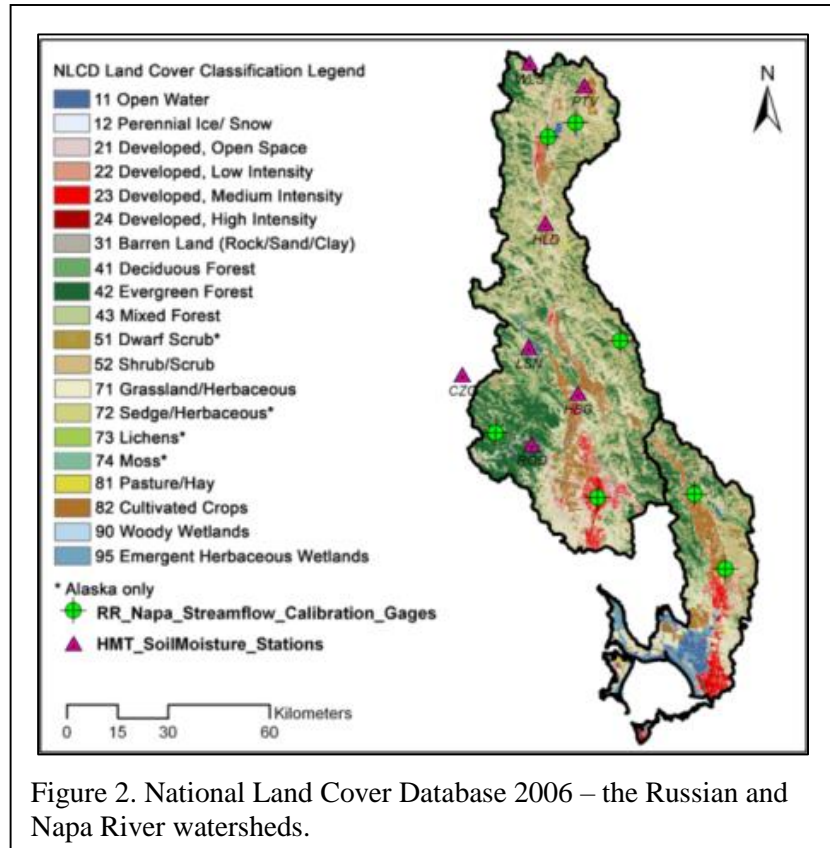


Figure 2. National Land Cover Database 2006 – the Russian and Napa River watersheds.

East Fork Russian River. Daily diversions through the Potter Valley project have averaged 197 cfs for the 50-year period. The Potter Valley diversion flows comprise a substantial portion of the flows reaching Lake Mendocino, perhaps 40% if accounting for consumptive uses for the irrigation usage. Potter Valley diversions have been reduced in recent years due to regulatory actions taken by the California Water Resources Control Board.

Lake Sonoma, located on Dry Creek in the lower part of the Russian River basin, was formed by Warm Springs Dam in 1982. It has a design capacity of 381,000 AF with a water supply pool of 212,000 acre-feet. It controls a Dry Creek drainage area of approximately 130 sq. mi., or approximately 9 percent of the total Russian River basin. Just downstream of Lake Sonoma, Warm Springs Hatchery, located at the reservoir outlet, produces Coho salmon and Steelhead for waters in the Russian River drainage. Together these two federally regulated large dams have a combined drainage area of 235 square miles and storage capacity of 450,000 acre-feet to diminish peak winter flows. These facilities have been credited with reducing floodwaters by four feet in the Guerneville area during the February 1986 storm and for reducing the flood crest level by an estimated 7-10 feet overall.

Releases from these dams are used to sustain water flows in the summer months and to support water supplies downstream. The State Water Resources Control Board adopted Decision 1610 requiring a minimum streamflow for the Russian River and Dry Creek (SCWA, 1996). In a normal year, the minimum river flow requirement at the Hacienda Bridge, upstream from Guerneville, is 125 cubic feet per second (cfs). In a dry year these quantities are reduced to 75 cfs. In a critically dry year these quantities are further reduced to 25 cfs.

These are the current minimum flow requirements and are subject to change given on-going water management planning activities. The actual flows maintained are typically much greater, even in a critically dry year, for both operational reasons and because of the unregulated runoff from the Russian River watershed (SCWA, 1996).

A concern with reservoirs in a river system is how to account for water capture and releases as part of the process for forecasting river flows. The NWS river forecast processes typically emphasize forecasting of “natural” flows which do not account for water management influences. To address this shortcoming an application was developed to couple the RDHM with a water management model; this application is described later in this report.

Several municipal water supply systems are located along the Russian River (Kennedy/Jenks 2007). Municipal pumping rates vary seasonally. The typical water usage pattern for this area is for the highest water demand to occur in the summer months and the lowest demand to occur in the winter months. Typically, the groundwater wells for these systems are completed in the alluvial aquifer near to the River. Wells completed in the highly permeable alluvial sediments are capable of producing pumping rates in

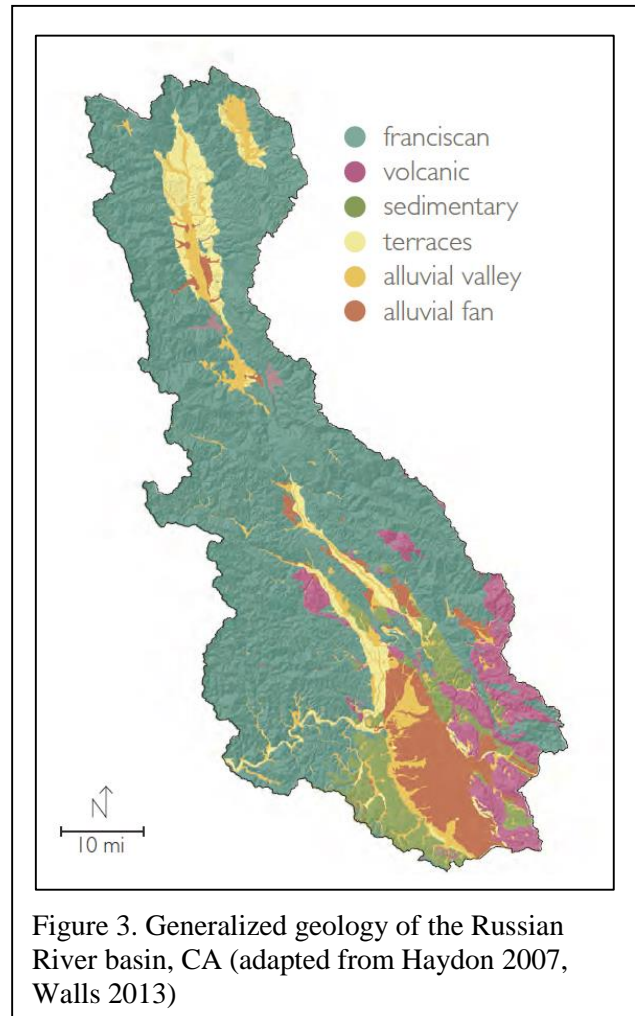


Figure 3. Generalized geology of the Russian River basin, CA (adapted from Haydon 2007, Walls 2013)

excess of 1,000 gallons per minute (gpm). Wells located near the Russian River are able to induce leakage from the Russian River to sustain higher flow rates. The SCWA has the largest well system and delivers water to over 375,000 residents in its service area, which includes most of urban Sonoma County and portions of northern Marin County. SCWA (2007) holds water rights of 75,000 acre-ft/yr from the Russian River and Dry Creek. Based on an analysis of future needs, up to 89,000 acre-ft/yr are anticipated in the future (SCWA 1996).

Vineyards are the predominant crop type (Kennedy/Jenks 2007). The alluvial valleys along the Russian River have a high density of land dedicated to vineyards (Figure 4). Agricultural pumping wells tend to be located near to the land they irrigate. Therefore, agricultural pumping tends to be distributed over a large number of wells. In the Russian River Valley, annual irrigation rates typically range from 6 to 18 inches per year of applied water per acre depending on vine age, location, varieties and weather conditions for a given year (Lewis et al., 2006, DWR, 2003). Metzger and others (2006) estimated that of the 13,500 acre-ft/yr of irrigation in Cloverdale and Alexander Valley, about 78 percent was met solely by groundwater, about 6 percent was met solely by surface water, and about 1 percent was met by a combination of ground and surface water; about 15 percent had an unknown source.

Seasonally, irrigation of vineyards varies from little to none in the winter to a maximum in the summer. Of the typical range from 6 to 18 inches per year of applied water per acre of vineyards, about 85 percent is applied during the most intensive irrigation months of May through August (California Water Atlas, 1979). Of that total, approximately 50 percent of the annual demand occurs over a 60-day period typically late June to early August. During September and October, irrigation is scaled back to stress the grapes and during the harvest. About 15 percent of the applied water is used in September and October. Typically, little to no irrigation occurs during November through April while the vines are dormant and/or sufficient precipitation is available. These percentages may vary due to precipitation conditions for a given year and local variation in climate, soil and irrigation practices.

Utilization of spray irrigation for frost protection of vineyards has become a wide-spread practice during March and April after leaves and grape clusters have begun to form. Spraying to protect vines typically requires between 1.5 and 2.5 inches of water (Kennedy/Jenks 2007; Ryder, 1994). Ponds, wells, river diversions and recycled water are typically used as sources of frost protection water. Frost damage can occur when temperatures fall below freezing in the spring. Healdsburg and Cloverdale average 2 days of below freezing temperatures during March and April; however, temperatures in the area may vary by elevation and local microclimates (USDA, 1972). Spray irrigation may also be used to cool the grapes during hot summer periods.

All streams tributary to the Napa River go dry in summer (Rantz 1965). The Napa River is a perennial stream at the St. Helena gaging station but is usually dry at the Napa gaging station for one or more months during the summer. This loss in streamflow between the two gaging stations is attributed to pumping for irrigation both from the stream and from the ground-water reservoir.

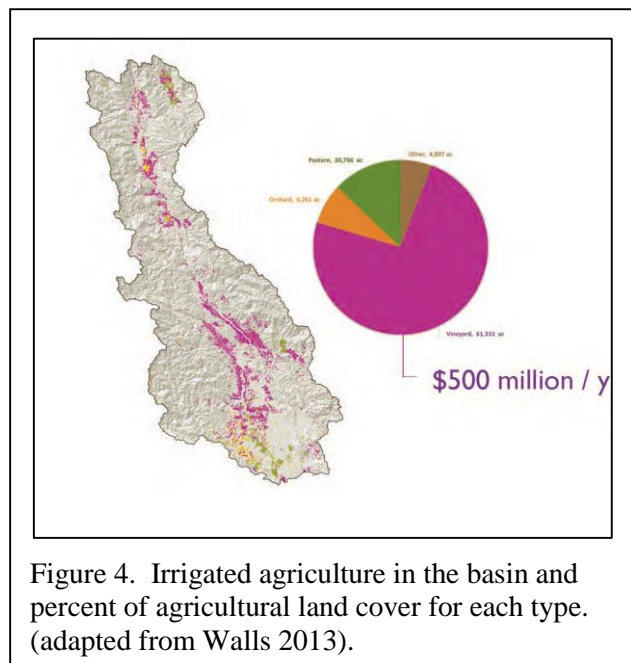


Figure 4. Irrigated agriculture in the basin and percent of agricultural land cover for each type. (adapted from Walls 2013).

2.6 Precipitation

Atmospheric Rivers

According to a recent Department of Water Resources report California's Flood Future: Recommendations for Managing the State's Flood Risk (2013, <http://www.water.ca.gov/sfmp/>) - many parts of California, including the Bay area, are at risk of catastrophic flooding. In addition to public safety, existing infrastructure dedicated to transportation, water supply, and waste water can be negatively impacted by both long- and short-duration heavy rainfall events. Rain storms are highly variable in time and space and are not fully resolvable using current rain gauge and weather radar information.

Recent studies (e.g. Ralph, et al 2012) have documented the important role that "atmospheric rivers" (ARs) of concentrated near-surface water vapor above the Pacific Ocean play in the storms and floods in California, Oregon, and Washington. By delivering large masses of warm, moist air

(sometimes directly from the Tropics, Fig 5), ARs establish conditions for the kinds of high snowlines and copious orographic rainfall that have caused the largest historical storms. In many California rivers, essentially all major historical floods have been associated with AR storms. Ralph et al. (2006) recently noted that every "declared" flood on the Russian River near Guerneville, California, during the past 10 years has been associated with the arrival of an AR.

Conversely, if AR events during the winter storm season do not occur, then there is threat of drought conditions and consequent impacts on water supply reliability. When an AR event occurs after a protracted dry spell, then it is called a "drought buster." Dettinger et al. (2011) documented the major roles that ARs also play in California's water supply, providing from 25% to 50% of an entire water-year's precipitation in just a few events.

Even today, California's aging water supply and flood protection infrastructure, including more than a thousand kilometers of levees, is challenged by punishing floods and increased standards for urban flood protection. Further, current climate-change projections for 21st Century California uniformly include warming by at least a couple of degrees, and, although great uncertainties remain about future changes in long-term average precipitation rates in California. It is generally expected that extreme precipitation episodes may become more extreme as the climate changes (Dettinger 2011).

Precipitation Climatology

The Russian River basin receives about 46.5 inches (1180 mm) of rain per year; about 30 in (760 mm) is normal for Santa Rosa. Certain areas, particularly in the north-west portion of the county around the Russian River, receive significantly more rainfall. The Guerneville area, for example, typically receives about 50 in (1,300 mm) of rain a year, with annual rain occasionally going as high as 70 in

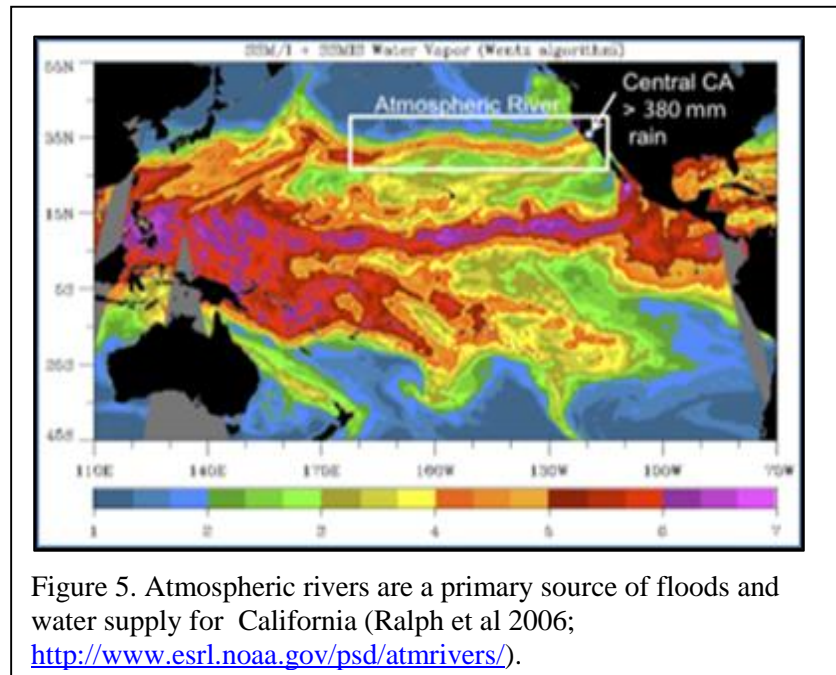


Figure 5. Atmospheric rivers are a primary source of floods and water supply for California (Ralph et al 2006; <http://www.esrl.noaa.gov/psd/atmrivers/>).

(1,800 mm). Nearby Cazadero typically receives about 72 in (1,800 mm) of rain a year, many times has reached over 100 in (2,500 mm) a year, and sometimes over 120 in (3,000 mm) of rain a year. The Cazadero region is the second wettest place in California. Snow is rare in Sonoma County except in the higher elevations on and around the Mayacamas Mountains. The Napa River basin is shielded from coastal storms and consequently has a lower annual average rainfall of about 31.5 inches (800 mm).

Average precipitation for the 30-year period 1981 to 2010 has been computed by the Parameter-Elevation Regressions on Independent Slopes Model (PRISM) of Daly and others (1994) at Oregon State University (<http://prism.nacse.org/>, Table 1). PRISM is designed to map climate in complex environmental regimes, including high mountainous terrain and rain shadows (Daly and others, 1994). PRISM uses point measurements, digital elevation models, and other spatial data to generate gridded estimates of monthly and yearly precipitation. PRISM fits separate precipitation/altitude relations to neighboring stations with the same topographic aspect to generate interpolated values. Thus, PRISM is automated to adjust its frame of reference to accommodate local and regional climatic differences, rain shadows and coastal effects to create a pattern of precipitation (Daly and others, 1994).

Table 1. PRISM Basin Average Precipitation [in] (1981 - 2010)

	Napa River Basin	Russian River Basin
Jan	5.9	8.9
Feb	6.1	8.5
Mar	4.4	6.5
Apr	1.9	3.0
May	1.1	1.7
Jun	0.2	0.3
Jul	0.0	0.0
Aug	0.1	0.1
Sep	0.2	0.4
Oct	1.6	2.4
Nov	3.8	5.7
Dec	6.0	9.0
Annual	31.5	46.5

The 30-year (1981 – 2010) annual precipitation normal from PRISM shows that annual precipitation distribution is a function of elevation and distance to the coastline (Figure 6). In the Russian River watershed, three juxtaposition zones assert the precipitation distribution: 1) ridges along the west boundary from the Laughlin Ridge to the Little Black Mountain by the Austin Creek have the highest precipitation; 2) the valleys from the Redwood valley in the north to the Santa Rosa Plain in the south constitutes the zones receives less rainfall; and 3) the Cow Mountain and the Mayacamas Mountains on the eastern boundary comprise the third zone with medium annual rainfall.

A variation of the PRISM procedure, called Mountain Mapper (Schaake et al 2004; CNRFC 2004) is used by the CNRFC to determine precipitation amounts used as input to their river flow forecasting model, the Sacramento Soil Moisture Accounting (SAC-SMA) model. The SAC-SMA is a so-called “lumped” model of watershed hydrology representing runoff from sub-basin areas which have uniform characteristics. For example, the CNRFC has 6 forecast points on the main stem in the Russian River basin and 2 forecast points in the Napa basin. The CNRFC generates precipitation mappings on the HRAP grid, nominally 4 km on a side (see below) for current rainfall amounts (called Quantitative Precipitation Estimates

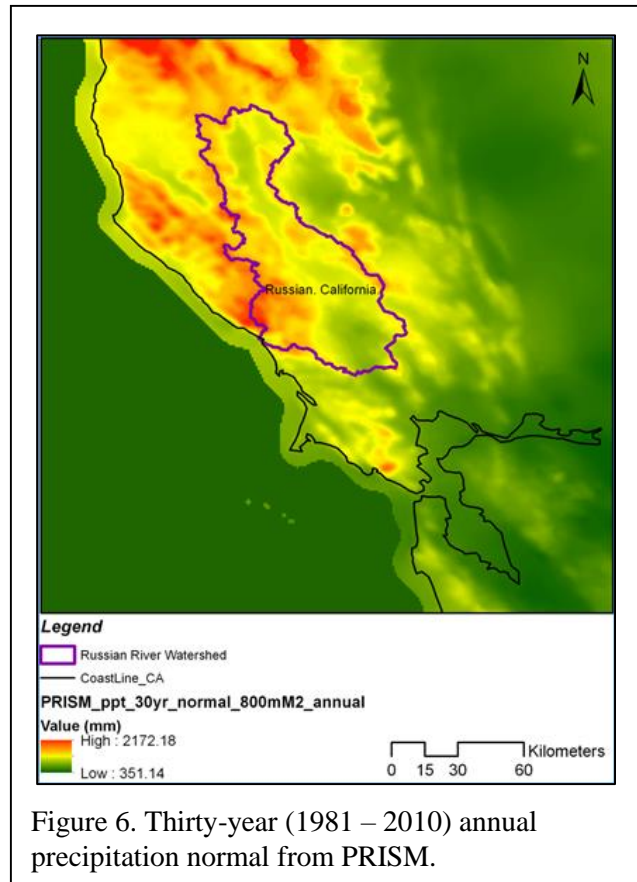


Figure 6. Thirty-year (1981 – 2010) annual precipitation normal from PRISM.

(QPE)) and forecasts (called Quantitative Precipitation Forecasts (QPF)). These gridded fields are a primary input to the distributed hydrologic model RDHM. The CNRFC remaps the gridded values to obtain Mean Areal Precipitation (MAP) for the watersheds represented in their NWSRFS hydrologic model.

The Mountain Mapper technique (Schaake et al 2004) uses an inverse distance weighting approach to estimate precipitation at ungaged locations from values at gaged locations while taking into account the climatology of precipitation at the gaged and ungaged locations. An important component of the CNRFC NWSRFS modeling involves calibration in preparation of a mean areal precipitation (MAP) time series for the forecast watersheds. When a basin is subdivided into elevation zones, a MAP time series must be created for each zone. Using the Calibration Assistance Program (CAP) PRISM data is used to relate historical gage data to zone climatology. The CNRFC data is used as the primary precipitation forcing data for this distributed hydrologic modeling study.

Rainfall in the region is generally associated with the winter season November through March. Winter storms often are associated with the atmospheric river (AR) phenomenon which has been associated with the highest rainfall events resulting in flooding and overall water supply (Ralph 2012). The seasonality graphs show the percentage of precipitation totals for a given duration that exceeded the precipitation frequency estimates for the duration and selected annual exceedance probabilities in each month for each region (Figure 7, NOAA Atlas 14 - <http://www.nws.noaa.gov/oh/hdsc/index.html>). Precipitation frequency characteristics are tabulated by the NOAA Atlas 14. Figure 7(a) illustrates the depth-duration frequency data for Santa Rosa, CA. For example, the 24-hour, 100-year precipitation is approximately 5 inches; the 10-day, 100-year precipitation at Santa Rosa is 16.0 inches. Results for Ukiah, CA are 8.6 in in 24 hours; the 10-day, 100-year precipitation at Ukiah is 25.2 inches.

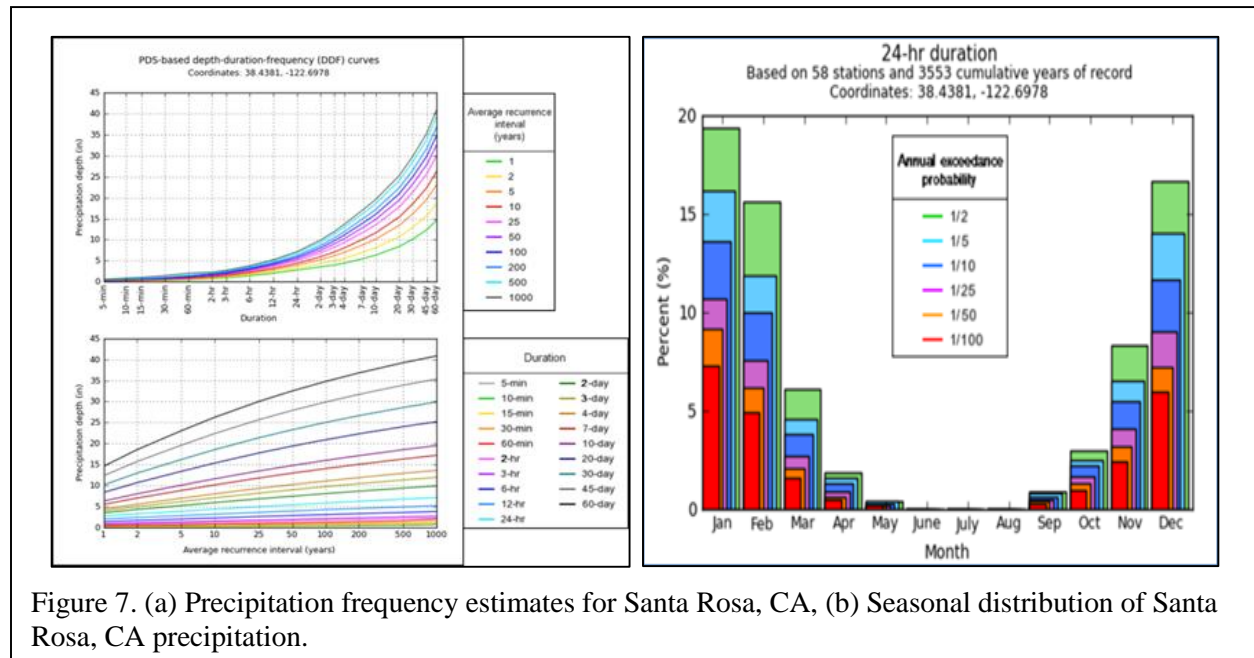


Figure 7. (a) Precipitation frequency estimates for Santa Rosa, CA, (b) Seasonal distribution of Santa Rosa, CA precipitation.

2.7 Surface Runoff

USGS Flow Gages

Surface runoff is determined primarily by stream flow gages operated by the USGS which has collected the longest and most reliable records (http://ca.water.usgs.gov/gmaps/st_rt_map.html). Other agencies such as the USACE, NMFS, SCWA and other entities collect flow records as well. Table 2 summarizes flow records for the Russian-Napa basins. River flows, represented as depth of water averaged over a drainage area, range from 3.1 ft/yr for tributaries draining the higher mountain headwaters (e.g. Austin Cr) to 1.78 ft for the basin upstream of the Guerneville gage (period 2002 – 2011). Flows in the Napa River are somewhat lower reflecting less rainfall farther from the Pacific coast. Streamflow records for these gages can be retrieved from the USGS web site. Figure 8 illustrates a typical retrieval.

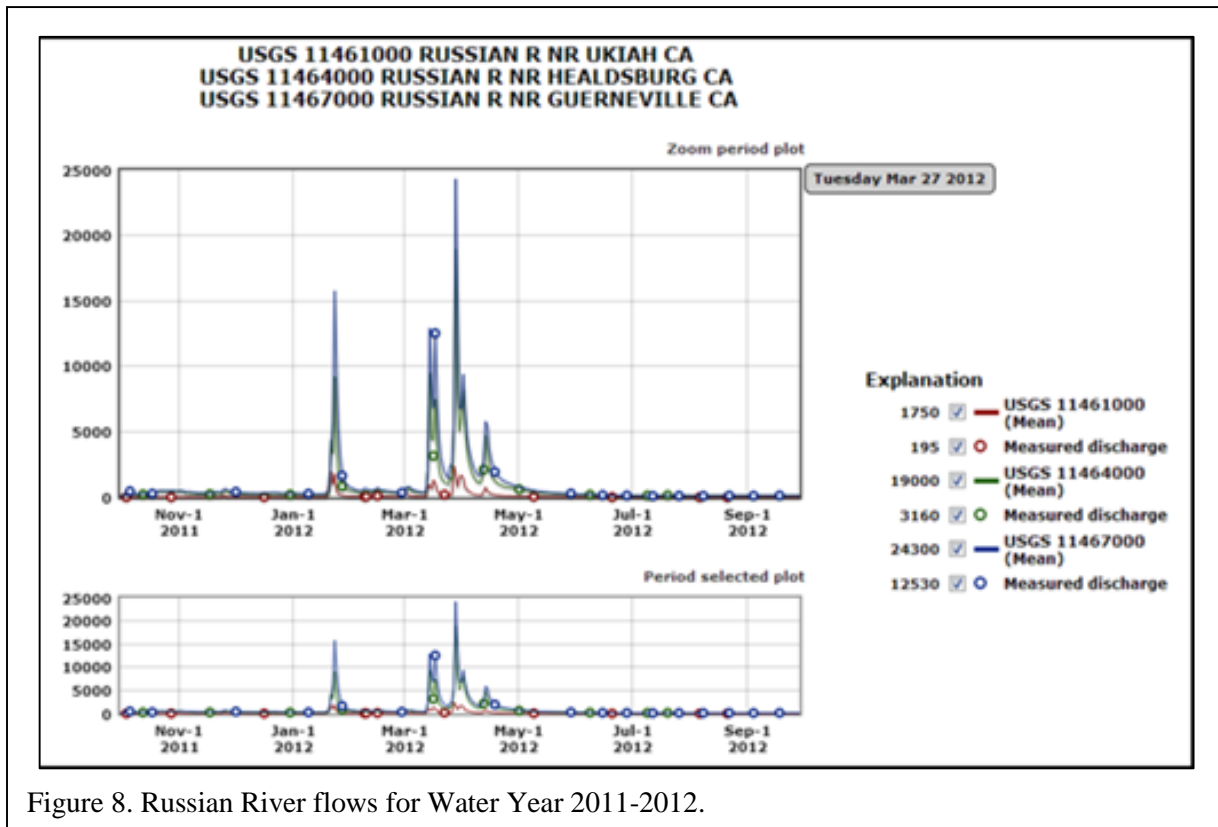


Figure 8. Russian River flows for Water Year 2011-2012.

Floods

The Russian River is one of the most flood-prone basins in California due to location near the coast and the influence of land-falling storms (atmospheric rivers). The gaging records at Guerneville (USGS 11467000 RUSSIAN R NR GUERNEVILLE CA; 1940-2014) show the annual peak flows routinely exceed 50,000 cfs. The peak flood flow was 102,000 cfs in 1964 (Figure 9). A review of the flood records for 23 USGS gauging stations on tributaries of the Russian River and nearby streams reveals that the unit mean-annual-flood (average peak discharge/watershed area) is roughly 100 cfs/sq.mi, for watersheds larger than 1.0 sq.mi. (SCWA 2012).

Table 2 Russian-Napa Rivers USGS Surface Water Gage Sites

Flow Gage Name	USGS gage #	Area [mi ²]	Area [km ²]	HRAP grids	Record period	Qann** [cfs]	Qann** [ft]	Comments
E Fk Russian River nr Calpella*	11461500	92.2	238.8	14.0	1-Oct-41	259	3.17	Diversions from Eel River through Potter Valley Powerplant
Potter Valley Powerhouse Tailrace	11471099	--	--	--	1-Oct-87	128	1.57	Records since 1987 incl. irrigation flows; diversions recently reduced
Lake Mendocino #		105.0	271.9	16.0				Built Nov 1958; Vtot=122KAF, Vcons=68.4KAF, Vflood=48.1KAF
Russian River nr Ukiah* #	11461000	100.0	259.0	15.2	1-Oct-11	187	2.11	Irrigation influences; CNRFC forecast point
Russian River nr Talmage	11462080	286.0	740.7	43.6	6-Aug-09			Regulated by Lake Mendocino
Russian River at Hopland #	11462500	362.0	937.6	55.1	1-Oct-39	659	2.06	Regulated by Lake Mendocino; CNRFC forecast point
Russian River nr Cloverdale #	11463000	503.0	1302.8	76.6	1-Aug-51	866	1.95	Regulated by Lake Mendocino; CNRFC forecast point
Big Sulphur Cr nr Cloverdale	11463200	85.5	221.4	13.0	1-Jul-57			Low flow gaging only after 2009
Big Sulphur Cr CAG Resort nr Cloverdale*	11463170	13.1	33.9	2.0	1-Oct-80	46	3.96	Two HRAPs, a very small response area
Russian River at Jintown	11463682	684.0	1771.6	104.2	1-Jul-09			Regulated by Lake Mendocino; No records above 400 cfs
Russian River at Digger Bend nr Healdsburg	11463980	791.0	2048.7	120.5	1-Oct-87			Regulated by Lake Mendocino; No records above 400 cfs
Russian River at Healdsburg #	11464000	793.0	2053.9	120.8	1-Oct-39	1331	1.90	Regulated by Lake Mendocino; CNRFC forecast point
Lake Sonoma #		130.0	336.7	19.8				Built Oct. 1983; Vtotal=381KAF, Vcons=245KAF, Vflood=136KAF
Dry Creek nr Geyserville	11465240	162.0	419.6	24.7	1-Oct-59			3.0 mi downstream from Warm Springs Dam
Dry Cr nr mouth	11465350	217.0	562.0	35.1	1-Oct-81			Regulated by Lake Sonoma; 0.25 mi upstream from mouth
Russian River nr Windsor	11465390	1022.0	2647.0	155.7	1-Jun-09			Regulated by Lakes Mendocino and Sonoma
Santa Rosa Creek at Willowside Rd	11466320	77.6	201.0	11.8	9-Dec-98			Backwater from Laguna de Santa Rosa
Santa Rosa Creek at Santa Rosa *	11466200	57.0	147.6	8.7	1-Dec-01	110	2.18	Water diverted into Spring Lake during floods
Laguna de Santa Rosa nr Sebastopol	11465750	79.6	206.2	12.1	18-Nov-98	84	1.20	Backwater effects on rating
Mark West Cr nr Mirabel Hgts	11466800	251.0	650.1	38.2	1-Oct-05			Low-flow records only since October 2009
Russian River at Guerneville #	11467002	1338.0	3465.4	203.8	1-Oct-39	2103	1.78	Regulated by Lakes Mendocino and Sonoma; CNRFC forecast point
Austin Cr nr Cazadero *	11467200	62.8	162.7	9.6	1-Jun-59	174	3.13	May 1959 to September 1966, October 2003 to current year
Russian River at mouth		1485.0	3846.1	226.2				Regulated by Lakes Mendocino and Sonoma
Napa River nr St. Helena* #	11456000	78.8	204.1	12.0	1-Oct-29	98	1.41	Some regulation by Bell Canyon Res (2.5kaf)
Napa River nr Napa* #	11458000	218.0	564.6	33.2	1-Oct-29	218	1.13	Regulated by Lake Hennessey (31kaf, 58 sq. mi.)
HRAP grid =		6.6	17.0			**2002-2011		

* = RDHM calibration sites
= CNRFC forecast site

*Highlighted rows are the sites used for calibration and verification purposes.

The history of flood events which Lake Mendocino (drainage area 102 sq. mi.) has experienced is of interest (Figure 10). For the 50-year period 1962 to 2012 the daily inflows were tabulated to compute the 10-day inflow volumes; the 10-day period was selected to represent a period for which inflow forecasts would be available. During the 50-year period there were 135 flood events having inflow volumes greater than 10,000 AF; approximately 2.7 events per year. There is a 1-in-2 chance that a flood event exceeding 21 KAF could occur in any year and a 1-in-10 chance a flood event exceeding 42 KAF. The figure below shows the frequency tabulations. The maximum flood event occurred in 1964 with a 10-day inflow volume of 83,000 AF. The largest event in recent years was the 2005 event at 60,700 AF. For comparison, the 10-day precipitation for the 2005 event was 30.2 inches; noteworthy is that this rainfall would be characterized as a 500-year frequency storm. If applied over the 105 sq. mi. drainage area this rainfall totals to 169,000 AF. Compared to this total the surface runoff volume at 60,700 AF is 36% and the soil moisture storage would be 108,000 AF or 64%. Assuming an effective porosity of 30%, the soil would be saturated to a depth of 5.4 ft. This estimate underscores the relevance of soil moisture accounting in the basin water budget.

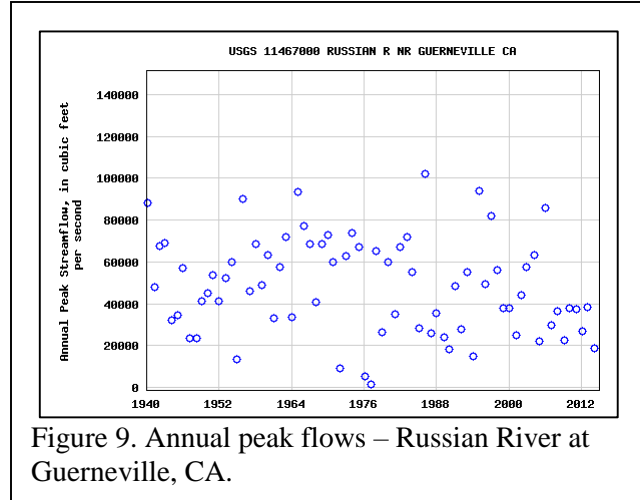


Figure 9. Annual peak flows – Russian River at Guerneville, CA.

Table 3. Flood frequency (cfs; from FEMA Flood Insurance Study - for Sonoma County, CA, 19 Feb 2014)

	DA [mi ²]	10-yr	50-yr	100-yr	500-yr
Mouth at Pacific	1,485	76,000	102,000	114,000	135,000
Upstr of Dry Creek	795	56,000	79,000	90,000	129,000
Upstr Oak Valley Cr	502	40,000	56,000	64,000	85,000
Austin Creek	63.2	14,900	22,100	24,600	30,400

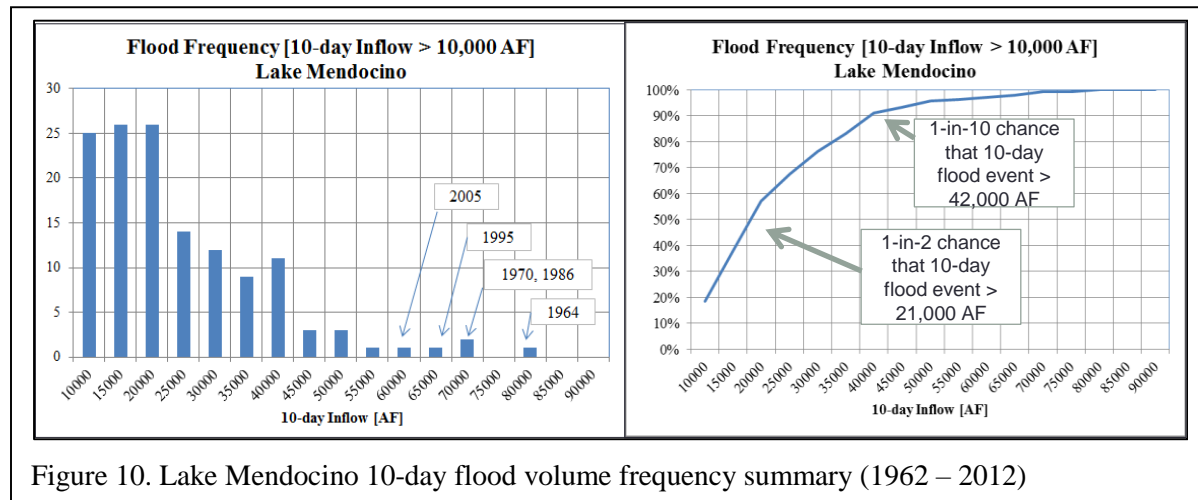


Figure 10. Lake Mendocino 10-day flood volume frequency summary (1962 – 2012)

Flood frequency characteristics for the Russian-Napa basins have been analyzed by the USGS based on regional regression analysis of basin characteristics (Gotvald et al 2012). The USGS approach uses generalized least squares regression to develop a set of equations for estimating flows with 50-, 20-, 10-, 4-, 2-, 1-, 0.5-, and 0.2-percent annual exceedance probabilities for ungaged basins in California. Table 3 lists the flood flow frequencies for a range of drainage area sizes.

Low Flows

A report by Rantz and Thompson (1967) presented an analysis of the surface-water hydrology of the coastal basins of California that lie between the north shore of San Francisco Bay and the south boundary of the Eel River basin. The report noted that flows in the summer and early fall are poorly sustained, and many of the smaller streams go dry. This seasonal distribution of runoff reflects not only the seasonal distribution of precipitation but also the influence exerted by the geologic characteristics of the California Coast Ranges. The low permeability of the soil and surficial rock and the limited capacity for subsurface storage impede infiltration, and as a result there is little lag between rainfall and runoff.

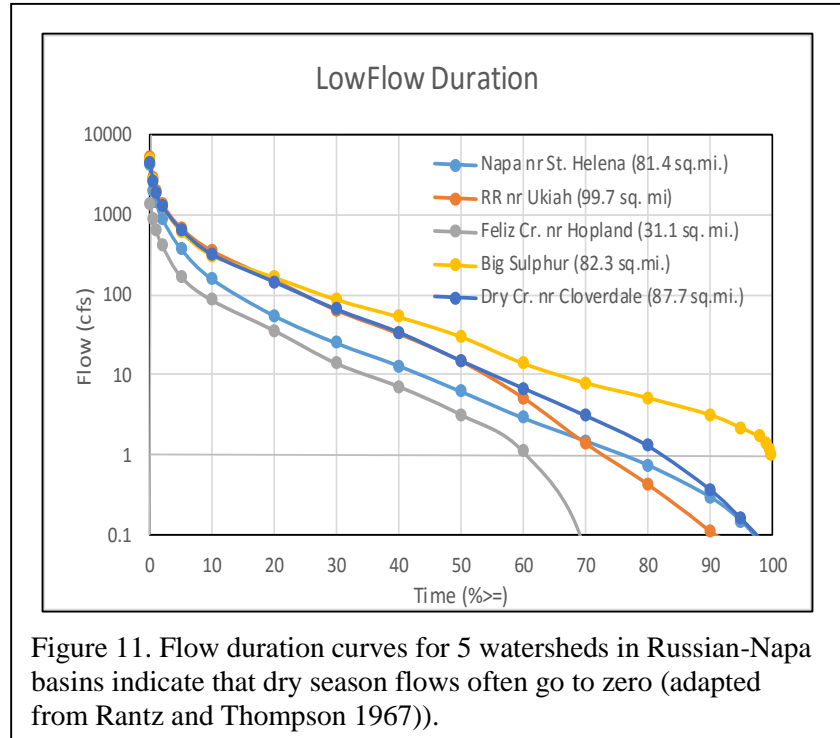


Figure 11. Flow duration curves for 5 watersheds in Russian-Napa basins indicate that dry season flows often go to zero (adapted from Rantz and Thompson 1967)).

For the Russian-Napa basins the Rantz and Thompson (1967) analysis indicated that the recurrence intervals of low flows sustained for periods ranging from 1 day to 274 days may be derived from the flow-duration curve. Their analysis covered the 30-year period 1931 – 1963. Figure 10 shows the flow duration curves for five watersheds in the Russian-Napa basins. Flow in the summer and early fall is poorly sustained and many small streams often go dry. Rantz and Thompson (1967) note that the very low flows are often associated with watersheds having low permeability soils and bedrock. There is also the sensitivity of low flows to pumping from wells in some locations. In terms of frequency, the 1-day discharge with a 10-year recurrence interval is about equivalent to the discharge at that station that is equaled or exceeded 99 percent of the time. As shown in Figure 10, for many small drainages this flow level is often zero. Note that in Figure 1 flows show as 0.1 cfs can be considered zero. For example, for the W.Br. Russian River nr Ukiah the flow is zero 10% of the time; for Feliz Creek the flow is zero 30% of the time.

2.8 Evapotranspiration

Evapotranspiration includes the transfer of water from surface-water bodies, soils, and vegetation to the atmosphere. As described by Metzger et al (2006) total annual evapotranspiration is greater than the soil-moisture deficit because plants continue to transpire water and water evaporates from water surfaces even during the cooler months of October to April. The mean annual potential evapotranspiration (PET or Eto) at Healdsburg between 1986 and 1994, calculated from hourly meteorological measurements, was 50.5 in. (California Department of Water Resources, accessed March 21, 2005). Actual evapotranspiration (Eta) is much less than Eto because most of the time soil moisture is below field capacity and many plants have periods of dormancy during part of the year, during which water consumption is greatly reduced.

For this study, Eta was estimated by comparing the soil moisture deficit (SMD) with the calculated Eto for the months May through September. The ratio of SMD to Eto for those months is 0.33. Eta for the entire year was estimated to be 16.7 in. by multiplying annual Eto (50.5 in.) by 0.33. This estimate is similar to estimates of Eta reported by the California Department of Water Resources (1980) for various crops. The estimate of Eta for orchards was about 19.7 inches per year (in/yr). Most of the study area is covered by native vegetation, which, with the exception of riparian vegetation, consumes less water than crops. So the mean Eta for the study area is probably less than 19.7 in. Total annual Eta for the study area can be calculated assuming an areally constant Eta. For the 81,280-acre study area, with an Eta ranging between 16.7 and 19.7 in., total Et is calculated to range between 113,000 and 133,000 acre-feet per year (acre-ft/yr).

2.9 Soil and Bedrock Moisture

The NOAA Physical Science Division, which manages the HMT program (initiated in 2004), began deploying soil moisture observing stations in support of hydrometeorological and air quality research in the year 2000 (Ralph et al. 2005; Zamora et al. 2003). These observing platforms have been designed to provide research quality observations of soil moisture and temperature on time scales ranging from minutes to decades. Zamora et al. (2011) outlined the observational strategies, instrumentation used by the HMT soil moisture observing networks, and presented some preliminary research results obtained by the networks. At present there are seven sites. (Figure 12, Table 4).

Soil moisture observations in the Russian River basin are made using Campbell Scientific Inc (CSI) CS616 soil water content reflectometers. Soil probes burial depths in the Californian HMT network have been standardized at 10 and 15 cm below surface. The Healdsburg site has been augmented with a CS616 probe at 20 cm depth. In addition, the Cazadero soil pit has been enlarged and additional probes have been installed at the standard USDA/SCAN probe depths of 5, 20, 50 and 100 cm.

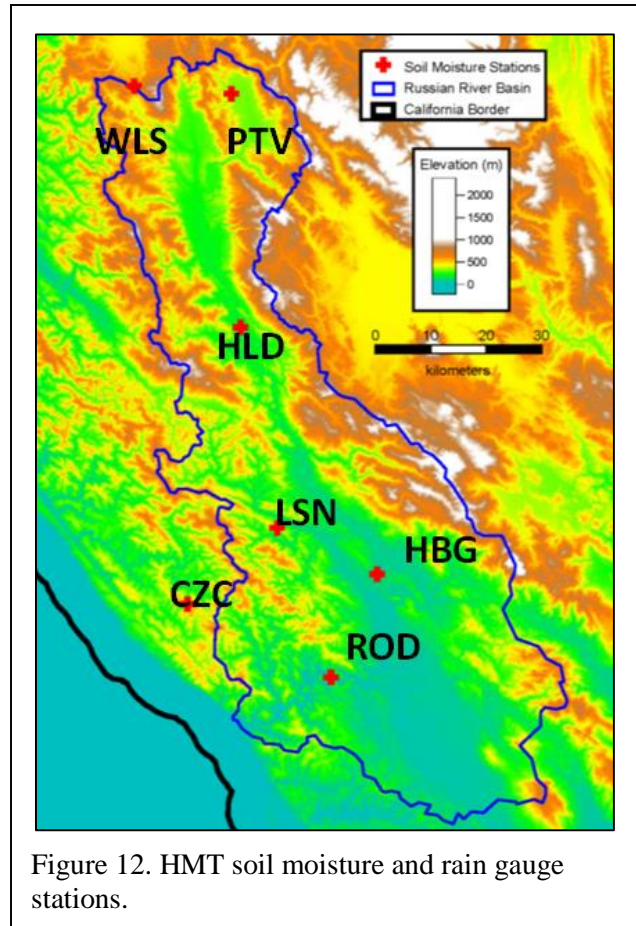


Figure 12. HMT soil moisture and rain gauge stations.

Table 4 HMT Soil Moisture Monitoring Stations.

Name	ID	Latitude	Longitude	Elevation [m]	Soil probe depths [cm]	Installation Date
Healdsburg	HBG	38.65	-122.87	62	10, 15, 20	12/29/2003
Cazadero	CZC	38.61	-123.22	475	5, 10, 15, 20, 50, 100	11/15/2005
Rio Nido	ROD	38.51	-122.96	30	10, 15	12/2/2006
Hopland	HLD	39	-123.12	165	10, 15	5/2/2010
Lake Sonoma	LSN	38.72	-123.05	398	10, 15	12/16/2010
Willits	WLS	39.35	-123.32	585	10, 15	12/16/2010
Potter Valley	PTV	39.34	-123.14	303	10, 15	4/20/2011

All soil probes are placed horizontally in the soil. Soil temperature observations are taken at each soil moisture probe depth using Campbell T-107 temperature probes. The temperature data are used for climatological studies and applying soil temperature corrections to the reflectometer measurements. All of the soil moisture stations deployed by NOAA/ESRL measure air temperature and relative humidity at 2.0 m. Precipitation measurements are made using Texas Electronics tipping-bucket rain gages.

The soils composition in the Russian River basin for all soil units in Sonoma and Mendocino counties based on the SSURGO soil surveys are shown in Figure 13. Soil physical properties, in particular saturated hydraulic conductivity and depth to restrictive layer information play a crucial role in the performance of the RDHM model. From an observational standpoint the soil electrical conductivity mapping can be used to locate regions in the basin where soil moisture probes may need to be recalibrated. With the exception of the alluvial river bed areas most of the soil units show a soil composition that is made up of nearly equal parts sand, silt and clay. All seven of the HMT soil moisture observing stations appear to be well situated within the average soil composition of the basin.

USDA SSURGO soil survey saturated hydraulic conductivity mapping for Sonoma and Mendocino counties from 0-20 cm depth indicates that there is some discrepancy between soil surveys completed at different times. The borders between soil survey areas that were completed at different times are distinct. In general, saturated hydraulic conductivity appears lower in the southernmost part of Sonoma county (Figure 14).

The largest apparent discrepancy between the SSURGO data sets and the PSD observations lies in the soil electrical conductivity (EC) mapping. The EC maps indicate that most of the basin has nearly zero EC and there are discontinuities in the mapping that do not appear related to the survey boundaries. High EC soils bias soil moisture measurements made using water content reflectometers. PSD has found that at least four of the seven soil moisture observing stations are located in soils where the EC is greater than 1.0 dS m^{-1} by direct measurement. These stations include Healdsburg, Willits, Potter Valley, and Rio Nido.

All soil moisture data collected by HMT is available at the web site (Figure 15). Comparisons of soil moisture observations with that generated by the RDHM are made in the following sections of this report.

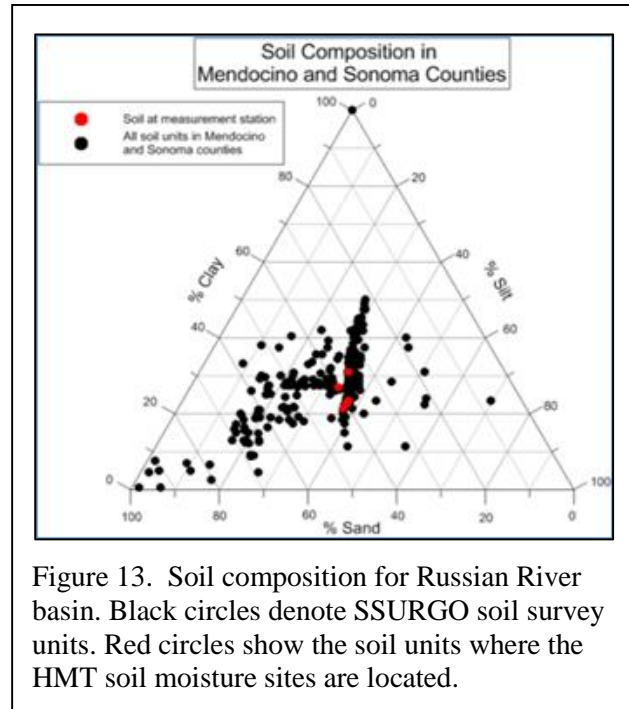


Figure 13. Soil composition for Russian River basin. Black circles denote SSURGO soil survey units. Red circles show the soil units where the HMT soil moisture sites are located.

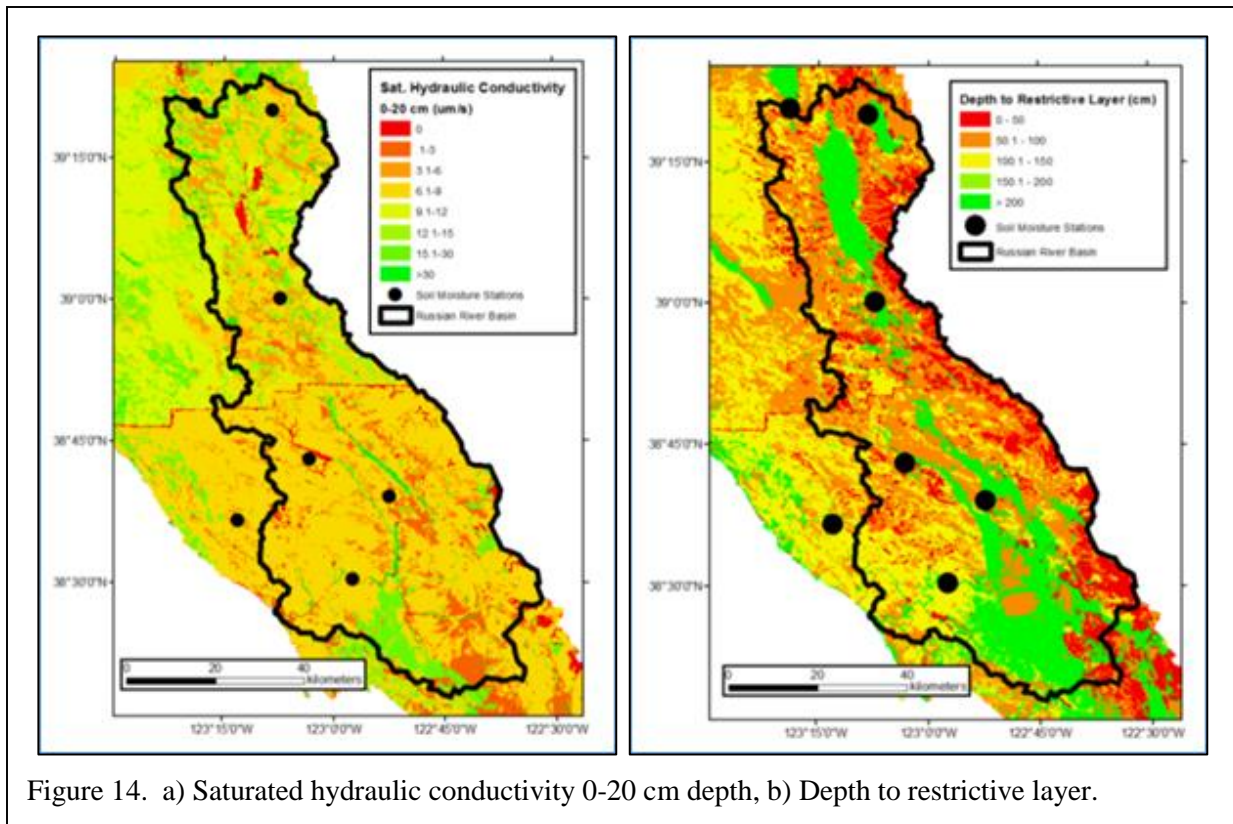


Figure 14. a) Saturated hydraulic conductivity 0-20 cm depth, b) Depth to restrictive layer.

2.10 Groundwater

Ground water includes all subsurface water below the water table but does not include moisture held in soils. Ground water is discharged from the watershed directly by springs and seepage into streams. Base flow in streams is sustained by ground-water discharge. Ground water is used by riparian vegetation that has roots extending below the water table. Plants growing outside the riparian zones can have roots that extend deep enough to extract ground water (Lewis and Burgy, 1964). Ground water can be evaporated directly to the atmosphere in locations where the water table is at, or very near, land surface. Ground water is also pumped from wells to provide supplies for irrigation, municipal, industrial, and domestic uses.

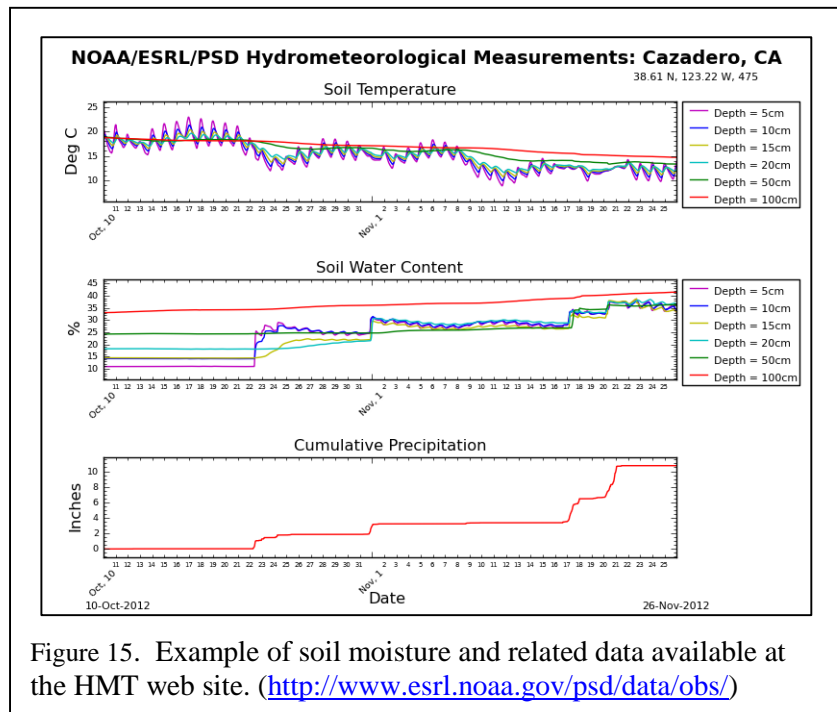


Figure 15. Example of soil moisture and related data available at the HMT web site. (<http://www.esrl.noaa.gov/psd/data/obs/>)

2.11 Water Budget

A basin-wide water budget was attempted by the SCWA (2012). Mean annual precipitation, for the 1931-1963 water-years, above the USGS Russian River near Guerneville, CA stream gauge is about 45 inches. The mean annual natural runoff, adjusted for the transfer from the Eel River, for the 1931-1963 water-years, at the Guerneville stream gauge is 19.1 inches (1,367,000 acre-feet) which is 42% of the mean annual precipitation. Subtracting the mean annual natural runoff from the mean annual precipitation gives a mean annual amount of water lost to evapotranspiration and percolation to deep groundwater above the Guerneville gauge of about 25.9 inches or 58% of mean annual rainfall for the 1931-1963 water-years (Rantz and Thompson, 1967).

A study by Metzger et al (2006) on the Alexander Valley (6800 ac) estimated an annual water budget; of 44 in/yr precipitation, 23.6 in/yr (54%) drains as streamflow, 18.7 in/yr (42%) evapotranspires, and 1.7 in/yr (4%) recharges the groundwater table (Figure 16). There is considerable uncertainty associated with this estimate because it was computed as residual from other, much larger water-budget components that have considerable uncertainties. The mean annual precipitation for water years 1952 through 2004 is estimated to be about 298,000 acre-ft/yr (44 in) based on

PRISM (Daly and others, 1994; Oregon State University Spatial Climate Analysis Service, accessed January 13, 2006). Part of this amount is absorbed by the soil and deep percolation; the amount absorbed varies from season to season and inter-annually depending on climatic variables and antecedent conditions in the watershed. The mean annual amount of precipitation absorbed by soils is the soil-moisture deficit replenishment, which is estimated to be about 75,000 acre-ft/yr (equivalent to 11 in. over the study area). This estimate was based on the quantity of precipitation received before stream discharge increased significantly. The soil-moisture deficit is caused by evapotranspiration during the dry months (generally May–September).

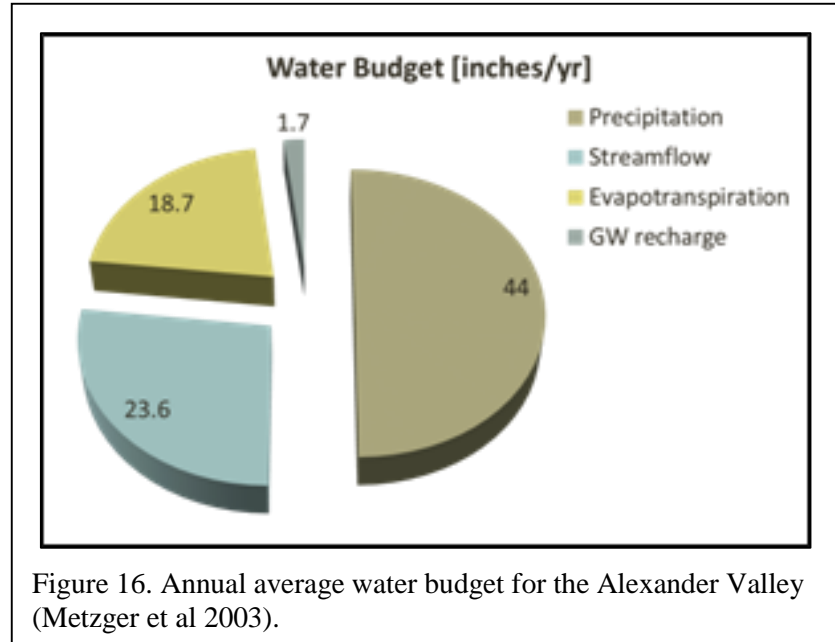


Figure 16. Annual average water budget for the Alexander Valley (Metzger et al 2003).

3. RUSSIAN-NAPA RIVERS DISTRIBUTED HYDROLOGIC MODEL

3.1 Description of Model

Overview

The Research Distributed Hydrologic Model (RDHM) is the DHM used for this study. RDHM is a conceptual hydrologic prediction model which can be used to account for runoff, streamflow, soil moisture, snowmelt, evapotranspiration, and various hydrologic states during storm events and inter-storm periods (Figure 17). RDHM was developed by NOAA National Weather Service (NWS) / Office of Hydrologic Development (OHD) (Koren et al., 2004; Smith et al., 2004) to provide an efficient interface for remote sensing-based products and atmospheric model outputs and to support operations at

NWS River Forecast Centers (RFCs). RDHM routes both surface and subsurface water flow. The required input forcings are precipitation and temperature. This simplified input greatly reduces the burden of forecasters as they attempt to promptly respond to various weather situations. The strength of the RDHM is its ability to represent forcings with high variability, such as high-resolution NEXRAD (e.g., MRMS) radar precipitation data. It represents the general functionality of the class of distributed hydrologic models (DHMs) operating on a gridded data structure.

The HRAP grid system is the spatial structure used by RDHM to fit the gridded parameters and forcing in terms of the spatial resolution and location. This HRAP-based model structure enables RDHM to support any grid cell resolution (e.g. 1 HRAP, ½ HRAP, ¼ HRAP, and so on). Within each cell, there are water balance components and kinematic overland and channel routing components, which together constitute the nucleus of the RDHM simulation mechanism. RDHM contains various modeling modules: Snow-17, Sacramento Soil Moisture Accounting (SAC-SMA), Continuous API (CONT-API), Frozen Ground (FRZ), Sacramento Soil Moisture Accounting Heat Transfer and Evapotranspiration (SACHTET) and Overland and Channel Routing (rutpix 7 and rutpix9). Different compositions of modeling techniques can be arranged to simulate snowmelt, streamflow and soil moisture based on local climate characteristics. The relationships between these modeling techniques are illustrated in Figure 18. For example, if the simulated watershed is an area that is snowing, the model will trigger Snow17 to simulate snowmelt. The rainfall forcing and engendered snowmelt will then be inserted into either SAC-SMA or CONT-API techniques to obtain surface runoff, base flow, and various other hydrologic states. If soil moisture is a desired output, one can then either run FRZ or SAC-HTET to get the result at various depths. In this process, surface runoff and base flow are treated differently. Surface runoff is entered into the hill-slope routing mechanism first, followed by channel routing, whereas the base flow fluctuation is brought into the channel routing mechanism directly by the model. To further explain how rainfall is dealt with over terrain, traverse soil, and through channels, we concentrate on dissecting the SAC-SMA model

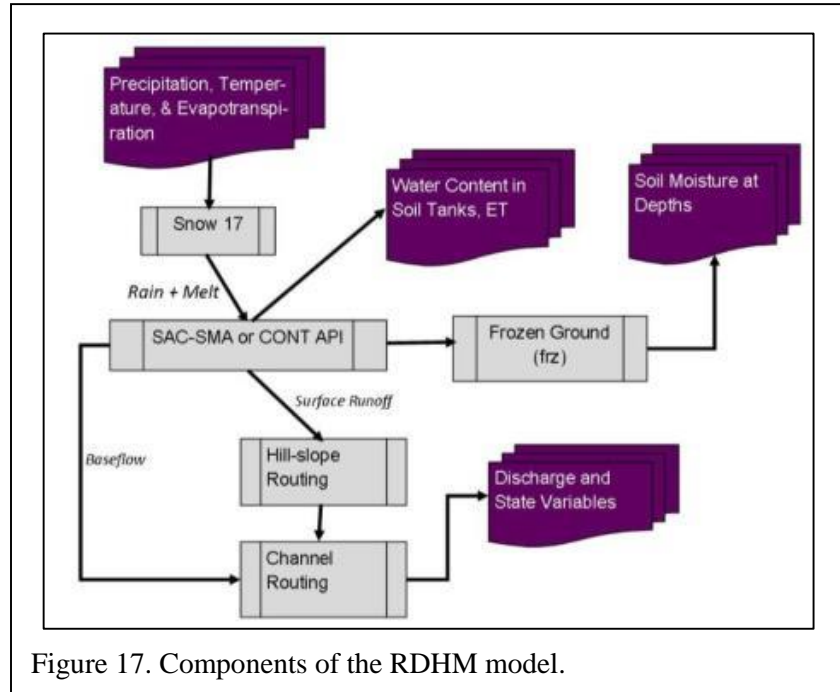


Figure 17. Components of the RDHM model.

and the routing technique via the illustration of a schematic diagram and the representation of the numerical equations.

Sacramento Soil Moisture Accounting

SAC-SMA conducts the water balance computation by taking rainfall and monthly potential evaporation demand as forcings to address water transference between the surface, upper and lower zones, and channels. To support this water balance mechanism, SAC-SMA uses 17 parameters and six state variables representing the water contents and flux dynamics between the surfaces, upper, and lower zones at each time step. These parameters include 6 soil water capacity (tank) parameters, 3 recession parameters, 4 percolation related parameters, and 4 non-modified (a priori grid data not available) parameters. Table 5 lists these parameters and states. The functions of these parameters in allocating between various storages and channels are displayed in Figure 19.

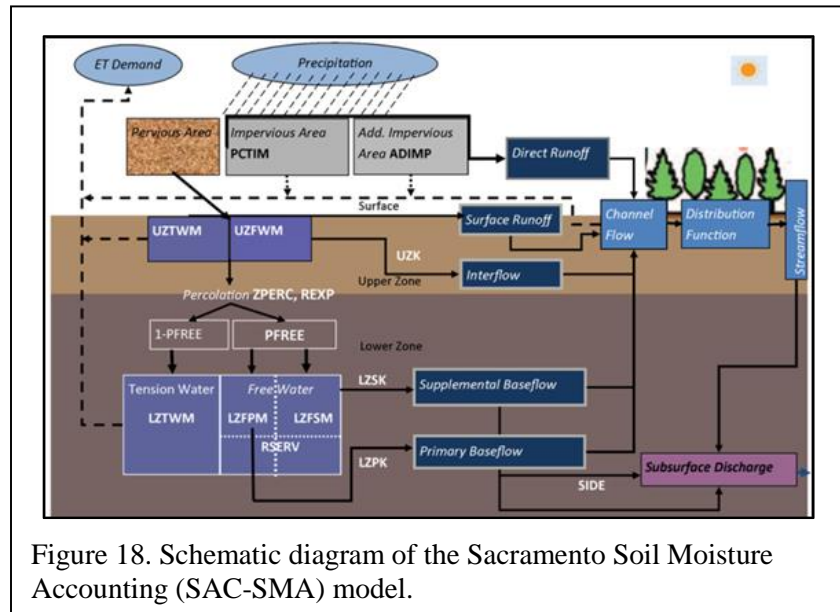


Figure 18. Schematic diagram of the Sacramento Soil Moisture Accounting (SAC-SMA) model.

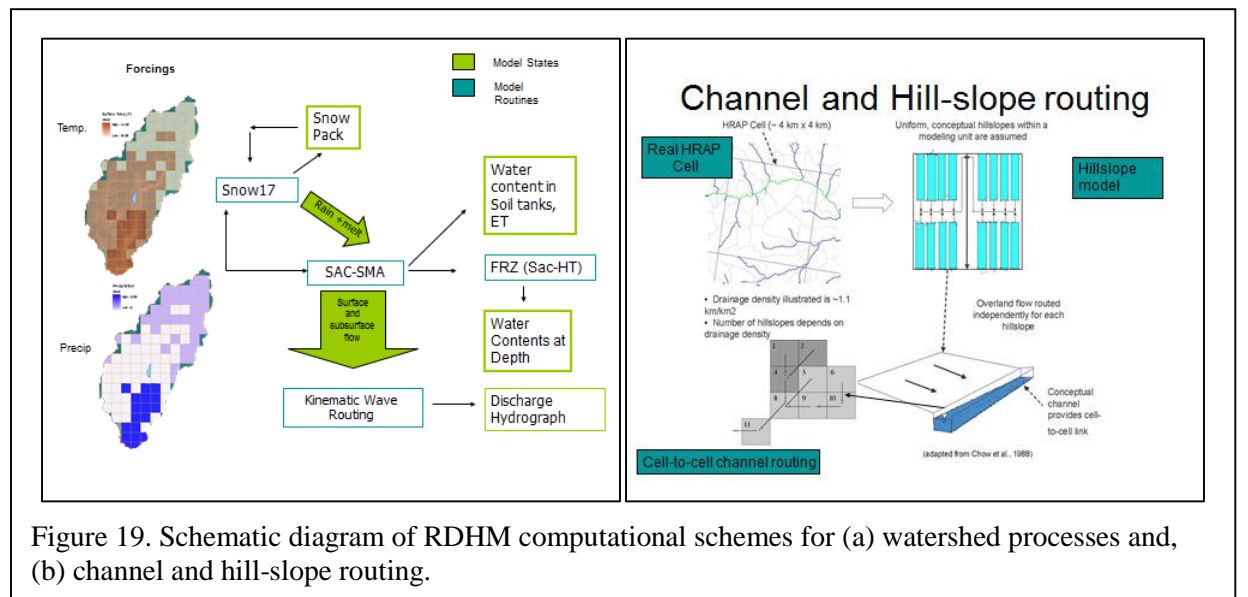


Figure 19. Schematic diagram of RDHM computational schemes for (a) watershed processes and, (b) channel and hill-slope routing.

Table 5. SAC-SMA model parameters and states with their realistic ranges or default values.

No.	Parameter /State	Description	Units	Parameter or State	Ranges or Default
Capacity					
1	UZTWM	Upper zone tension water capacity	mm	P	10 - 300
2	UZFWM	Upper zone free water capacity	mm	P	5 - 150
3	LZTWM	Lower zone tension water capacity	mm	P	10 - 500
4	LZFPF	Lower zone primary free water capacity	mm	P	10 - 1000
5	LZFSM	Lower zone supplemental free water capacity	mm	P	5 - 400
6	ADIMP	Max. fraction of an additional impervious area due to saturation	-	P	0.0 - 0.40
Recession Parameters					
7	UZK	Upper zone free water storage interflow depletion rate	1/day	P	0.1 - 0.75
8	LZPK	Lower zone primary free water storage depletion rate	1/day	P	0.001 - 0.05
9	LZSK	Lower zone supplemental free water storage depletion rate	1/day	P	0.01 - 0.35
Percolation and the Related					
10	ZPERC	Ratio of maximum and minimum percolation rates	-	P	5 - 350
11	REXP	Exponent of the percolation equation (Shape Parameter)	-	P	0.0 - 5.0
12	PCTIM	Permanent impervious area fraction of the watershed	-	P	0.001
13	PFREE	Fraction that goes directly to lower zone free water storage	-	P	0.0 - 0.8
Not Optimized					
14	RIVA	Riparian vegetation area fraction	-	P	0.001
15	SIDE	Ratio of deep percolation from lower zone free water storage	-	P	0
16	RSERV	Fraction of lower zone free water not transferable to tension water	-	P	0.3
17	EFC	Effective forest fraction	-	P	
States					
1	ADIMC	Tension water contents of the ADIMP area	mm	S	
2	UZTWC	Upper zone tension water contents	mm	S	
3	UZFWC	Upper zone free water contents	mm	S	
4	LZTWC	Lower zone tension water contents	mm	S	
5	LZFSM	Lower zone free supplemental water contents	mm	S	
6	LZFPF	Lower zone free primary water contents	mm	S	

Overland and Channel Routing

When an overflow of precipitation occurs, water at each grid will be routed kinematically downstream based on the connectivity network. The routing techniques in RDHM use two distinct routing regimes to model fast and slow runoff: hill-slope and channel routing. Three hill-slope routing parameters are used to characterize kinematic overland flow: hill-slope slope, hill-slope roughness (ROUGH), and drainage density (DS). Initially, based on the 30-m DEM data, the hill-slope slope (the SLOPH parameter) is calculated for each 30-m DEM cell using the ArcGIS slope function. The slope of the 30-m resolution is then aggregated to the HRAP resolution (~4 km) and transformed to XMRF format.

For the ROUGH parameter, on the other hand, a constant value of 0.15 is assigned for all grids based on two considerations: 1) a precise ROUGH value is very difficult to determine for a given land use category, and 2) hill-slope parameters are not as sensitive as channel parameters in a watershed study. Similarly, DS is assigned a spatially constant value of 2.5. In this study, we assumed these spatially constant values for both parameters and found that the simulation results were satisfactory. The equation for applying these hill-slope routing parameters is:

$$q_h = 2k_q D \frac{\sqrt{S_h}}{n_h} h^{5/3}, \quad (1)$$

where q_h is the discharge per unit area; k_q is a unit transformation coefficient equal to 10^5 ; D is stream channel density (km^{-1}); S_h is hill-slope slope; n_h is hill-slope roughness; and h is the average hill-slope water depth.

Channel Routing Parameters

For channel routing, RDHM has two options for computing the flow and the cross-sectional area of flow: the channel shape method and the rating curve method. Both of these two methods originate from the same basic equations, representing conservation of mass and the conservation of momentum. Based on the mass conservation principle and supposing an open channel where lateral inflow can be ignored, the continuity equation for gradually varied, unsteady flow is,

$$\frac{\partial A}{\partial t} + \frac{\partial Q}{\partial x} = 0, \quad (2)$$

where A is the cross-sectional area of flow; Q the discharge; and t and x denote the time and the distance along the channel, respectively.

The St. Venant equation is designed to accommodate the principles of the conservation of momentum and to individually characterize local acceleration, convective acceleration, hydrostatic pressure, and friction as well as gravity forces, as configured with the terms as below.

$$\frac{1}{g} \frac{\partial v}{\partial t} + \frac{V}{g} \frac{\partial V}{\partial x} + \frac{\partial h}{\partial x} + (S_f - S_0) = 0, \quad (3)$$

where v is velocity; V is the flow volume; h is the depth of flow, and S_f and S_0 are the friction and bed slope, respectively.

Based on Eq. (3), kinematic wave theory is used to induce a relationship between the discharge and the depth of flow. This relationship is a simple parabolic channel shape defined by

$$B = \alpha H^\beta, \quad (4)$$

where α is the top width parameter; β is the shape parameter; H is flow depth, and B is the channel top width.

The channel shape method requires four parameters as inputs: slope (S_c), roughness coefficient (n_c), shape parameter (β), and top width parameter (α). From equation (4), parameters α and β can be defined based on an assumed relationship between B and H . In this research, instead of the channel shape method, we employ the rating curve (rutpix9) channel routing method for the RDHM simulation. The two required parameters for the rating curve method operation, channel discharge per unit channel cross-section area, q_0 , and the power value, q_m , can be converted from the four parameters of the channel shape method using the following equations.

$$q_0 = \alpha^{-\frac{2}{3(\beta+1)}} (\beta+1)^{-\frac{2\beta}{3(\beta+1)}} \frac{\sqrt{S_c}}{n_c}, \quad (5)$$

$$q_m = \frac{\beta + \frac{5}{3}}{\beta + 1}, \quad (6)$$

Using Eq. (5) and (6), the OHD is able to provide a priori parameters for q_0 and q_m . The parameters q_0 and q_m are used to calculate the channel discharge using the equation

$$Q_c = q_0 A^{q_m}, \quad (7)$$

where Q_c is discharge in [$L^3 T^{-1}$].

3.2 Base Data

Digital Terrain Model

A digital elevation model (DEM) is often represented with a raster data structure, as opposed to a contour or triangulated irregular network (TIN) data structure (Moore et al., 1991), in the GIS processes to numerically represent terrain elevation variations within a uniform grid framework. The gridded DEM is used in hydrologic analyses to derive watershed boundaries, flow direction, stream networks, and flow length. This format of the terrain representation makes the geomorphology factors easy to manipulate, aligns with gridded data on precipitation and soils. The USGS develops and distributes DEMs at various resolutions, ranging from 10-m resolution at the hillslope scales to the 30 arc-second resolution for characterizing terrain at the continental scales.

As an example, two different resolution DEM's are snapped respectively to the 1 HRAP (4.12 km at 38.0 N) and 1/16 HRAP (~1.03 km) resolution grids (Figure 19). In the RDHM, DEM's are used to create the connectivity files necessary to move water between the HRAP pixels. To create the connectivity file, the flow direction layer, whose values at each pixel indicate the water flow directions, need to be generated first. The D8 algorithm (O'Callaghan and Mark, 1984 & Jenson and Domingue, 1988) is often employed for this purpose. In the D8 algorithm, water at each grid cell is assumed to flow a direction with the steepest descent to one of the neighboring pixels. While this D8 steepest decent algorithm has been successfully used to locate stream networks at high resolution (less than 90 m), it has been found by the

researchers not accurate when applied to DEMs with ~ 1 km or coarser resolutions (e.g. O'Donnell et al., 1999). Unfortunately, coarse resolutions of 1 to 4 km are of interest for RDHM implementation. To resolve this problem, the COTAT (Cell Outlet Tracing

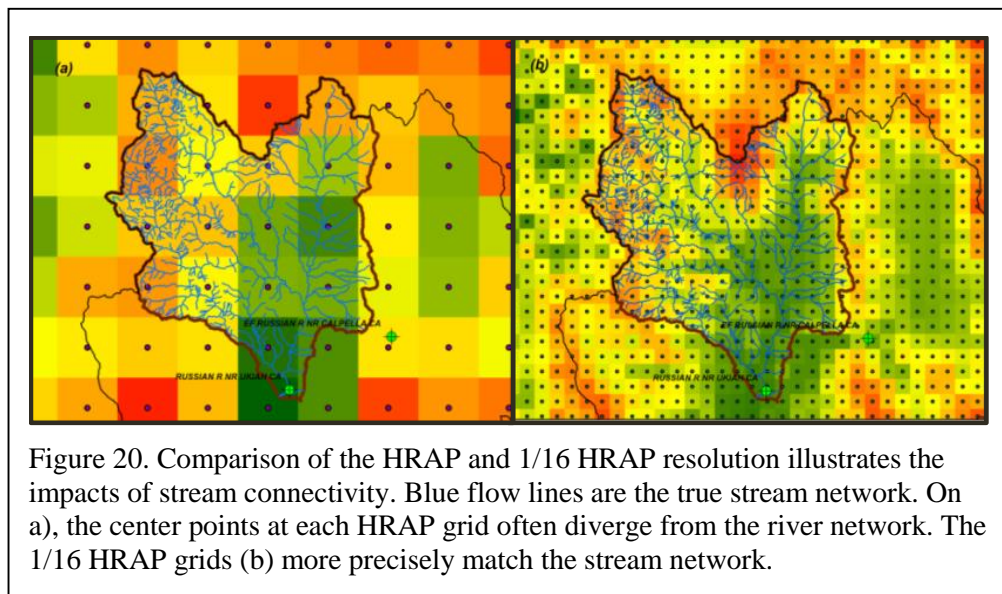


Figure 20. Comparison of the HRAP and 1/16 HRAP resolution illustrates the impacts of stream connectivity. Blue flow lines are the true stream network. On a), the center points at each HRAP grid often diverge from the river network. The 1/16 HRAP grids (b) more precisely match the stream network.

with an Area Threshold) algorithm is applied (Reed 2003) to generate flow direction layers for the grid cells at coarse resolutions. COTAT traces downstream along the higher-resolution flow network from each outlet pixel, thus accurate flow directions can be assigned to the coarse-resolution cells. Currently, the algorithm can utilize the NHDPlus version 2 data (30 m resolution) directly and output flow direction layers at coarse resolutions (HRAP, ¼ HRAP, or 1/16 HRAP) in the HRAP coordinate system. In Figure 20, notice that the DEM at a 1/16 HRAP (~1 km) resolution shows higher maximum elevation and larger spatial variability.

HRAP and 1/16 HRAP models

RDHM can be executed at any HRAP grid resolution, such as 1-HRAP, 4-HRAP ¼-HRAP, etc. NEXRAD radar-rainfall Stage II and Stage III estimates are defined on the HRAP grid which is defined in a projected plane relative to a spherical earth datum (Fulton 1998). This projection is a quasi-rectangular grid whose cell size is nominally 4 km on a side but ranges from about 3.5 km in southern contiguous U.S. latitudes to about 4.5 km in northern contiguous U.S. latitudes. In the Russian-Napa basins an HRAP grid size is 4.12 km on a side. The distributed hydrologic model is based on the HRAP grid and sub-partitions of this (i.e. 1 km grid is 1/16 of an HRAP, actually 1.03 km on a side. Table 6 presents the HRAP grid size at various latitudes (adapted from Reed and Maidment 1995).

Higher resolution grids have a greater correspondence between natural and model flow routing mechanism. With the DEMs as the background, Figure 20 displays that the 1/16 HRAP grids can form flow sequence that closely resemble natural channels. The degree of portrayal a model routing characterizing natural flow function sometimes dramatically influences streamflow simulation, especially for imitating flow at the stations near to the junction of a main stem and tributaries. For example, because HRAP [30, 474] contains water flow from East Fork Russian River sub-watershed, the streamflow simulation for the USGS Ukiah station needs to be executed at the HRAP [30, 475] grid instead of HRAP [30, 474] (Figure 20). For the 1-HRAP resolution simulation, picking an upstream grid instead for modeling is an approach to eliminate possible flow networking errors accompanied with the coarse resolution imitation.

Table 6. HRAP Cell Size on the Earth's Surface

Latitude	Location	Side Length [km]	Area [sq. km.]
25	Miami, FL	3.63	13.18
30	Houston, TX	3.83	14.66
35	Memphis, TN	4.02	16.13
38	Santa Rosa, CA	4.12	17.00
40	Indianapolis, IN	4.19	17.58
45	Minneapolis, MN	4.36	18.98
50	Winnipeg, Manitoba	4.51	20.32

Land Use / Land Cover

The study site has a complex terrain with the land cover dominated by “Evergreen Forest”, “Scrub/Shrub”, and “Grass Land”. Among these dominant land covers are the clusters of the lands classified as “Cultivated Crops (Vineyard)” and “Developed”. Figure 2 (shown earlier) is the National Land Cover Dataset (NLCD 2006) showing the land cover distribution of in the Russian and Napa watersheds. Land cover can influence streamflow and soil moisture fluctuation through the functions of evapotranspiration and direct runoff.

Two factors determine the formation of direct runoff: impervious area (PCTIM) and additional impervious area (ADIMP). While PCTIM can be easily decided using the NLCD, the assessment of ADIMP is much difficult. In fact, setting the ADIMP parameter at a constant in the calibration process sometimes abuse the direct runoff mechanism. ADIMP is the synergy of climate, vegetation, and soil property; therefore, it should become a dynamic parameter. Deeper discussions will be convened in a later section of this report. In this section, we showed the calculation of the fraction of the impervious area within each sub-watershed. The calculation is based on the equation below.

$$F_{imp} = \frac{\sum_{i=0}^{100} f_i \times 30 \times 30 \times N_i}{A} \quad (8)$$

where F_{imp} is the fraction of the impervious areas within each sub-watershed; f_i denotes a fraction ($i\%$) of a 30-m * 30-m pixel as imperviousness; N_i represents the number of the pixels which have $i\%$ of the pixel area as imperviousness; and A is the drainage area of the sub-watershed.

As an example, the distribution of the imperviousness percentage in the Upper and Lower Santa Rosa Creek watershed is shown in Figure 21. By applying Equation (8), the impervious area fraction of the Upper and Lower Santa Rosa Creek watershed can be derived. The percentage of impervious surface for some subwatersheds (HUC-10 level) are tabulated in Table 7. Most of the HUC-10 subwatersheds in the Russian and Napa watersheds have small fractions of impervious surface except for the Upper and Lower Santa Rosa Creek where the city of Santa Rosa is located.

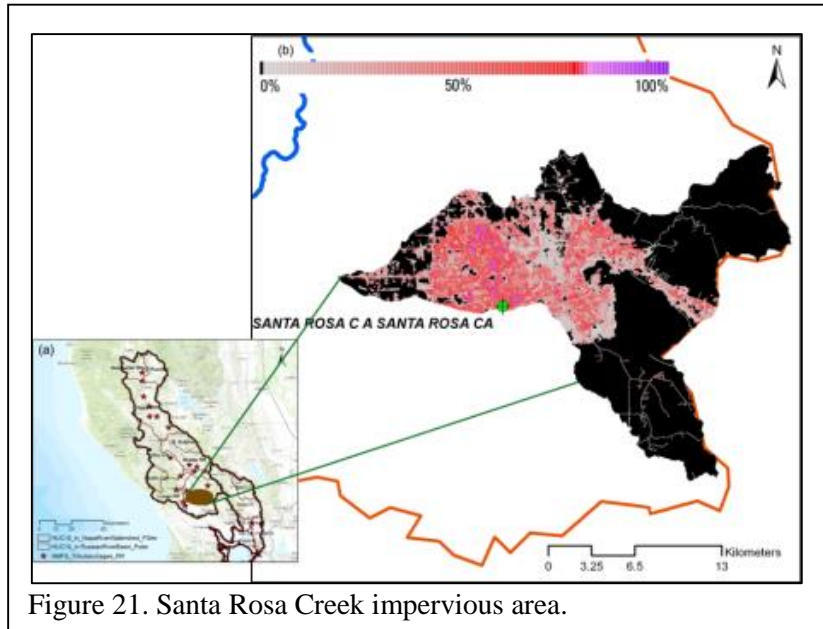


Figure 21. Santa Rosa Creek impervious area.

Compared to the imperviousness fraction calculated in this section, the a-priori PCTIM value at 1 HRAP resolution provided by OHD is quite accurate, so no further adjustment is necessary for PCTIM in the model calibration process.

Table 7. Percentage impervious area for watersheds

Watershed (Streamflow Station)	Austin Creek (Cazadero)	E.Fk. Russian River (Calpella)	W. Fk. Russian River (Ukiah)	Napa River (Napa)	Santa Rosa Cr. (Santa Rosa)	Napa River (St. Helena)	Big Sulphur Creek (nr Cloverdale)
Impervious Area (%)	0	0.26	1.1	2.8	12.9	1.9	0.26

SAC-SMA A Priori Parameters

The NWS Office of Hydrologic Development has developed a procedure to derive the SAC-SMA model parameters based on soil texture data (Koren et al 2000). To quantify relationships of model parameters with soil properties, the assumption was made that the SAC-SMA tension water storages relate to an available soil water, and that free water storages relate to gravitational soil water. Porosity, field capacity, and wilting point derived from STATSGO dominant soil texture for eleven standard layers were used in estimating available and gravitational water storages. SCS runoff curve numbers and saturated hydraulic conductivity of different soils were also used. Analytical relationships were derived

for 11 SAC-SMA model parameters. Preliminary tests on a few basins in different regions suggest that most parameters derived from soil properties agreed reasonably well with calibrated parameters for those basins. Accuracy statistics of hydrographs simulated using calibrated and derived parameters were also close. It means that parameters derived from soils data are very reasonable, and can be improved by using calibration if observed historical data are available.

After testing in the model calibration process, we confirmed that the a priori parameters created by OHD acquire the spatial variability of basin physical properties and improve hydrologic simulation performance. These parameter estimates were obtained based on a finer-scale soil database, the Soil Survey Geographic Database (SSURGO), combined with high-resolution land use/land cover data.

Figures 22 to 24 illustrate the a priori parameters for the Napa and the Russian River watersheds created by OHD. Anderson et al. (2006) described the relationships between the soil texture of the soil database and the SAC-SMA parameters. To calculate these parameters using SSURGO or STATSGO, model component storages expressed in water depth need to be converted to actual depths within the soil profile. This is achieved by deciding the split between the upper and lower soil zones (Z_{up}). By applying the theory of an initial rain abstraction from the curve number method developed by Natural Resources Conservation Service (NRCS), Z_{up} can be determined.

$$Z_{up} = 5.08 \times \frac{1000 / CN - 10}{\theta_s - \theta_{fld}}, \quad (9)$$

where CN is the curve number; θ_s and θ_{fld} represents saturated moisture content and field capacity, respectively.

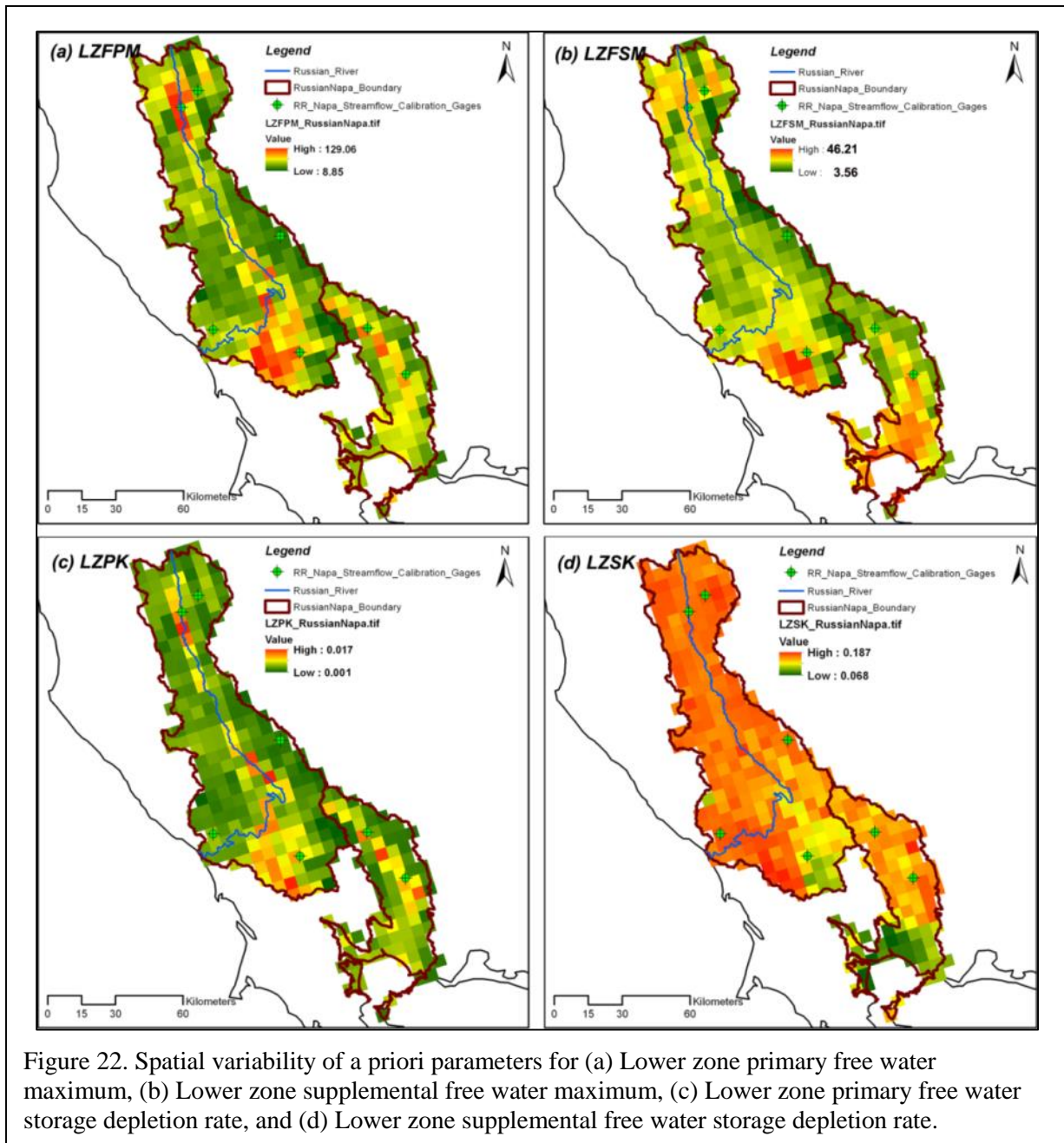
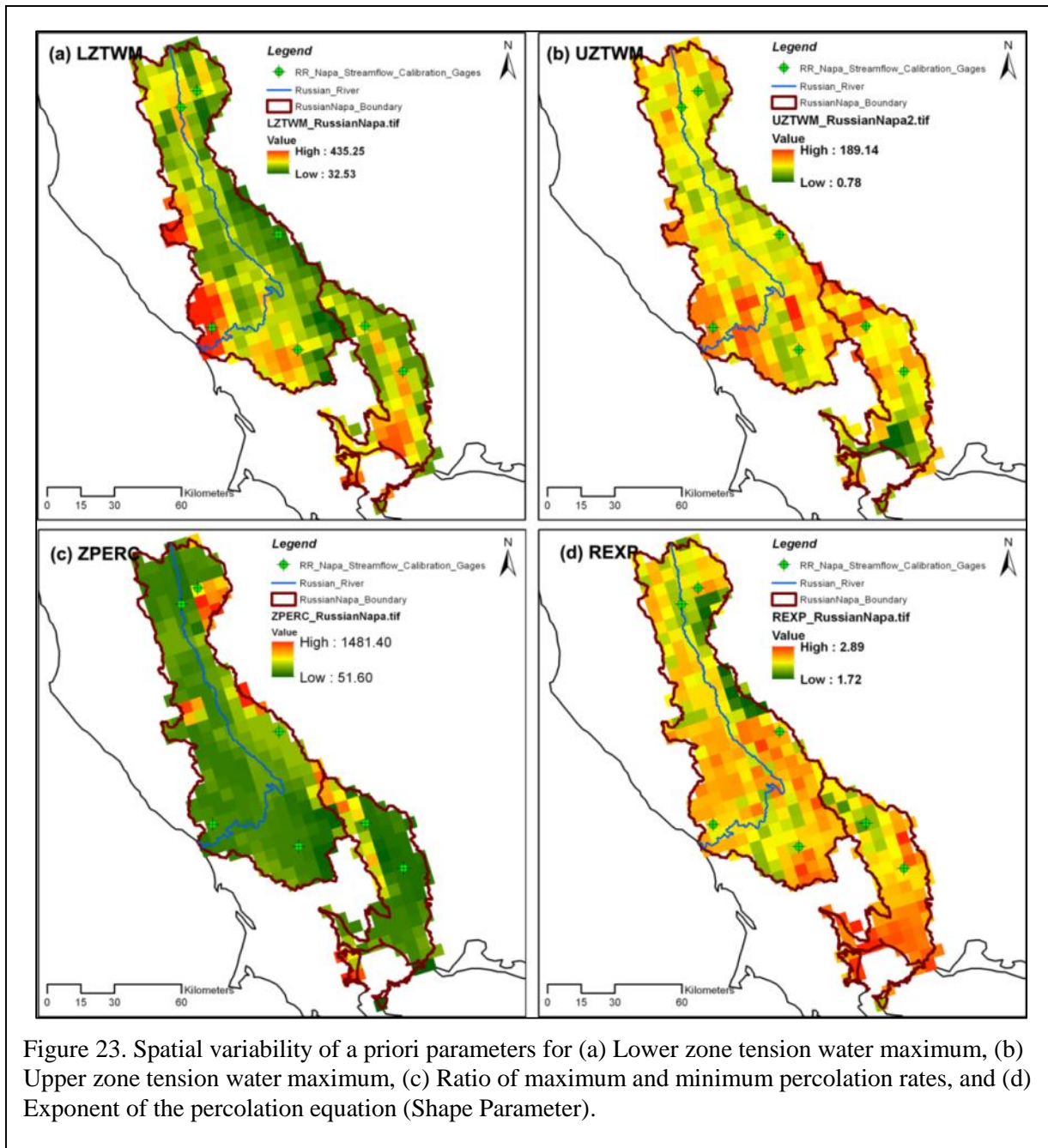
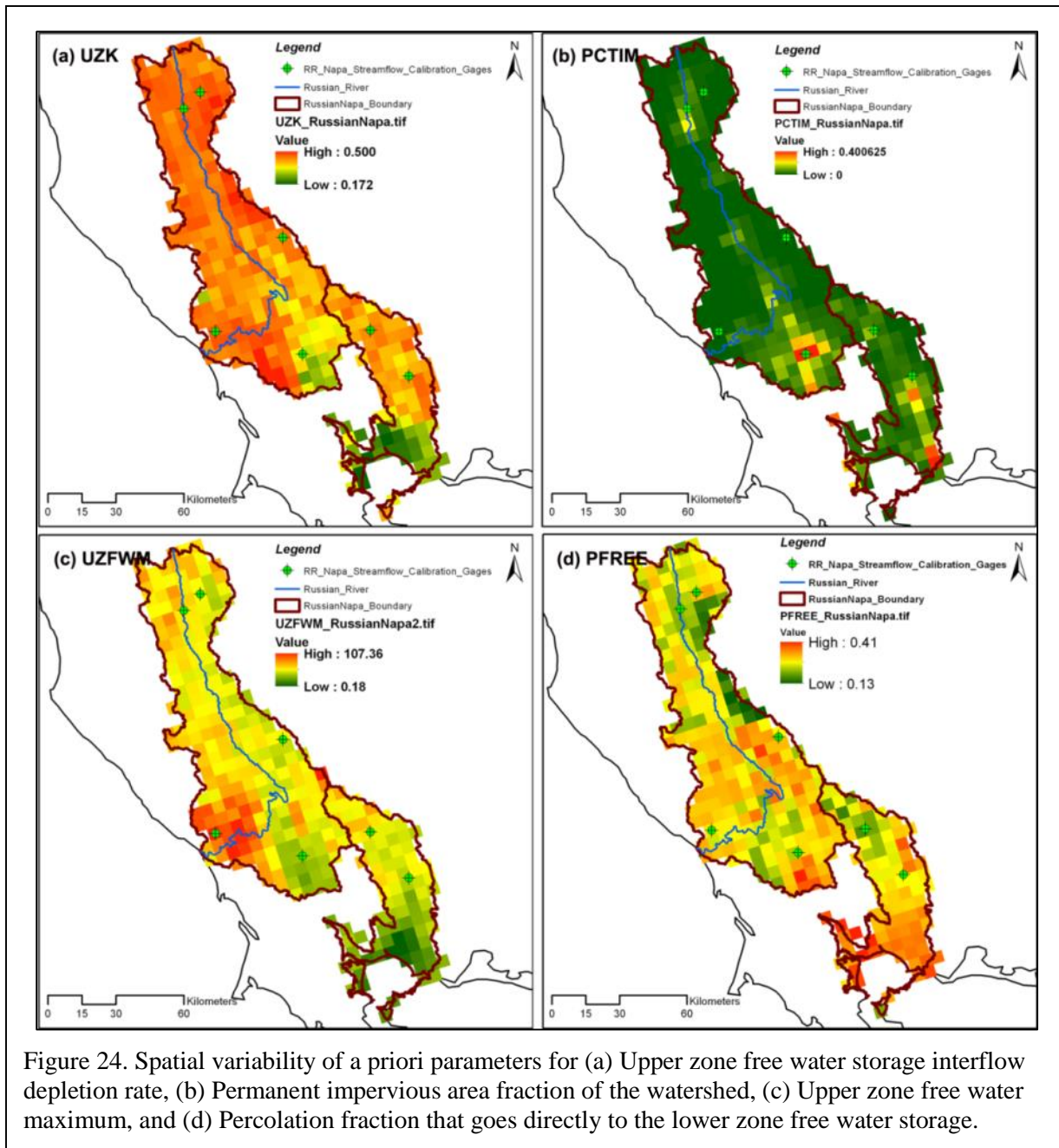


Figure 22. Spatial variability of a priori parameters for (a) Lower zone primary free water maximum, (b) Lower zone supplemental free water maximum, (c) Lower zone primary free water storage depletion rate, and (d) Lower zone supplemental free water storage depletion rate.





3.3 Precipitation

CNRFC Quantitative Precipitation Estimation (QPE)

The California Nevada RFC (CNRFC) 6-hourly QPE product is an exclusively gauge-based precipitation product based on a technique known as “Mountain Mapper” (Schaake et al. 2004). The archived CNRFC QPE data starts from January 2004, but temperature data is only available after November 2010. To make the data period for the precipitation and temperature forcing consistent, we initiated the operation of the RDHM with a warm-up period arranged from Nov. 2010 to Jan. 2011.

Two aspects compose the application of the Mountain Mapper technique (Schaake et al 2004) in the NWS river forecast system: 1) comparison of the precipitation climatology at gauged and ungauged locations and 2) application of the inverse distance weighting (IDW) method to interpolate the fraction of the monthly normal calculated at the gauges to the ungauged pixels. First, if the pixels to be estimated and the precipitation gauges are located in the same climatologic zones, an IDW will be directly used for interpolation. The function of IDW in interpolating precipitation observed at multiple gauges for an intended location can be expressed as:

$$Y = \frac{\sum_{i=1}^n W_i R_i}{\sum_{i=1}^n W_i}, \quad (10)$$

where Y is the interpolated precipitation at an ungauged location; R_i is the precipitation amount observed at gauge i with $i = 1 \dots n$; and

$$W_i = \frac{1}{d_i^2}, \quad (11)$$

where d_i denotes the distance from gage i to the pixel to be estimated. Second, if the variable precipitation climatology occurs due to orographic phenomenon or large (synoptic) scale atmospheric conditions, the Mountain Mapper procedure will be implemented. The Mountain Mapper procedure is somewhat different from the algorithm expressed with Eq. (8) and (9). The equations will become:

$$F_Y = \frac{\sum_{i=1}^n W_i F_{R_i}}{\sum_{i=1}^n W_i}, \quad (12)$$

where F_Y represents the interpolated precipitation as a fraction of normal and F_{R_i} can be expressed as

$$F_{R_i} = \frac{R_i}{\bar{R}}, \quad (13)$$

where \bar{R} is the monthly normal (i.e. average of monthly precipitation from 1981 to 2010) and can be obtained from either the PRISM (Parameter-elevation Regressions on Independent Slopes Model) climate mapping system or analyses from gage observations. Thus, the interpolated number is a fraction of normal. This application of the fraction of normal concept ensures that the variable climatology can be better captured against the normal climatology. After fractions of normal are interpolated, Mountain Mapper can then generate estimated precipitation for all the grids by simply multiplying the interpolated fraction to the precipitation monthly normal obtained from the PRISM.

$$Y = F_{R_i} \bar{Y}, \quad (14)$$

where \bar{Y} is the monthly normal from PRISM.

As an illustration, Figure 25 displays a CNRFC QPE product generated using the Mountain Mapper procedure. This QPE example is at the HRAP grids at the Geographic Coordinate System (GCS, i.e. Lat/Lon).

A validation study by the forecasters from OHD and CNRFC has shown that the interpolation involving the Mountain Mapper process using PRISM can effectually reduce the estimation bias for the locations where orographic influences are moderate or less. For the places where there is no orographic effect, involvement of PRISM climatology produces no difference compared to the standard IDW technique.

Although involvement of PRISM in Mountain Mapper can remove much of the bias in the estimates, many studies have pointed out the limitations of PRISM monthly climatology. This

limitation is especially apparent in storm events with fast moving wet air masses or with storm tracks that are different from climatology. The synoptic atmospheric conditions of these anomalous events will yield precipitation patterns with spatial variation which are not consistent with the PRISM climatology.

To evaluate the performance of the Mountain Mapper procedure in different sub-watersheds, HMT observations at the Willits and Cazadero stations were used to calculate the accuracy of the CNRFC QPE at both locations. Note that HMT data are not routinely used to generate the CNRFC QPE products and are therefore used for independent validation. The validation period is from 2011/02/01 (February 1, 2011) to 2012/03/30 (March 30, 2013). Inspection of Figure 26 shows that the CNRFC QPE at Cazadero has a bias approaching 30 percent (underestimate); the Willits site shows almost no bias. Willits also has a higher Nash-Sutcliffe efficiency (NSE), 0.91 compared to Cazadero (0.69), such that the CNRFC QPE at the Willits station was shown to be more accurately estimated than at the Cazadero station. There are two reasons that may have caused this difference. First, although both sites are in elevated terrain (Willits is at 585m and Cazadero is at 475m), the terrain is less variable in Willits compared to Cazadero. The PRISM climatology may be inadequate in capturing the precipitation distribution patterns of storms moving through the areas with higher topographic variation, such as the Cazadero site in the Austin Creek watershed. Unlike the Austin Creek watershed, the headwater watershed of the Russian River, where the Willits station is situated, has less variation in topography. Second, the CNRFC QPE is a gauge-only product and therefore heavily relies on the reliability of the gauge data at neighboring stations. For the QPE pixel corresponding to the HMT Cazadero station, it is very difficult to find reliable gauge data nearby, leading to a degraded quality of the precipitation estimation at that pixel. However, for the estimation at the pixel corresponding to the Willits station, a high quality gauge, Willits Howard (WILC1), is located close to the watershed and can furnish more accurate local precipitation estimation.

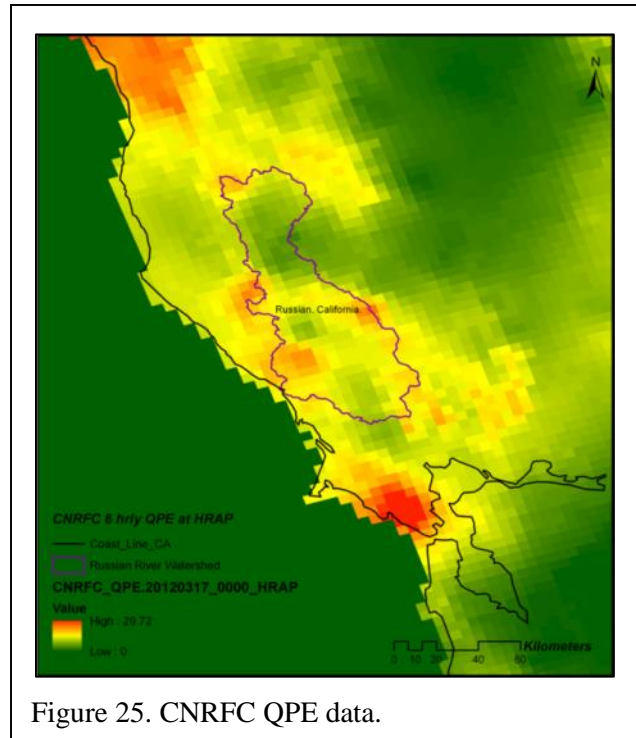


Figure 25. CNRFC QPE data.

Another validation of the CNRFC QPE data was made by Zamora et al (2015). CNRFC supplied the required input forcing grids of precipitation and temperature and an evaluation was conducted at several other locations in the Russian basin. The CNRFC 6-hr QPE grids are gage only products that are created using Mountain Mapper and PRISM (Daly et al. 1994).

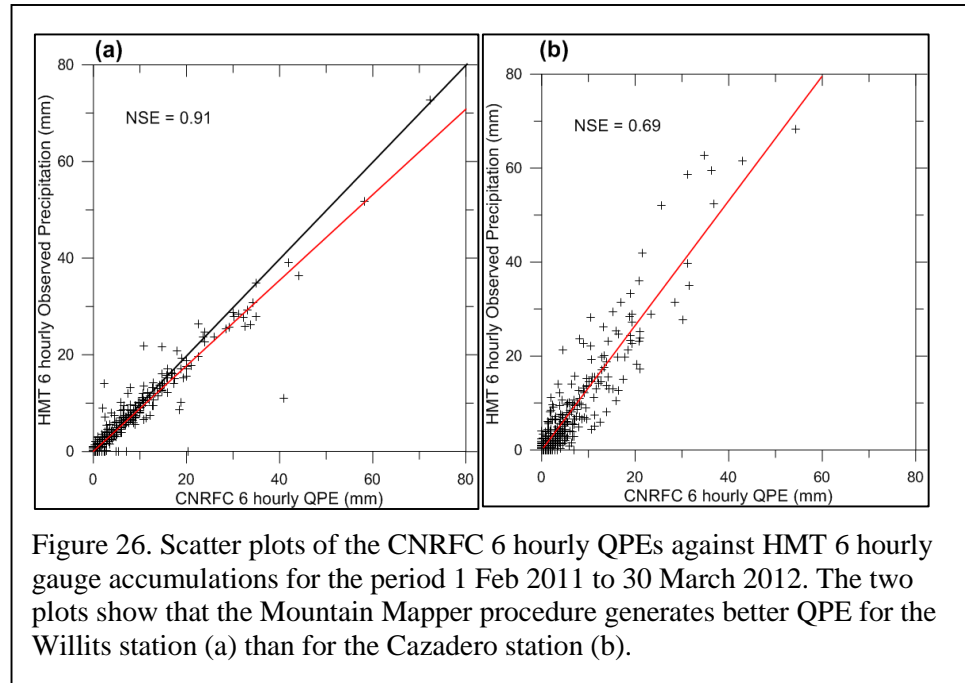


Figure 26. Scatter plots of the CNRFC 6 hourly QPEs against HMT 6 hourly gauge accumulations for the period 1 Feb 2011 to 30 March 2012. The two plots show that the Mountain Mapper procedure generates better QPE for the Willits station (a) than for the Cazadero station (b).

Example comparisons are shown in Figure 27 for Healdsburg (HBG) and Hopland (HLD), as well as the Willits and Cazadero sites previously discussed. Comparison of the best fit line for these sites with a 1:1 line shows that the

precipitation at HLD and HBG shows a significant negative bias (underestimate), ranging from 10% to 20%; similar to Cazadero (CZC) described above. These comparisons point to the difficulty in using a monthly climatology (PRISM) to adjust precipitation estimates from rain gauges. The Nash-Sutcliffe (NS) efficiency computed using the HMT observed precipitation at HLD and the RDHM grid point nearest HLD (0.86) suggest that the CNRFC QPE grids do a reasonable job of estimating the precipitation near HLD (Fig 27).

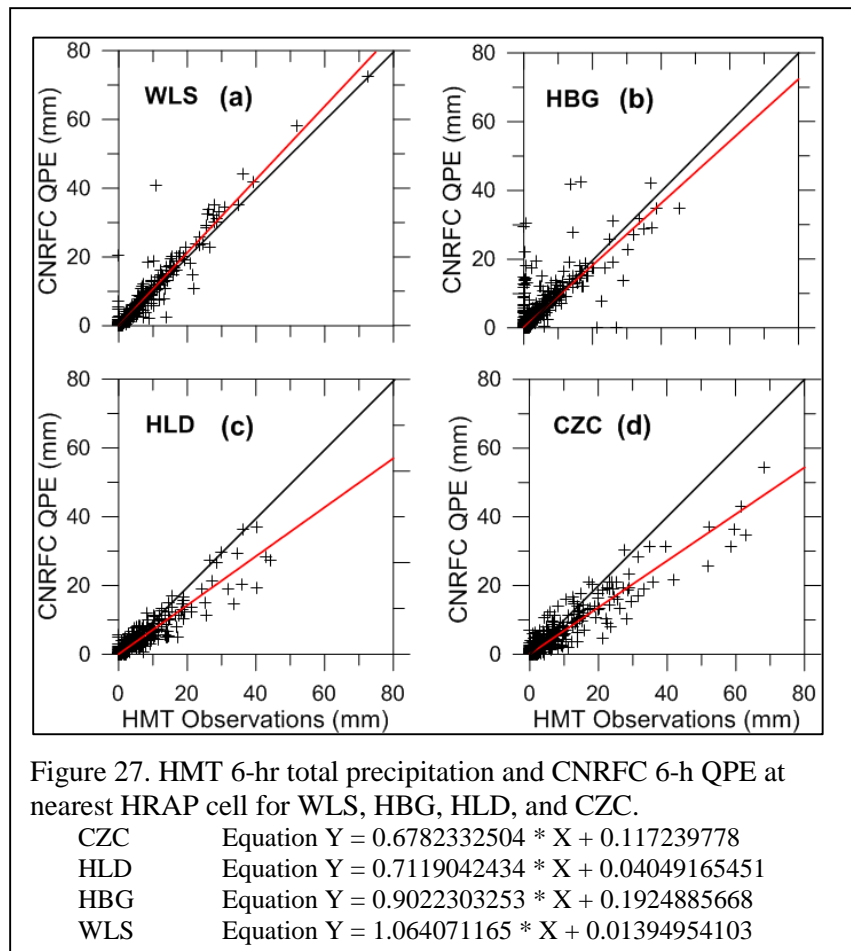
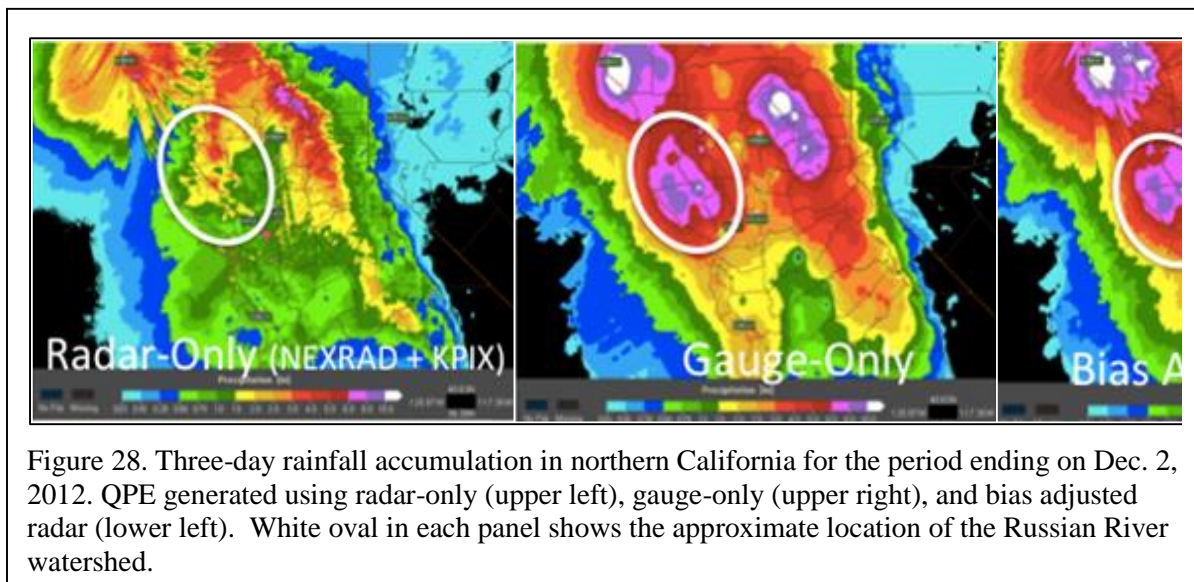


Figure 27. HMT 6-hr total precipitation and CNRFC 6-h QPE at nearest HRAP cell for WLS, HBG, HLD, and CZC.

MRMS – KPIX

Radar-based QPE products are increasingly being used to produce high spatial and temporal resolution precipitation mapping over relatively large areas. Multiple radar data, including gap-filling radars, are merged in an effort to obtain better rainfall estimates in regions having variable terrain. The Multi-Radar Multi-Sensor System (MRMS, Glaudemans et al 2008) and the Multi-Sensor Precipitation Estimator (MPE, Zhang et al 2011) systems are used by NOAA to derive high quality QPE data. Because both radar and gauge-based QPE have their limitations, MRMS and MPE generate QPE product suites using combinations of radar and gauge data (i.e., radar-only, gauge-only, radar and gauge combined). MPE and MRMS have their own methodologies for mosaicking radar data and combining gauge information so that one system may perform better than another for a given region and storm type event. As such, both systems are available for the NWS. It is important to note that there are often large differences in QPE depending on which sensors are used, especially for an area like the Russian River where orographic terrain, low rain gauge density, and relatively poor radar coverage make QPE challenging (see Figure 28). For this study, MRMS is primarily used to test the impact of higher resolution QPE (e.g., hourly QPE from MRMS) generated from multiple sources (e.g., gauge and radar) compared to the CNRFC QPE product (6 hourly gauge only).



The MRMS data processing system, as shown in Figure 29, is composed of three components: the meteorological model data extraction algorithm, the single-radar processing algorithm, and the multi-radar processing algorithm. The meteorological model data extraction algorithm, which extracts surface temperatures and model sounding files using RUC (Rapid Update Cycle) or RAP (Rapid Refresh), plays an ancillary role in the MRMS processing system. The insertion of surface temperatures and model sounding files into the single-radar processing algorithm executes quality control and calculates the hybrid scan of reflectivity. The single-radar processing algorithm first ingests single radar reflectivity data (NEXRAD), such as the respective radars of KDAX, KMUX, KBBX and KBHX used in this research, in polar coordinates and then transfers it to NetCDF format. Data from a commercial T.V. station radar, KPIX, is also used in this analysis. The KPIX radar provides much better coverage of the lower Russian River watershed compared to NEXRAD; however, the radar calibration is often suspect and caution must be exercised when using KPIX data.

After radar data ingest, a neural-net based quality control program is implemented in order to remove radar artifacts such as ground return, range-aliased radar return, and insect and bird clutter. So far, the neural network quality control function hasn't been trained for the KPIX C-band radar data, therefore any artifacts of the KPIX data will be kept in integration. Following the quality control process, a hybrid

scan of reflectivity is calculated for each radar input. “Hybrid scan” combines multiple scans of reflectivity at various tilt angles into one hybrid scan. The last step in the single-radar processing algorithm is the calculation of the vertical-profile-of-reflectivity (VPR) correction. The VPR correction is used to compensate for the fact that the radar observes precipitation in the cloud (as inferred from the radar reflectivity), often many thousands of feet above the ground level. The radar reflectivity, which is used to convert the observations into rain rate, can be significantly different at cloud vs ground level and it is often useful to extrapolate the radar reflectivity observed at cloud level to the ground via a VPR correction. Although VPR can improve radar QPE, research has shown that rain gauge data is still needed in most cases to remove bias from the radar-based estimates (Vignal et al. 2000; Bellon et al. 2005).

The multiple-radar processing algorithm (shown in purple in Figure 29) is plugged in after the VPR and hybrid scan are calculated. In addition to generating mosaics of the data from multiple radars, the main functions of this component is to generate a variety of radar and gauge QPE products, including rainfall products based on raw Z (reflectivity) without any correction, raw Z with gauge correction, gauge-only interpolation with raw Z quality controlled, gauge-only interpolation with VPR-corrected Z quality controlled, VPR-corrected Z with gauge correction, and VPR-corrected Z. In this step, the data is also transformed to Cartesian coordinates. A radar QPE layer with VPR and gauge correction generated from the MRMS system at 0.01 degree (~1.1 km) resolution is displayed in Figure 30. The displayed layer was registered to the geographic coordinate system (Lat/Lon) with a spatial resolution 0.01 degree (~1.1 km). The data is a gauge corrected QPE based on VPR-corrected reflectivity from all of the radars (KDAX, KMUX, KBBX and KBHX).

Willie et al. (2015) conducted an evaluation of MRMS QPE products using HMT and several other gauges as independent validation. Not surprisingly, the results of that study showed that, for the limited number of heavy rainfall events in the Russian basin that were examined, the gauge-adjusted radar QPE product outperformed the radar-only and gauge-only QPEs for hourly rainfall, based on normalized standard error and bias metrics. Moreover, the study found that, although KPIX improved the overall quality of the radar-only QPE, this radar had minimal impact on the gauge adjusted radar QPE performance. In other words, once a gauge bias adjustment was applied, it made little difference whether KPIX data was used or whether only NEXRAD data was used.

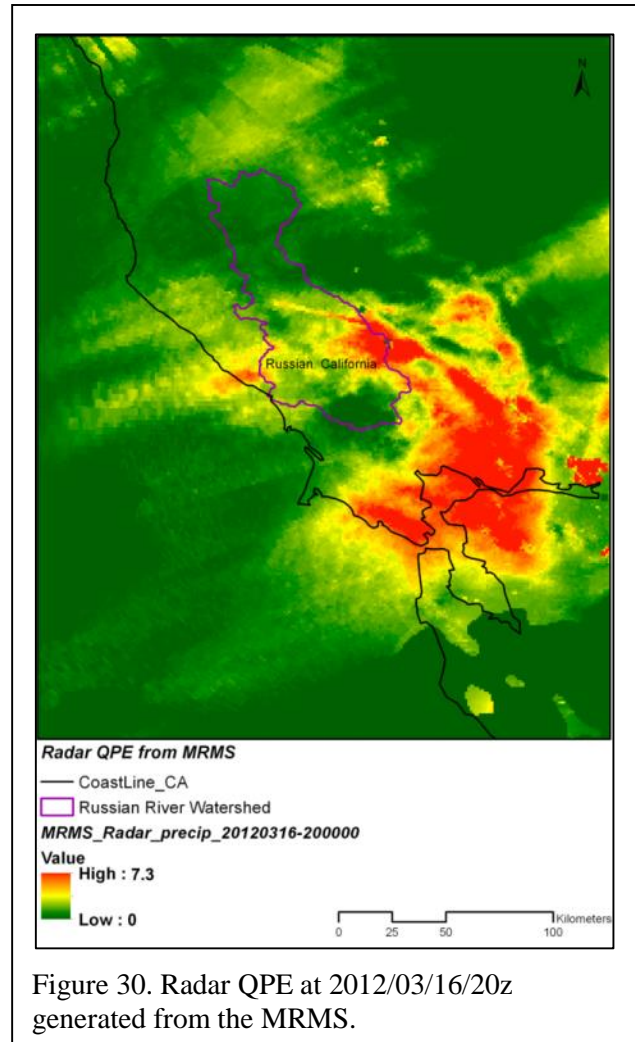


Figure 30. Radar QPE at 2012/03/16/20z generated from the MRMS.

3.4 Soil Moisture

Soil Moisture Observation Network

The existing HMT legacy soil moisture stations located at Cazadero (CZC), Healdsburg (HBG) and Rio Nido (ROD), have been augmented with stations located at Hopland (HLD), Lake Sonoma (LSN), Potter Valley (PTV), and Willits, CA (WLS) (Figure 11). Table 8 summarizes the station locations, elevation, soil probe burial depths, and date of installation for the Russian River basin soil moisture observing network.

Soil Moisture Instrumentation

Soil moisture observations in the Russian River basin are made using Campbell Scientific Inc (CSI) CS616 soil water content reflectometers. Soil probe burial depths in the Californian HMT network have been standardized at 10 and 15 cm below surface. The Healdsburg site has been augmented with a CSI CS616 probe at 20 cm depth. The Cazadero site soil pit has been enlarged and additional probes have been installed at the standard USDA/SCAN probe depths of 5, 20, 50 and 100 cm. All soil probes are placed horizontally in the soil.

Soil temperature observations are taken at each soil moisture probe depth using Campbell T-107 temperature probes. The temperature data are used for climatological studies and applying soil temperature corrections to the reflectometer measurements

All of the soil moisture stations deployed by HMT in the Russian River basin measure air temperature and relative humidity at 2.0 m. Precipitation measurements are made using Texas Electronics tipping-bucket rain gages, Table 8 summarizes the instrumentation used at the soil moisture observational locations along with the accuracies of the instruments supplied by the manufacturers.

The soil observing stations are queried at hourly intervals over voice telephone line from a central data collection/archiving system operated by NOAA/ESRL in Boulder, CO. The provisional data are made available in near real-time (1-hr latency) to the NWS RFCs, WFOs, and NCEP via SHEF, and FTP. In addition, the data are also available in both graphical and numerical form on the NOAA/ESRL web server located in Boulder, CO. <http://www.esrl.noaa.gov/psd/data/obs/datadisplay/>

Soil Moisture Sensor Calibration

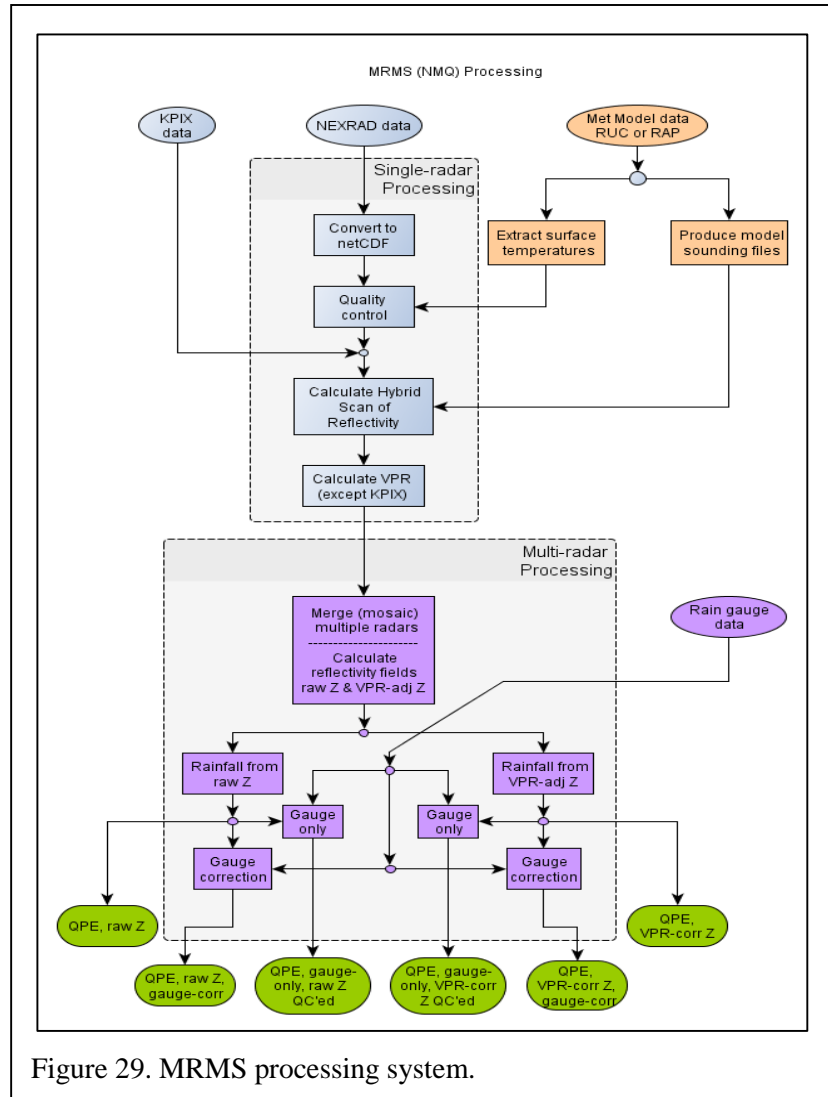


Figure 29. MRMS processing system.

Traditionally, gravimetric sampling using soil cores has been used to determine soil volumetric water content (VWC). The method, which requires oven drying soil core samples while error prone, is typically used to calibrate probes that measure soil moisture. Errors can arise from sampling, transporting, and weighing the samples before and after drying. The process of obtaining soil core samples destroys the natural state of the soil around the sampling area, and great care must be taken to minimize the disturbance. Gravimetric sampling also requires intensive manual labor which makes the procedure costly from an economic point of view.

The soil probes deployed at Cazadero, Rio Nido, and Healdsburg have been calibrated gravimetrically.

Table 8. Soil moisture station data summary.

Variable	System	Type	Accuracy
Air Temperature	Vaisälä HMP-45C	Thermistor	± 0.4 °C
Relative Humidity	Humicap®	Capacitor	± 2% (0 to 90% RH) ± 4% (90 to 100% RH)
Precipitation	Texas Electronics	Tipping Bucket	± 1% (Up to .254 mm/hr) 0,- 3% (25.4 to 50.8 mm/hr) 0, -5% (50.8 to 76.2 mm/hr)
Soil Temperature	CSI T107	Themistor	± 0.4 °C (Worst Case)
Soil Wetness	CSI CS616	Reflectometer	± 2.0 %

A procedure for the HMT sites selected for gravimetric calibration has been developed. After the probes have been placed in the wall of the soil pit, soil cores are extracted from the adjacent walls of the pit. If the soil through the depth of the pit is uniform, three to five ~ 50 g soil cores are taken at a single sampling depth. If multiple soil horizons are present and a soil probe is located in one of those horizons, additional cores are removed at that depth. The soil cores are then dried as soon as possible using a Denver Instruments Laboratory IR-50 infrared moisture analyzer at the standard temperature of 105° C. After recording the moist and dry weights of the cores, the cores are checked for rocks or excessive organic material. The bulk density and VWC are then calculated for the uncontaminated cores. This procedure is repeated periodically at each soil moisture site during the annual precipitation cycle in an attempt to capture expressively dry and moist soil conditions. Every effort is made to preserve the soil state of the site and at the same time extract soil cores that are representative.

Finally, a regression analysis is calculated that provides a calibration function for each soil type that has been found at an observing location. In addition, the raw output period of the reflectometer is corrected for changes in soil temperature using T107 soil temperature probe data gathered at the same depth as the reflectometer using the procedure suggested by CSI. The dielectric properties of soil are weakly dependent on temperature. The correction attempts to minimize the impact of soil temperature on the CS616 reflectometer VWC observations.

Figure 31 shows the difference between the CSI supplied calibration and calibrations derived using gravimetric sampling at the Healdsburg, CA observing location.

The general calibration function that relates the output period of the reflectometer to VWC is assumed quadratic. As one can see the calibration curve derived using the gravimetric samples taken at Healdsburg is flatter at the longer periods. According to documentation provided by CSI, the calibrations for the probes were derived in the laboratory using air-dried and saturated soils. The soils contained some silt and clay but were generally considered sandy loams with an electrical conductivity $\leq 0.5 \text{ dS m}^{-1}$ and a bulk density $\leq 1.55 \text{ g cm}^{-3}$. CSI states that the reflectometer response can change when the soil electrical conductivity exceeds 0.5 dS m^{-1} . The USDA SSURGO county soil survey published for the area around the Healdsburg site indicates that the soil series is a Montara Cobbly Clay Loam with clay content in the first 15.0 cm of 31.0 % and a bulk electrical conductivity of 1.0 dS m^{-1} . We have found similar discrepancies between the CSI supplied calibration and those derived by NOAA/ESRL using the gravimetric method in soils that have high clay contents and/or an electrical conductivity $\geq 0.5 \text{ dS m}^{-1}$ based on the USGS Soil Surveys.

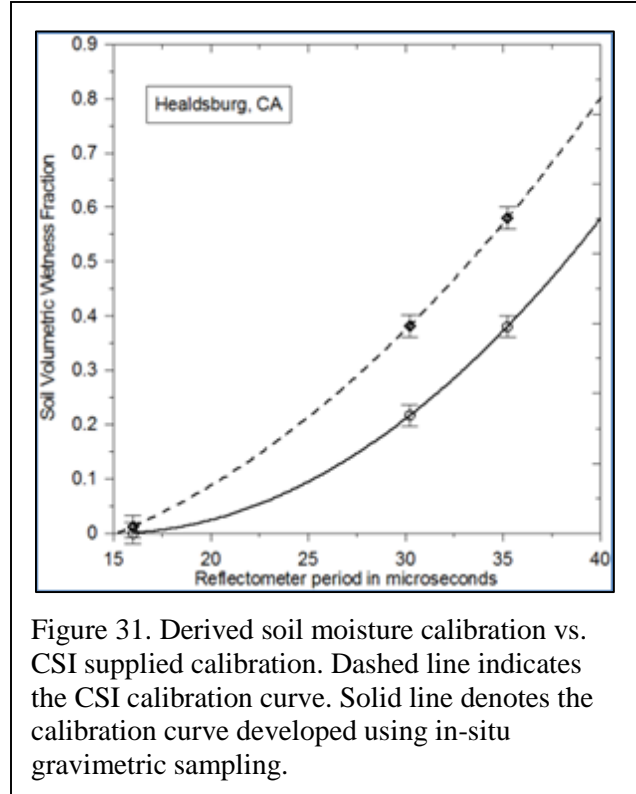


Figure 31. Derived soil moisture calibration vs. CSI supplied calibration. Dashed line indicates the CSI calibration curve. Solid line denotes the calibration curve developed using in-situ gravimetric sampling.

This calibration procedure has limitations. Identifying soil layers where soil cores are extracted and the elimination of non-representative cores after drying are carried out subjectively. The number of samples used in the initial regression analyses can be as few as six and it may not be possible in the years following the site installation to capture the wettest and driest soil conditions using gravimetric sampling.

Alternatives to Gravimetric Calibration

Two alternative methods have been explored. The first uses the soil wetness fraction observed using the CS616 probes and the manufacturer supplied calibrations, and the Available Water Capacity (AWC) estimated at nearby sites. The second relies on reflectometers that are designed to compensate for changes in soil electrical conductivity by making measurements of electrical conductivity simultaneously with the VWC measurement.

The AWC is the difference between field capacity (FC) and soil dry (SD). Field capacity is the VWC after all excess water has been drained by gravity, and is generally reached 2-3 days after a precipitation event. SD is the VWC of a volume of soil when water can no longer be extracted from the soil by either gravity or evapotranspiration. PSD had developed objective methods of determining FC and SD using seasonal VWC measurements. The definition of SD used in this report should not be confused with wilting point. Water can be removed from the soil by evapotranspiration when suction pressures are lower than -1500 J/kg .

Field capacity is determined by fitting four days of post-precipitation VWC decay measured at a specific observing location with an exponential decay function. The function takes the second derivative of the fitted function and determines where the second derivative crosses a threshold VWC value. This threshold is determined by the slope of the original decay function, such that soils with quickly declining VWC cross the threshold later than soils with slowly declining VWC. Scaling the threshold with slope is based on the assumption that if a soil is still draining extremely quickly after a rain event, it is likely still

undergoing drainage due to gravity and has therefore not dropped to field capacity. This analysis is performed on any significant precipitation event present in the data set, allowing the averaging of a large (~15 event) sample size and thus reducing errors from any anomalous events.

SD was estimated by looking at the soil dry downs at a location from the last spring season precipitation event to late September. The minimum VWC valued reached during that period is considered SD. FC and SD values derived for gravimetrically calibrated and uncalibrated stations are shown in Table 9. Two case studies from soil moisture measurement stations in the Russian River basin show the value of measuring *in situ* soil moisture rather than relying on USDA estimates of AWC. Field capacities were calculated for 15 large precipitation events between 2007 and 2012 at Cazadero, CA and 16 large events at Healdsburg, CA. Mean field capacity at Cazadero was 25.2% with individual event field capacities ranging from 22.0% to 26.9%. Healdsburg showed a mean field capacity of 36.5% with a range of 34.4% to 39.9%. The USDA soil survey reported a field capacity of 26.1% for the soil unit in which the Cazadero station is placed, but only 18.7% for the unit at the Healdsburg site. Our field-based analysis shows a field capacity at Healdsburg that is nearly double that reported by the USDA.

Table 9. Soil sensor calibration parameters.

Site	Mean FC	USDA FC	Mean SD	Corrected FC	Corrected SD
CZC	0.25	0.26	0.09	N/A	N/A
HBG	0.37	0.19	0.09	N/A	N/A
HLD	0.24	0.22	0.05	N/A	N/A
LSN	0.34	0.26	0.10	N/A	N/A
PTV	0.37	0.20	0.15	0.27	.05
ROD	0.46	0.16	0.17	0.36	.07
WLS	0.42	0.22	0.16	0.32	.06

The FC estimated from the observations at PTV, ROD, and WLS were anomalously high when compared to other stations in the basin (Table 9). However, the AWC or difference between FC and SD for all three stations averaged 0.26 suggesting that a simple bias correction can be applied to the stations in question. After correction the values of FC and SD show better agreement with the other stations in the basin indicating that the AWC can be used to correct and in worst case identify stations such as HBG where gravimetric calibration must be carried out.

Some commercially manufactured soil moisture reflectometers claim to be self-calibrating. A CS-650L reflectometer has been installed and tested at the HBG soil moisture station. Initial results from the self-calibrating probe are not encouraging. Figure 31 shows the soil water content estimated at 15 cm depth from the gravimetrically calibrated CS-616 probe and the soil water measured by the self-calibrating CS-650L probe located at the same depth. The CS-650 obviously over estimates soil water content consistently measuring values 12% greater than the co-located gravimetrically calibrated CS-616 probe. In addition, it appears that temperature compensation is not being applied to the measurements because soil water content values are peaking during the time when one expects the losses to evapotranspiration to be the largest.

Groundwater Recharge

RDHM is a conceptual surface hydrology model designed principally for simulating various hydrologic states. However, the model is not equipped with a comprehensive method to represent groundwater hydrogeological processes. In the RDHM, the ZPERC, REXP, PFREE, and SIDE parameters are used to represent the groundwater recharge processes. These parameters control the percolation rate, percolation curve, and the fraction of deep percolation to free water reservoirs. First, the ZPERC, REXP, and PFREE percolation domains are limited to influencing the variations of tension and free water in lower zones (unsaturated zones) instead of affecting the rise and fall of the water table in

unconfined aquifers. Second, although the SIDE parameter allows modelers to eliminate a portion of water by removing it from base flow to deep groundwater recharge, it neglects the interactions between groundwater and the river network.

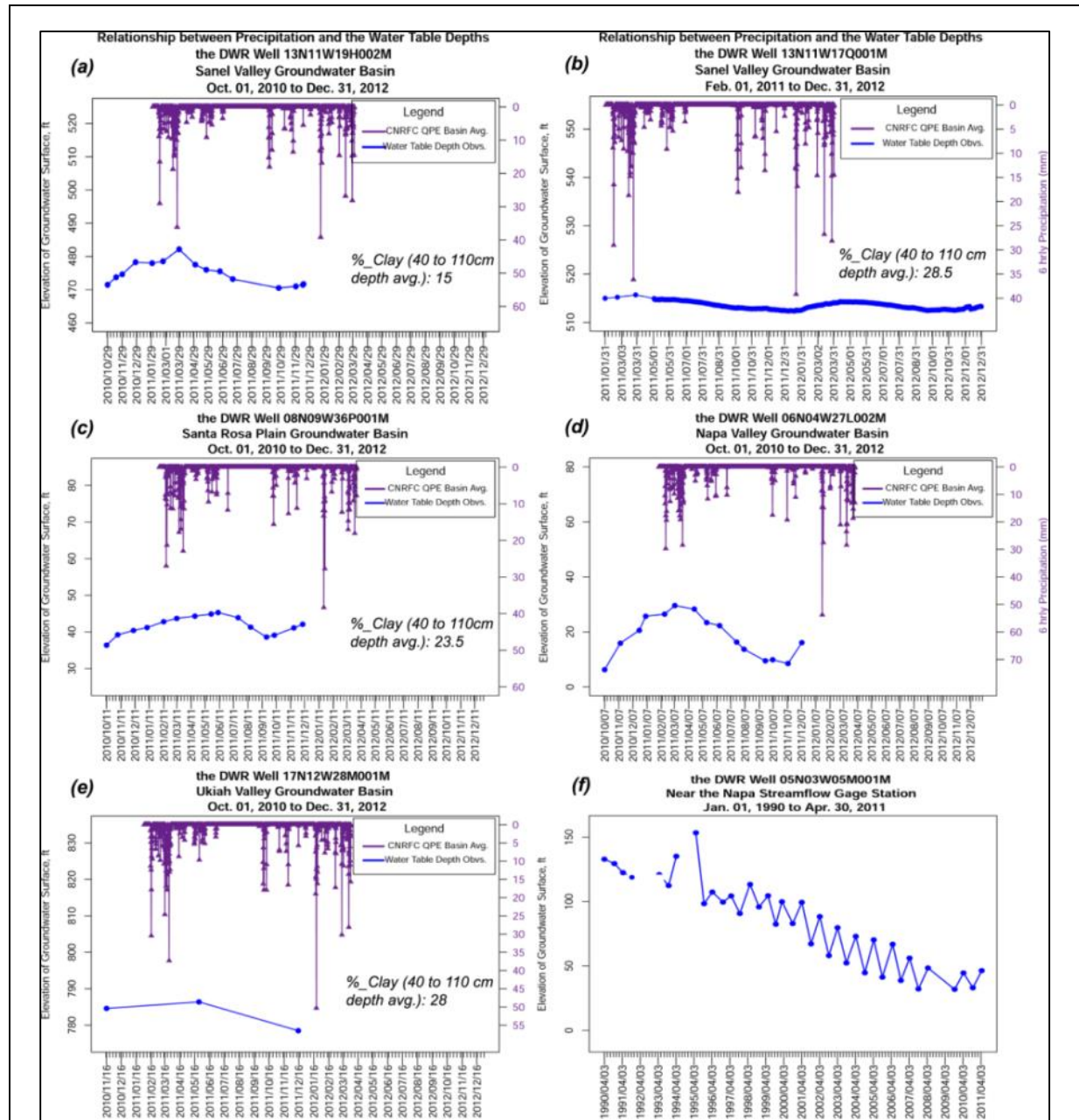


Figure 32. Response of well water table depths to precipitation at different locations underscores the influence of the deeper subsurface conditions in groundwater recharge.

For a distributed model, this disconnection makes RDHM less than ideal for modeling the spatial variation of groundwater. Thus, the main job of SIDE in RDHM is to attenuate base flow, being involved in the complicated trade-off interactions with the other parameters in the calibration process. Anderson (2002) realized that this would distort the original purpose of SIDE, advising that the calibration of SIDE should be constrained to circumstances where significant deep groundwater recharge has been demonstrated as an important part of the water balance.

To make the SIDE parameter independent from the model trade-off effects and to enable the RDHM with the capability to link the routing mechanism and water table dynamics together, we analyzed the influences of the soil properties on the water table responses to precipitation. The water table elevation data is extracted from the California Department of Water Resources (DWR) and precipitation is the CNRFC QPE data. The comparison, illustrated in Figure 32, shows that the soil properties and locations of the well have dominant power on the water table oscillation. The water table fluctuation at Well 13N11W19H002M (Panel a) shows more sensitivity to the moderate and large rainfall events than the other wells, reflecting the reality that low “percentage of clay” (15% in the surrounding area) makes groundwater more responsive to meteorological conditions. A similar water table response is found at Well 08N09W36P001M (Panel c). This well is characterized by its high “percentage of silt” and a location adjacent to the Mark West Creek in the Santa Rosa Plain. Well 13N11W17Q001M (Panel b) displays different behavior. With its “percentage of clay” soil property 28.5, the influence of rainfall events is attenuated and the resulting water table changes are small. These observed relationships between groundwater dynamics and soil property combining locations confirm the need to incorporate physically based representation of aquifers into the hydrologic and land surface processes.

3.5. Evapotranspiration

ET Instruments and Observations Summary

In association with the soil moisture monitoring stations the HMT program has deployed a surface flux observing platform at the Cazadero site (Figure 33). The goals include evaluating the evapotranspiration and soil moisture parameterizations utilized in the RDHM hydrological model. High quality observations of the radiative, sensible, latent, ground heat flux, and soil moisture are compared with the potential ET (PET) evapotranspiration values estimated by the RDHM model. RDHM adjusts the climatic monthly PET values based on the surface temperature used to force the model. High quality observations of each component of the surface energy balance have made a detailed evaluation of RDHM evapotranspiration (ET) performance possible.

The instrumentation includes the following:

- Wind and Temperature: Applied Technology Incorporated Sonic Anemometer/Thermometers
- Water Vapor: Licor LI-7500 fast response gas analyzer
- Direct beam solar radiation: Eppley Normal Incidence Pyroheliometer
- Incoming diffuse solar radiation: Eppley Black and White Pyranometer
- Outgoing diffuse solar radiation: Eppley Black and White Pyranometer
- Incoming IR radiation: Eppley Precision Pyrgeometer
- Outgoing IR radiation: Eppley Precision Pyrgeometer
- Ground Heat Flux: Radiation Energy Balance System soil heat flux plates
- Soil Moisture: Campbell Scientific Water Content Refectometers
- Soil Temperature: Campbell Scientific 107 Thermistors
- Aerosol Optical Depth: Carter-Scott sun photometer
- Irradiance calculated using Baseline Surface Radiation protocols

Typical forcing fields used in hydrological modeling are surface air temperature and precipitation. These parameters are routinely reported at standard meteorological surface observing locations. However, numerous

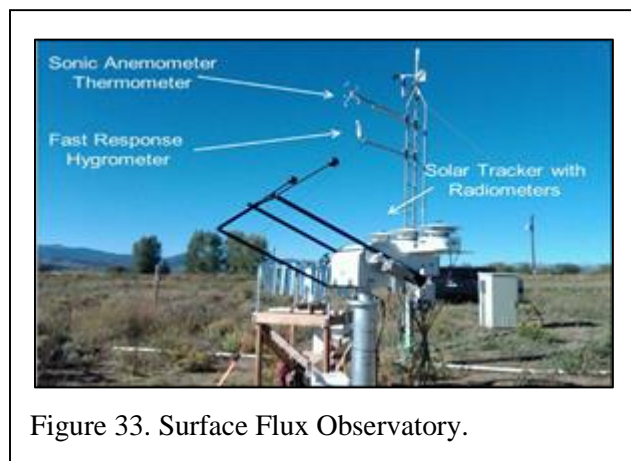
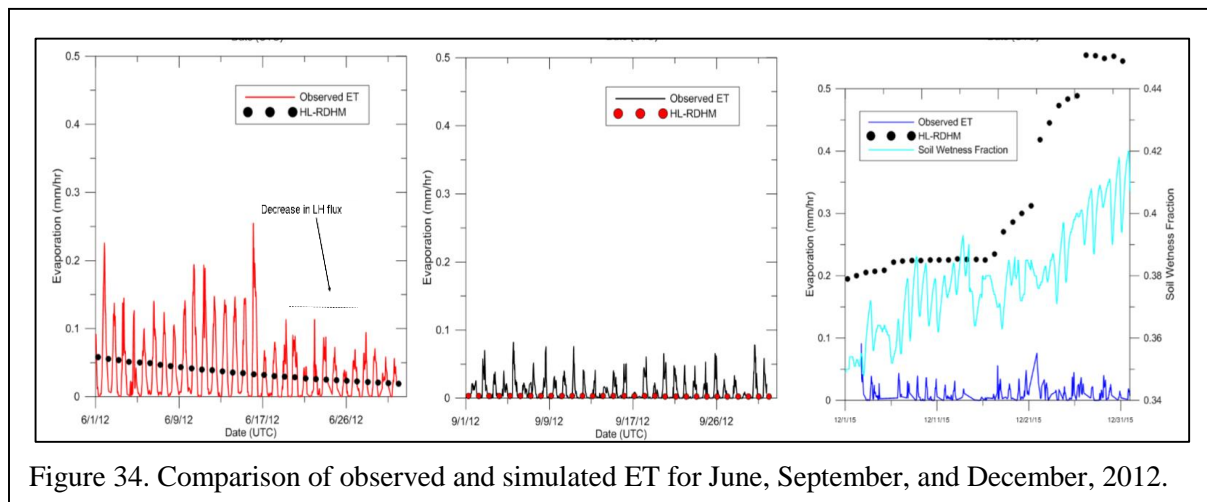


Figure 33. Surface Flux Observatory.

assumptions must be made in order to specify evapotranspiration using surface air temperature observations. They include ignoring the difference between surface air temperature and skin temperature, using climatological values of 10 m wind speed to specify the near surface wind speed, and making a priori assumptions about the Bowen ratio. Thus, the entire surface energy balance is specified using a single variable (air temperature). In reality estimating the surface energy balance requires observations of net irradiance, sensible heat flux, latent heat flux, and ground heat flux.

Evaporation estimated using surface air temperature observations can increase the level of uncertainty in hydrological model simulations. Evaporation estimated from a fully observed surface energy balance can be used to quantify this uncertainty. The results presented here suggest that the HMT flux observations can play an important role in hydrological model evaluation and development. Figure 34 compares observed and simulated ET.



Typical forcing fields used in hydrological modeling are surface air temperature and precipitation. These parameters are routinely reported at standard meteorological surface observing locations. However, numerous assumptions must be made in order to specify evapotranspiration using surface air temperature observations. They include ignoring the difference between surface air temperature and skin temperature, using climatological values of 10 m wind speed to specify the near surface wind speed, and making a priori assumptions about the Bowen ratio. Thus, the entire surface energy balance is specified using a single variable (air temperature). In reality estimating the surface energy balance requires observations of net irradiance, sensible heat flux, latent heat flux, and ground heat flux.

Evaporation estimated using surface air temperature observations can increase the level of uncertainty in hydrological model simulations of streamflow and soil moisture. Evaporation estimated from a fully observed surface energy balance can be used to quantify this uncertainty. The results shown in this study suggest that arbitrary manual calibration of SAC-HT to the hydrograph can lead to unrealistic values of evapotranspiration.

Conclusions of the comparison include:

- Spring and summer evapotranspiration controlled primarily by soil moisture.
- Observations show that evaporation is energy limited during the month of December, However, SAC-HT overestimates evapotranspiration when compared with the observations.
- Saturated soil conditions and SAC-HT manual calibration may account for this discrepancy. In this study the climatological values of ET were changed in the manual calibration process.
- SAC-HT underestimates evapotranspiration in late summer.
- SAC-HT evapotranspiration values showed the best agreement during spring dry-down.
- SAC-HT systematically underestimated peak daily evapotranspiration due to 6-hr time step.

4. ASSESSMENT OF THE DISTRIBUTED HYDROLOGIC MODEL

4.1 RDHM Simulations of Surface Runoff

The RDHM was implemented and applied for the period Oct. 1, 2010 through Mar. 31, 2012 with the following distinctions:

- Model warmup period - Oct. 2010 through Jan. 2011
- Calibration period - Feb. 2011 through Dec. 2011
- Verification period – Jan. 2012 through Mar. 2012

The model warmup period was to establish the initial states (e.g. soil moisture) prior to the calibration period. The model calibration period was used to make RDHM parameters adjustments to obtain close correspondence to observed flows. The model verification period was to assess model performance allowing for no parameter adjustments. The primary emphasis for calibration-verification was for total water balance and flood events. However, an independent verification was conducted for low flows using data provided by the NMFS.

4.2. Calibration Procedure

RDHM parameter calibrations were conducted at 7 streamflow gage stations: Austin Creek Cazadero, Santa Rosa Creek near Santa Rosa, Russian River near Ukiah, East Fork Russian River near Calpella, Napa River near Napa, Napa River near St. Helena, and Big Sulphur Cr CAG nr Cloverdale (Table 2, Figure 35).

Table 2 lists all of the USGS gaging sites in the Russian-Napa Rivers. Highlighted are the sites used for calibration and verification purposes. Since the RDHM simulates so-called “natural” flows it is important to acknowledge how water management operations for reservoir storage and diversions would influence the gaged flow records used to guide calibration efforts. For example, calibration was not addressed for the main stem Russian River due to regulation by Lakes Mendocino and Sonoma; such regulation is not represented by the RDHM. Three of the calibration sites drain watersheds that do not have major flow regulation except for irrigation diversions; include Austin Cr. nr Cazadero, W.Br. Russian River nr Ukiah, and Napa River nr St. Helena. These three watersheds received emphasis for calibration efforts for flood peaks and low flows even though irrigation diversions may influence low flows. Other watersheds have water management activities that may influence overall water balance and low flows, although flood flows may be minimally effected. Santa Rosa Cr. near Santa Rosa has some flow diversions to Spring Lake. Flows for the E.Fk. Russian River near Capella are influenced by the transbasin flows from the Eel River through the Potter Valley diversion, as well as irrigation operations in Potter Valley. The Napa River near Napa is influenced by Lake Hennessey (31,000 AF, 54 sq. mi.) which can influence flood peaks when the water storage levels are low. The Big Sulphur Cr CAG Resort near Cloverdale has a small drainage area (13.1 sq. mi.; 2 HRAP grids); it also has diversions for industrial use when flows are above 10 ft³/s.

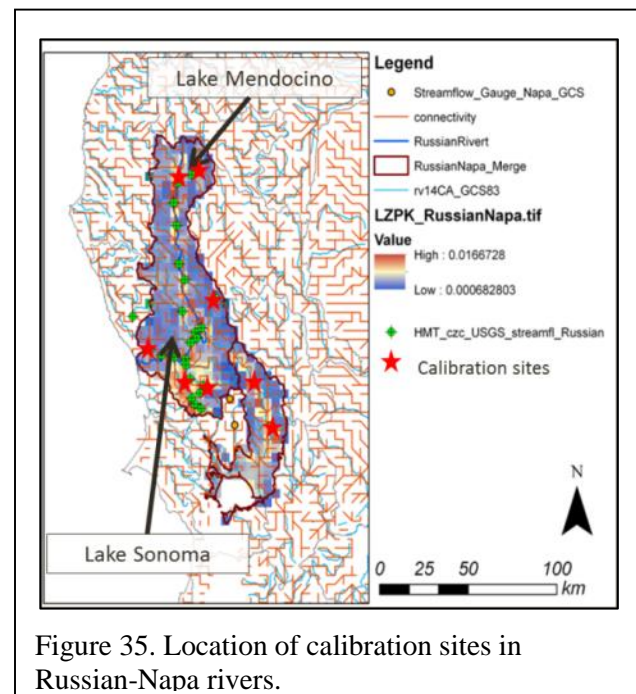


Figure 35. Location of calibration sites in Russian-Napa rivers.

Since RDHM is a highly dimensional and non-linear model, creation of an explicit calibration approach which can be duplicated by others for other watersheds is required for advancing RDHM towards being an operational model. This manual calibration process was greatly informed by work of Anderson (2002) who conducted extensive sensitivity analyses on SACSMA procedures and provided guidance on the sequence of steps for parameter adjustments.

To simplify the parameter estimation process, OHD has created *a priori* parameters based on SSURGO soil information. The calibration work aimed to refine these parameters to reflect local physiographic and vegetative characteristics of the calibration watersheds. The stream flow time series of the calibration period is segregated into categories of dry/wet periods, low-moderate/high flow, or dry/saturated soil.

Two preparatory tasks are needed before initiating calibration: 1) selection of the corresponding HRAP pixels for simulation and 2) identification of the dominant parameters for each period or event. First, to guarantee a hydrologic correspondence between the observation station and the simulated pixel, the HRAP pixels picked for simulation need to reflect the real flow sequence of the observed station in the context of the stream network. The National Hydrograph Dataset (NHD) stream network was used to supplement this HRAP pixel selection process.

Secondly, to identify the dominant parameters for the various periods or events, it was initially assumed no interactive effects occurred among the SAC-SMA parameters. Isolation of the parameter effects in the preliminary runs (sensitivity test) resulted in identification of the dominant parameters for the events (or periods) of the various categories. Figure 36 illustrates events of various categories and their corresponding parameters. The streamflow time series of the calibration period is simply segregated into categories of dry/wet periods, low-moderate/high flow, or dry/saturated soil. Table 10 summarizes the dominant parameter effects for each category of periods or events. The calibration period was first segregated into dry/wet periods with discharge into high and moderate-low flow stages.

The dominant parameters in dry periods are indicated by their exclusively influencing events (a). For example, UZTWM is used to determine when storm runoff after a dry period will first occur and to adjust the quantity of this recharge. In (b), the hydrograph in wet periods is further separated into the categories where upper zone tension water deficit is substantial (Event (1)), when the discharge rise is small to moderate (Feb. 19, 2011 to Mar. 19, 2011), and when soil is close to saturated or already saturated (Event (2) and (3)). The corresponding parameters are listed. The grayed-out parameters should not be

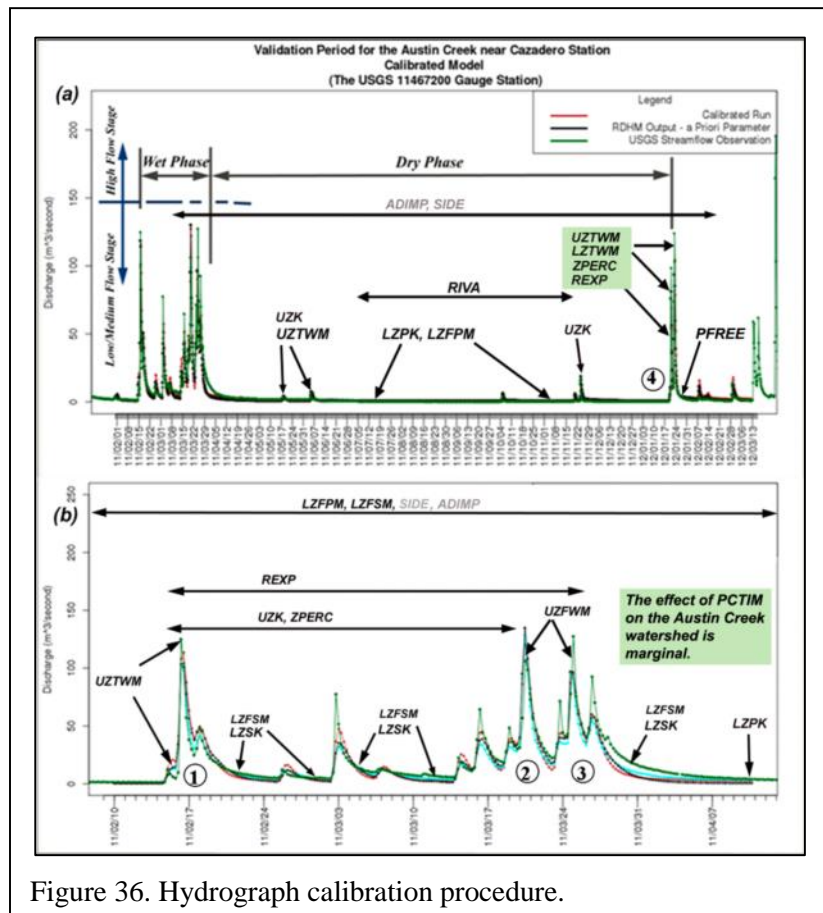


Figure 36. Hydrograph calibration procedure.

calibrated until the final step even though they appear sensitive to the flow fluctuation.

Table 10. Dominant parameters of the various periods and their effects.

	<i>Period</i>	<i>Parameter</i>	<i>Primary Effect</i>
Dry	Entire Dry Phase	SIDE	Control base flow and interflow in dry periods.
	Dry Phase, Primary Base flow	LZFPM, LZPK, PFREE, SIDE	Adjust primary base flow.
	Very Dry Phase, Significant ET Demand	RIVA	Determines whether ET from riparian vegetation occurs and draws down base flow.
	Dry Phase, Low to Moderate Events	UZK, ADIMP	Controls timing of interflow and determines quantity of direct runoff from low intensity events when soil is dry.
	Dry Phase, the First Small/Moderate Event after a Period of 2-3 Months from the Prior Storm Event	UZTWM, LZSK, LZFSM	Determines when storm and direct runoff will first occur after two to three months of dry period.
	Dry Phase, the First Moderate/Big Event after a Long Dry Period (longer than 3 months)	LZTWM, ZPERC, REXP, UZK, LZPK, LZFPM	Controls the timing and quantity of the first rise after long dry periods.
Wet	Entire Wet Phase	LZFPM, LZPK, LZFSM, LZSK, SIDE, ADIMP, REXP	Controls base flows and rises of various sizes.
	Wet Phase, Substantial Upper Zone Tension Water Exist (~ 2 -3 months after the prior event)	UZTWM, ZPERC, REXP, UZK	Controls discharge when the soil is still somewhat dry; especially influential on surface runoff and interflow.
	Wet Phase, Supplemental Base flow	LZSK, LZFSM	Controls the amount and the slope of the supplemental recession.
	Wet Phase, Small/Moderate Rises between Major Events	UZK, ADIMP, ZPERC, REXP	Controls the discharge amount for small to moderate rises.
	Wet Phase, Saturated or Near Saturated Soil	UZFWM	Controls when surface runoff occurs.

After completing these preparations, the calibration iterations can then proceed. Calibration involves judgements of multiple hydrographs and adjustment of related parameters simultaneously. Deliberations on parameter interactions and appreciation of model behaviors are critical for a successful calibration. Unfortunately, the expertise accumulated by one modeler in this non-linear calibration process is very difficult to transfer to another modeler. In fact, the complex tradeoffs of the model's behaviors often result in several possible calibration answers (sets of parameter values or sometimes unrealistic values) that generate equally "good" streamflow simulations (Qiao et al., 2013). Thus, the procedures used by one modeler are not necessarily the same as another's.

To resolve this problem and to create a standardized calibration procedure, the process developed for this research stresses an alternate categorization framework (i.e. tuning parameters alternately between

characteristics such as dry versus wet, saturated versus non-saturated, and peak versus low flow). For instance, if the calibration began with addressing the parameters which control peak flow after a long dry period, successive adjustments should be focused on the parameters controlling low flow (i.e. LZFP, LZPK, LZFSM, and LZSK) in the wet period. Table 10 tabulates the effects of the dominant parameters for each category of events/periods and can be used to organize the calibration sequence oscillating between peak and low flow as well dry and wet soil.

To make the table simple to use, we further categorized the events and periods based on the degree of soil saturation. For the dry soil peak flow period, evaluated parameters should include UZTWM, LZTWM, UZK, ADIMP, ZPERC, and REXP. For the dry soil base flow period, controlling parameters should be PFREE, LZPK, LZFP, SIDE, RIVA, and PCTIM. On the other hand, for saturated or near saturated soil peak flow events, UZFWM and REXP should be evaluated, whereas LZSK, LZFSM, LZFP, UZK, ADIMP, SIDE, REXP, and ZPERC should be evaluated for saturated soil low/moderate flow events. Among these parameters, UZFWM can also be used to control the timing when surface runoff occurs. In practice, the parameters listed in the same rows on Table 10 need to be adjusted simultaneously at some point in the later stages of calibration because their interactive effects can be influential. In addition to low flow, LZPK, LZSK, LZFP, and LZFSM also influence the peak flow quantity and should be thoroughly tested to evaluate the trade-off effect between high rises and base flow. As an example, to calibrate the parameters for the first event after a long dry period, such as the 23-Jan-2012 event (Event (4)) shown in Figure 36, LZTWM needs to be tuned simultaneously with ZPERC, REXP, UZK, LZPK, and LZFP.

Figure 37 illustrates a calibration framework using an alternate categorization. We started by calibrating the parameters which control discharge of the first storm events after a lengthy dry period. By the occurrence of this event, a lower zone or upper zone tension water deficit develops in the soil. Thus, the calibration of the relevant parameters, LZTWM and UZTWM, becomes relatively straightforward. Through a process of trial and error, the observed and simulated hydrographs can be made reasonably close. Since this represents the first attempt, modelers are encouraged to modify LZTWM and UZTWM to introduce a surplus over the USGS observations. This allows for subsequent adjustment on the lower zone free water-related parameters because their modifications will soon decrease peak flow.

In our study period, the best storm events for this evaluation are Events (1) and (4). The effects of both parameters on hydrographs are different: LZTWM has a longer impact on streamflow than UZTWM does. Soil can become more resilient if LZTWM is increased. The adjustment of LZTWM can influence the surface flow quantity and timing of interflow and recession flow for one to two months, while the change of UZTWM causes an instant change of flow centering on the first event after a dry period of two to three months. Therefore, the optimal storm event for evaluating UZTWM and LZTWM is given by the first moderate rain event after two to three months of dry period and the first event after a long dry period (i.e. longer than three months).

The influence of UZTWM will become significantly weaker after that first event. After calibrating UZTWM and LZTWM, we then focused on tuning the dominant parameters controlling primary base flow and supplemental base flow: LZFP, LZPK, LZFSM, and LZSK. The calibration of LZFP and LZPK is executed for the dry phase (2011/05/01 to 2012/01/15), whereas LZFSM and LZSK is executed for the wet phase (2011/02/15 to 2011/04/30). Adjusting these four parameters is simple, but one must pay attention to the impact of their combination in changing the magnitude of peak flow. In the Sacramento model, the term of PBASE is used to represent this combination in the related percolation equation:

$$PBASE = LZFSM * LZSK + LZFP * LZSK \quad (15)$$

The function of PBASE is to specify the saturated percolation rate. It can bring down peak flow when the PBASE value is raised and vice versa. Among these four parameters, LZFSM is especially dominant

in influencing peak flow and percolation rate. It requires modelers to simultaneously evaluate its impact on peak flow while adjusting supplemental base flow.

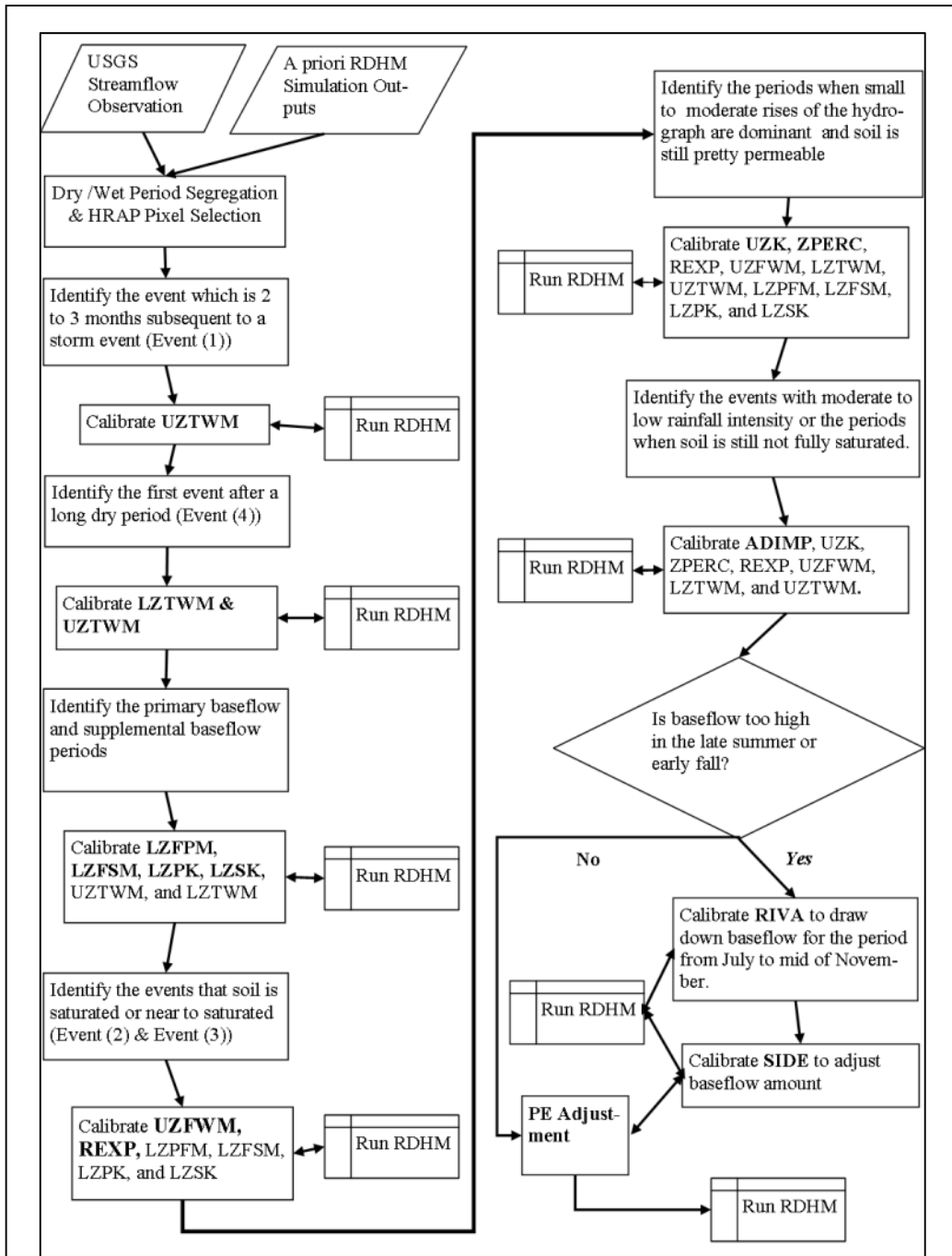


Figure 37. Sequence of steps to calibrate SAC-SMA module of RDHM. The bold abbreviations are the dominant parameters and should be calibrated first. But the other parameters (e.g. plain text) listed in the box still need to be adjusted because of the complex model trade-off caused by the different parameters.

Regardless of REXP and ZPERC, most of the parameters which control the streamflow fluctuation in relatively dry soil conditions have been resolved at this point. Thus, we proceeded to focus on events with large amounts of precipitation and near-saturated soil conditions. Event 3 in Figure 36 is such an event, strongly influenced by UZFWM, which is the dominant parameter for these events. By adjusting UZFWM, the relative division of storm runoff into surface flow and interflow will be changed. Therefore, it can be used not only for changing amounts of peak flow but also for controlling the timing of peak occurrence. The lower the UZFWM value, the higher the peak flow amount and the earlier the time of peak flow occurrence. Depending on the characteristics of the watersheds, sometimes UZFWM and REXP must be calibrated together. REXP is especially influential when the soil has not been fully saturated or is still permeable. The wetter the soil, the smaller the effect that REXP has on discharge. Therefore, for watersheds with a high percentage of sand, UZFWM and REXP should be considered together.

The larger the REXP value, the higher the rises at peaks. However, instead of calibrating REXP individually as a compromising factor to UZFWM, one should be thinking in terms of the structure of the percolation curve for that specific watershed. REXP is the parameter deciding the shape of the percolation curve. For example, soil in the Austin Creek watershed is composed of predominantly clay soil in the shallow layer but sandy soil in the deeper layers, according to SSURGO. Though these soil characteristics in the Austin Creek watershed are well represented by a priori parameters, in practice the REXP may need to be slightly scaled down to reflect the reality that evergreen forest-covered watersheds normally have a straighter percolation curve. The deep root system of evergreen plants and scrubs increases the percolation rate, so that the watershed resembles a sandy soil dominant watershed. Once the REXP can be determined, UZFWM can be calibrated. After calibrating UZFWM and REXP for relatively wet soil conditions, we then focus on adjusting UZK and ZPERC because UZK dominates small to moderate rises in the hydrograph and ZPERC determines percolation rate when the soil is dry. These are the events in which no surface runoff is generated.

For watersheds with highly permeable soils and little or no surface runoff, interflow will dominate the response from all storm events (Anderson, 2002). It is especially prominent when LZTWC is less than LZTWM, which normally occurs after a long dry period. UZK, on the other hand, was used to control the timing of interflow and is even influential for small to moderate rises. The larger the UZK value, the higher the rises. To evaluate the model trade-off effects of all of the parameters, which have influence on small to moderate rises in the dry soil conditions, in addition to ZPERC and UZK, parameters such as UZTWM, LZTWM, LZSK, LZFSM, LZPK, and LZFP, need to be recalibrated marginally at this step.

The impact of ADIMP lasts longer in the distributed model. It controls the hydrologic response in events with small to moderate rainfall intensity across dry and wet periods. Even when the soil is saturated and surface runoff is present, ADIMP still impacts flow in some watersheds. However, ADIMP should not be calibrated too early in the adjustment stages because the discharge output is very sensitive to its modification and a decent matching between the simulated and observed peak flow hydrographs using only ADIMP can be misleading. In fact, the whole watershed cannot be modeled using this feature – only the portions of the watershed which are adjacent to the channels and drain directly into the channel system are controlled by ADIMP. Modelers should always keep in mind that ADIMP has only a minimal effect on large events where surface runoff predominates. After completing the calibration of ADIMP, the major parameters of SACSMA model should be tuned to their optimal positions.

At this point, attention can then turn to the remaining two parameters: RIVA and SIDE. Both of the parameters are related to base flow quantity. Nevertheless, calibration for both parameters may be not necessary. Therefore, before calibration, one should examine if the overall base flow is still too high or if the base flow in the late summer and fall (July to November) is too high. If the overall base flow is too high, SIDE can be assigned a value that decreases base flow. If base flow from July to November is still too high, one can change the RIVA value to reduce base flow. The purpose of RIVA in RDHM is to represent sharp drawdowns in streamflow in dry periods, perhaps associated with riparian vegetation.

4.3. Calibration and Verification Results

The parameter calibrations were executed at 7 USGS streamflow gage stations: Austin Creek Cazadero, Santa Rosa Creek near Santa Rosa, Russian River near Ukiah, East Fork Russian River near Calpella, Napa River near St. Helena, Napa River near Napa, and Big Sulfur Creek. Summary data for calibration results are tabulated in Table A-1, and verification results in Table A-2.

Statistics for comparison of the observed versus simulated flows are computed for the calibration and verification periods, and for the each of the seven flood events. The equations used to define these statistics are presented by Moriasi et al. (2007). For the total simulation periods the metrics included 1) runoff volume, 2) Nash-Sutcliff correlation, and 3) percent bias. For the flood events the following comparison statistics were computed, 1) Runoff Volume (RO_v, feet), 2) Peak Flow [ft³/s], 3) time to peak [hrs], 4) Nash-Sutcliff efficiency (NSE, dimensionless), 5) percent bias (PBIAS%), and 6) R_{mod} (= Mod. Corre. Coef., dimensionless). We also conducted an independent verification of the model's low flow performance using stream flow data collected by the NMFS for a number of tributaries to the Russian River.

The Nash-Sutcliff coefficient is used to assess the predictive accuracy of the hydrological model; it represents how well the simulated hydrograph matches the observed flows for all time steps.

$$E = 1 - \frac{\sum_{t=1}^T (Q_o^t - Q_m^t)^2}{\sum_{t=1}^T (Q_o^t - \bar{Q}_o)^2} \quad (16)$$

where Q_o is observed discharge, Q_m is modeled discharge, and Q_{o^t} is observed discharge at time t. For the entire calibration period, the average N-S is 0.84; for the verification period the average N-S is 0.75. N-S values greater than 0.70 are characterized as “good” (Boyle, et al 2001).

RO Volume. RO Volume can be expressed as:

$$RO_v = \frac{\sum_{i=T_\alpha}^{T_\omega} Q_i * 6 * 60 * 60}{A} \quad (17)$$

where RO_v is the runoff volume expressed as depth (ft); T_α and T_ω represent the starting time and ending time of the runoff event, respectively; Q_i is streamflow (m³/s) time series simulated for the calibrated station.; A is drainage area. Differences in RO_v between observed and simulated flow accumulation periods are tabulated as percent bias (PBIAS); these values were computed for the total simulation period as well as for specific flood events.

$$PBIAS = \left[\left(\sum_{i=1}^n (X_i^{obs} - X_i^{sim}) \right) * 100 / \sum_{i=1}^n X_i^{obs} \right] \quad (18)$$

In addition, we restate the generalized water budget:

$$Precipitation = Surface\ Runoff - Evapotranspiration +/- Groundwater\ Storage +/- Transbasin\ Diversions. \quad (19)$$

Assessment of the RDHM performance necessarily involves the various components of the budget equation.

Total Period Simulation Performance

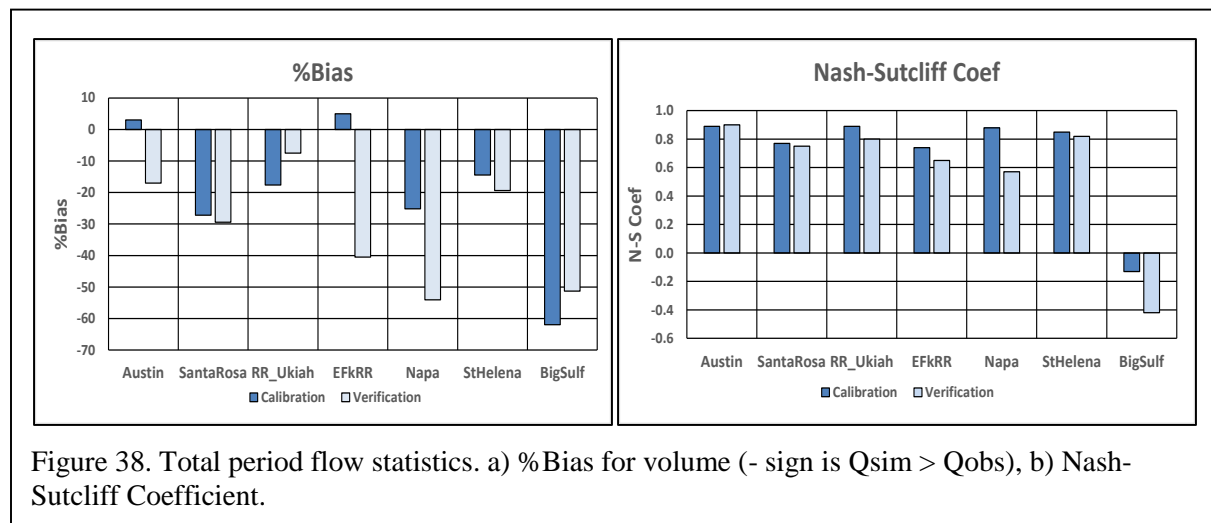
Accuracy statistics at the 7 stations are tabulated for the calibration (Appendix A, Table A-1) and verification periods (Appendix A, Table A-2; figures 38, 39 and 40). Interpretation of the results requires

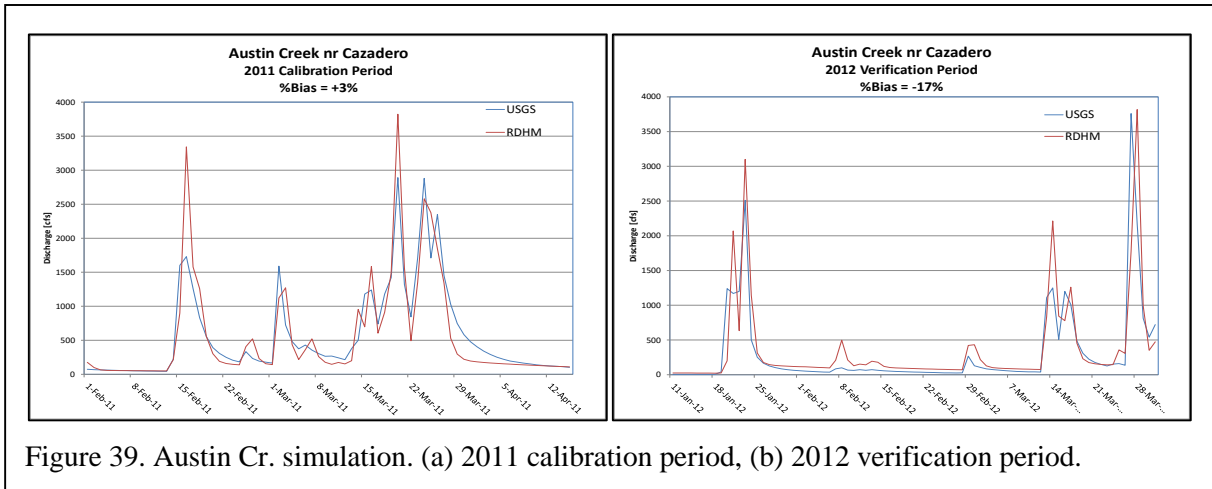
some understanding of factors influencing precipitation and runoff in the watersheds. The Big Sulfur Creek case is problematic for all indicators; this is likely due to its very small drainage area (13.1 sq. mi., 2 HRAP grids) and location near the peak of the Sonoma Mts. where precipitation tracking and forecasting is difficult and a small deviation in storm tracking could miss the small basin completely. The model performance for this basin suggests that flood forecasting for small basins in variable terrain can be highly uncertain.

For the 6 stations (not including Big Sulfur Creek) the calibration averages are %Bias -15% and NSE 0.84, and the verification averages are %Bias -26% and NSE 0.75. The results for NSE are considered good (i.e. > 0.70). This indicates the simulated flows closely match the timing and magnitude of watershed observed flows suggesting that the model reflects the influence of precipitation and watershed factors. The results for %Bias are not considered good, and indicate errors in the precipitation data as suggested by the comparison of CNRFC QPE with independent HMT data described above, and/or the RDHM misrepresentations of the water budget.

The 6-station %Bias statistics are influenced by higher values for three of the watersheds which have water management influences not represented in the model. We did not compute model statistics for the main stem Russian River downstream of Ukiah because RDHM does not represent operations of Lake Mendocino. Streamflow observed at the “E. Fk. Russian R near Calpella”, “Santa Rosa Creek near Santa Rosa”, and “Napa R near Napa” stations may also be impacted by either the trans-basin water diversions (EFk Russian Potter Valley Project, %Bias +5%) or reservoir capture (Lake Hennessey), thus the simulation accuracy declines at these stations.

The three watersheds performing best (Austin, WfK Russian, Napa R nr St. Helena) have lesser water management influences. Even so the average %Bias is -17%; Austin Cr was best at -8%. The consistent overestimation of surface runoff may be due to several factors including the identified QPE precipitation bias (underestimation) and misrepresentation of groundwater storage dynamics.





An identified concern is with the first runoff event of the winter season. For examples, calibration efforts for Austin Creek showed a very low %Bias at +3% for the winter season 2011 (Figure 40), but entering into the 2012 winter verification season the %Bias increased significantly to -17%. Divergence between observed and simulated flows begins with the first event in January 2012, and then continues with the 2 smaller events in February 2012 and the 3 larger events in March 2012. The cumulative runoff volume comparison highlights this divergence (Figure 40). These results highlight a need for model adjustments after prolonged dry periods prior to significant rainfall events.

Flood Events Simulation Performance

During the calibration/verification period there were seven (7) flood events which provided a basis for assessing model performance for flood peaks and related metrics; 3 events occurred during the calibration period and 4 events occurred during the verification period (January to March 2012). Given the 7 gage sites and 7 events there are 49 total events for performance assessment of flood simulations.

To assess model performance at the different stations and in the different storm events, we plotted observed and simulated differences in event runoff volume (%Bias), NSCs, peak flows, and time-to-peak.

%Bias

In general, simulated flood event volumes exceed observed volumes. Several reasons are suggested for this. First, the identified bias in the precipitation forcings was in the range 10% to 20% underestimation. Secondly, events 1, 4 and 5 occur after prolonged dry periods occurring 2/16/2011, 1/23/2012 and 3/14/2012 respectively. It seems that the RDHM does not well represent rainfall abstractions to soil and deeper bedrock moisture replenishment for these events. This phenomenon requires that better estimation of initial moisture conditions be established after prolonged dry periods. Additionally, RDHM soil moisture accounting procedures may be inadequate for the soil and bedrock moisture conditions in the basins.

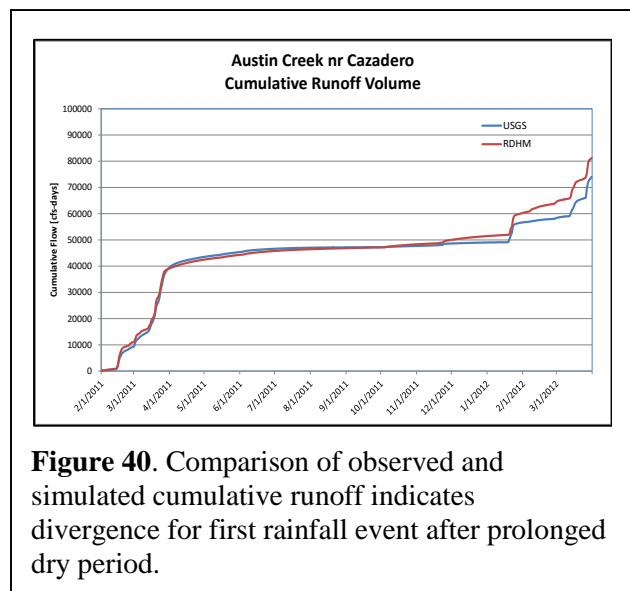


Figure 40. Comparison of observed and simulated cumulative runoff indicates divergence for first rainfall event after prolonged dry period.

Thirdly, several of the basins have reservoirs which can capture significant amounts of runoff, especially after prolonged dry periods when storage levels have been drawn down. The Napa River nr Napa is one example of this as Lake Hennessy (31 KAF, 50 sq. mi.) can control 25% of the upstream flows. However, checking with the City of Napa's Water Division indicates that Lake Hennessy was near capacity throughout the period 2011 - 2012. Water management influences are also suspected for Santa Rosa Creek nr Santa Rosa. Thirdly, it seems evident that flow simulations for the Big Sulfur watershed are a result of precipitation missing the basin.

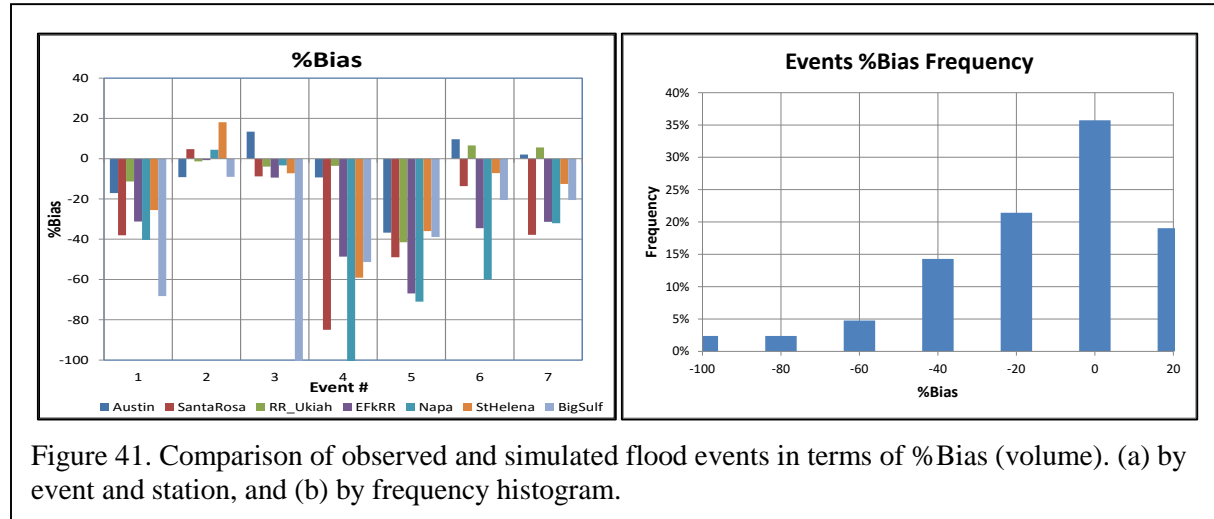


Figure 41. Comparison of observed and simulated flood events in terms of %Bias (volume). (a) by event and station, and (b) by frequency histogram.

Nash-Sutcliff Coefficient

Assessment of RDHM performance based on the Nash-Sutcliff coefficient also presents mixed results (Figure 42). The N-S for approximately one-third of the events exceeds 0.70 which is considered good performance. This is what might be expected when the precipitation is well defined and there are minimal water management influences. There is another third of the events where the model performance moderates as a result of precipitation mis-definition, poor accounting of soil moisture and water management influences. The lower third of event simulations exhibit poor performance; these are considered mainly due to precipitation field mis-placement but may also be influenced by water management and RDHM mis-representation of soil and bedrock moisture dynamics.

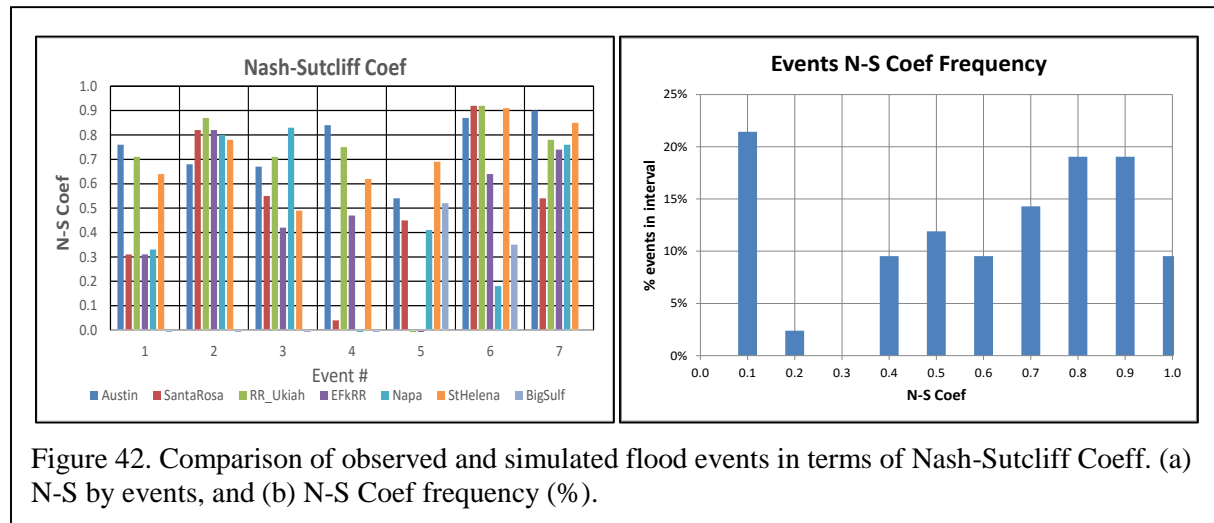


Figure 42. Comparison of observed and simulated flood events in terms of Nash-Sutcliff Coef. (a) N-S by events, and (b) N-S Coef frequency (%).

Flood Peaks

Peak flows generated by the RDHM correlate moderately well with observed discharges although there is a consistent underestimate of the peaks by 10% to 20%. Figure 43 illustrates the correlation between observed and simulated flood peaks for all events. The histogram plot of percent differences in peak flows reinforces the observation that the RDHM generates peak flows that are less than observed. Much of this underestimation can be attributed to underestimation of the precipitation. Other reasons for the differences may be in part ascribed to the 6-hour time step used for the RDHM simulation which would smooth out high intensity rain cells in time and space. (Note that the observed peak flows are tabulated as the maximum of the 6-hr averages of the 15-min observed flows.)

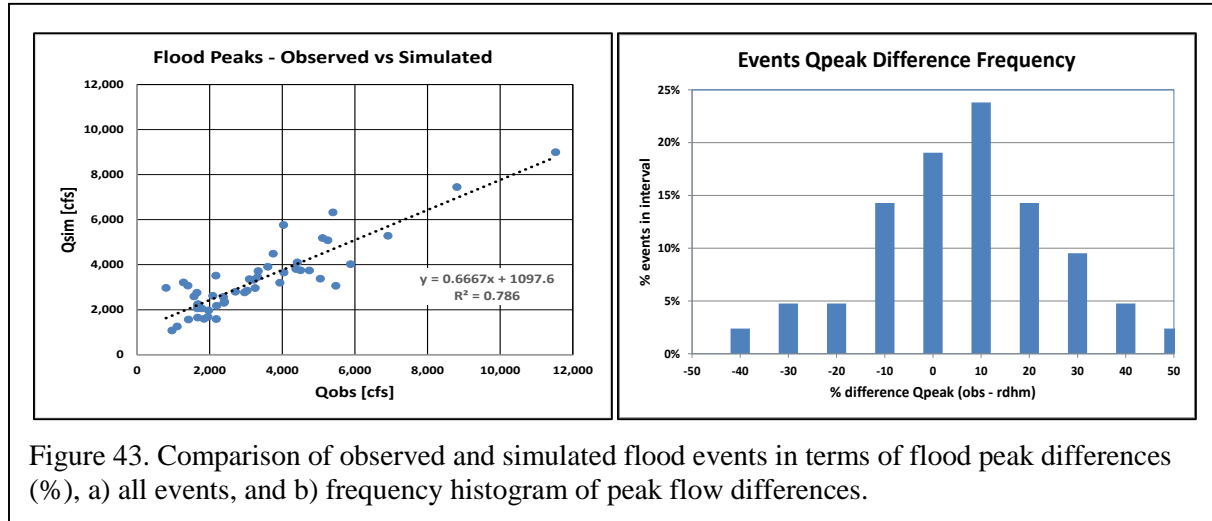


Figure 43. Comparison of observed and simulated flood events in terms of flood peak differences (%), a) all events, and b) frequency histogram of peak flow differences.

Time-to-Peak

Differences in the time-to-peak for the 7 events indicate good correspondence with observed peaks for most sites and events (Figure 44). Notable exceptions to this include a) Event 1 was evidently a poor precipitation definition in the Napa and Santa Rosa basins as the observed flood peak occurred more than 24 hours prior to the simulated event; and b) the Big Sulfur headwater basin had consistently early simulated flood peaks, some in excess of 24 hours (not shown).

Low Flow Simulation Assessment

The ability of the RDHM to simulate low flows in the Russian River tributaries is of interest to fisheries biologists because these flows occur during critical spawning periods for the endangered fish species in the basin. The Sac-HT conceptual model, used by the NWS nationwide, has been used primarily to forecast flood events. However, as a continuous simulation model the Sac-HT was designed to represent the complete hydrologic response for all time periods. In addition, the NWS strategic planning report has established a goal to support ecosystem sustainability and services which would involve forecasting flow conditions for fishes and related aquatic flora and fauna. Therefore, it is of interest to examine how the RDHM does in representing flow regimes relevant to ecosystem services.

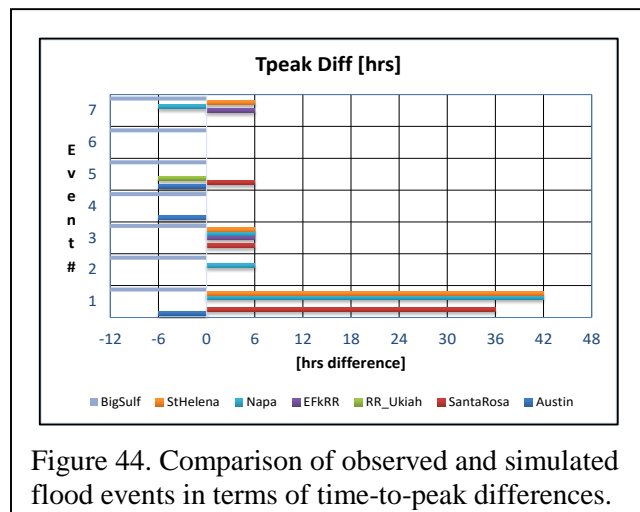


Figure 44. Comparison of observed and simulated flood events in terms of time-to-peak differences.

To accomplish this assessment, the RDHM simulation results were compared to observed flows at a number of stream gage locations. Given the RDHM is a continuous simulation tool it carries forward after flood events to represent the hydrograph recessions and dry period low flows. For this task, 2 USGS gages used for RDHM calibration and verification for flood events are also calibrated for low flow performance. In addition, the NMFS has established 16 low flow gaging sites on tributaries to the main stem Russian River to gather data supportive to their fisheries habitat restoration activities. Given that the NMFS gage sites have not been used for RDHM calibration purposes then the comparison of observed to simulated flows serves as an independent verification of model performance for low flows. It is important to note, however, that the rating curves established for the NMFS sites were for low flows only; extrapolation of the ratings to estimate medium and high flows was not considered valid.

The NMFS gage sites are shown in Figure 45 and listed in Table 11. As presented the sites are listed in descending order by drainage area ranging from 50 sq. to 3.5 sq. mi. An issue for the RDHM is how well the (approx.) 4 km grids correspond to the gaged watershed drainage areas. Noted in the table is the number of RDHM grids in each watershed. To account for the differences in drainage area the RDHM flows were scaled by the ratio of drainage areas.

Various statistics and graphics were computed to make the comparison between the simulated and observed low flows. Figure 46 illustrates the procedures for the W. Br. Russian River. Analysis tableaus for the other stations are included in Appendix B.

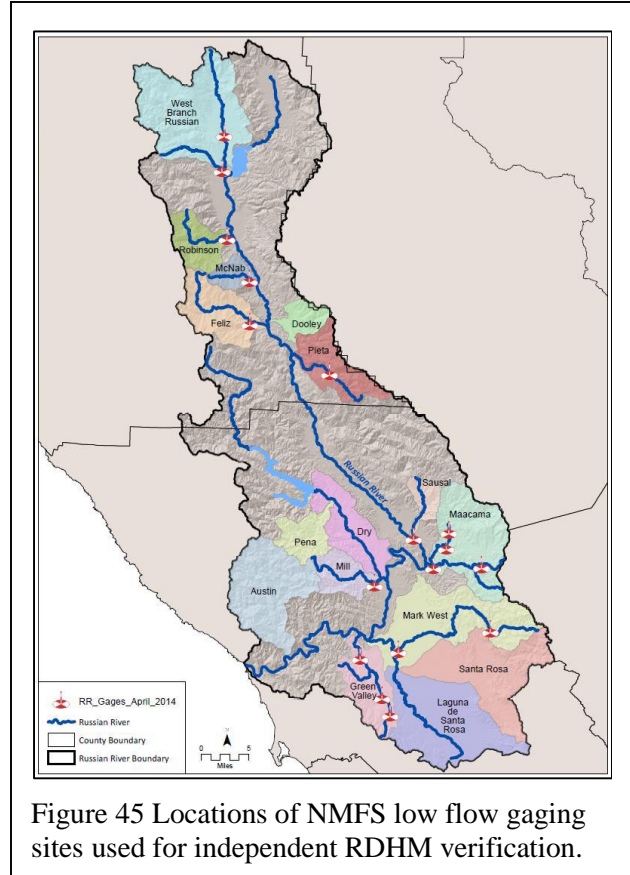


Figure 45 Locations of NMFS low flow gaging sites used for independent RDHM verification.

Figure 46 illustrates procedures for comparison of RDHM and observed flows – W.Br. Russian River. Table 12 and Figure 47 show summary statistics for the low flow comparisons at the 15 NMFS gaging sites and the 3 USGS sites. Focused low flow calibration efforts were applied for the USGS sites at Austin Cr nr Cazadero and the W.Br. Russian River nr Ukiah. Correlations between observed and simulated low flows are quite high averaging 87%. Nash-Sutcliff Coefficients (NSE) exhibit wide variability. Low flow bias expressed in terms of cubic feet per second per sq. mi (cfs/mi) averages -0.55 cfs/mi with StdDev of 1.09 cfs/mi. These

statistics are strongly influenced by large positive bias values for sites 5 (Pena Cr) and 15 (Mill Cr). Ignoring these sites then the average bias is 0.12 cfs/mi (StdDev 0.41 cfs/mi). Twelve (12) of the 15 NMFS sites have positive biases (80%) indicating that the RDHM consistently underestimates low flows. Noteworthy is that the two calibration sites at USGS gages have average low flow bias of -0.015 cfs/mi. The Austin Creek basin (Site 17) has a low flow bias of -0.010 cfs/mi (equivalent to 0.83 cfs for the 62.8 sq. mi. basin); this basin was the focus of extended calibration efforts and indicates the best correspondence between observed and simulated flows that might be obtained.

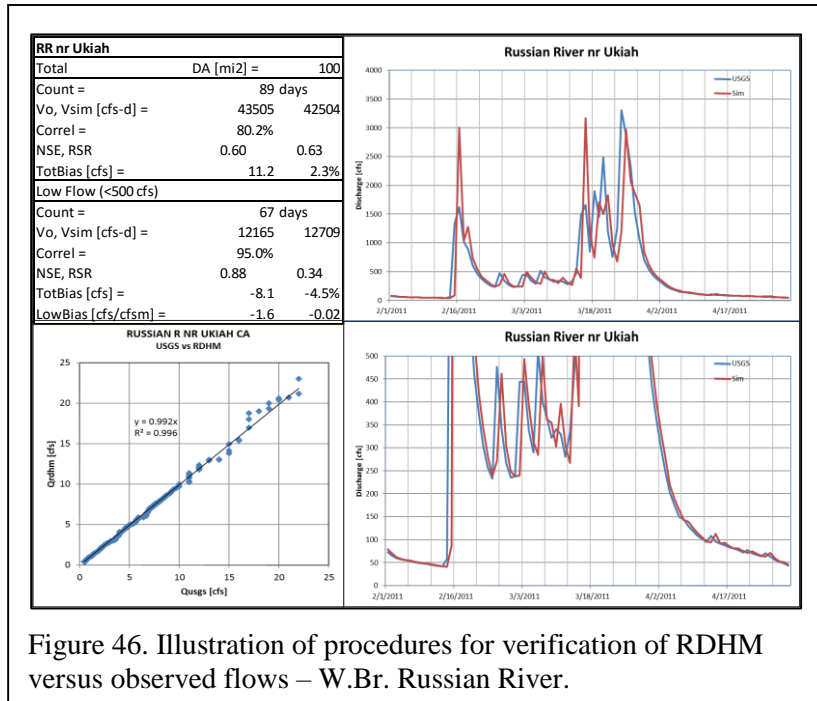


Figure 46. Illustration of procedures for verification of RDHM versus observed flows – W.Br. Russian River.

Table 11. Streamflow gaging stations used for low flow verification. (Note: Stations 16, 17, 18 were used for the RDHM calibration presented above.)

#	NMFS Sites	Lat	Long	Area				HRAP Grids
				Area (sq mi)	Area (sq km)	RDHM (sq km)	Area Ratio [%]	
1	Mark West Creek at River Road	38.48192	-122.83276	50.2	130.0	136.7	-5.2%	8
2	Green Valley Creek near Martinelli Road	38.48923	-122.91888	37.4	96.9	85.3	11.9%	5
3	Feliz Creek nr Hopland	38.97228	-123.14197	31.2	80.8	51.7	36.0%	3
4	Franz Creek at Chalk Hill Road	38.60990	-122.76930	23.0	59.6	51.3	13.9%	3
5	Pena Creek	38.70154	-122.96856	22.7	58.8	68.5	-16.5%	4
6	Dooley Creek	38.97137	-123.08109	14.9	38.6	51.7	-34.0%	3
7	Redwood Creek at HWY 128	38.64013	-122.74559	14.0	36.3	34.3	5.4%	2
8	Mark West Creek at Calistoga Road	38.51628	-122.65521	13.7	35.5	34.1	3.9%	2
9	Atascadero Creek at Mill Station Road	38.38467	-122.84532	13.6	35.2	34.1	3.2%	2
10	Sausal Creek at E. Soda Rock Ln	38.65380	-122.80954	12.6	32.6	34.3	-5.1%	2
11	York Creek at N. State Street	39.20339	-123.20685	11.7	30.3	34.6	-14.2%	2
12	McNab Creek	39.03798	-123.14634	8.3	21.5	17.2	20.0%	1
13	Atascadero Creek at Water Trough Road	38.41088	-122.86180	4.8	12.4	51.1	-311.0%	3
14	Bidwell Creek at Laufenburg Ranch	38.61389	-122.67598	4.6	11.9	17.1	-43.5%	1
15	Mill Creek below Felta Creek	38.58075	-122.88283	3.5	9.1	17.1	-88.6%	1
16	Santa Rosa Creek at Santa Rosa	38.43667	-122.72361	57.0	147.6	136.5	7.5%	8
17	Austin Creek nr Casadero	38.50667	-123.06861	62.8	162.7	188.1	-15.7%	11
18	West Branch Russian River nr Ukiah	39.19556	-123.19389	100.0	259.0	242.3	6.4%	14

Note in Figure 46 the correlation between the RDHM flows and the USGS gage flows is very high. This affirms the accuracy of the RDHM when calibrated. This correlation also allows the long term flow statistics at the USGS gage site to be used. The RDHM can represent a given flow regime (e.g. mean annual flow) at the gage; it also provides a rationale for determining what the MAF may be at any location within the watershed upstream.

A caveat on estimating low flows is that this flow regime can be strongly influenced by water management practices of diversions, return flows and releases from storage. Note in Figure 4 (b) that the observed flows indicate fluctuations attributable to water management operations for which no data exists. To accurately account for these factors requires modeling of these water management practices which in turn requires accurate data on what these practices entail. An application of such water management modeling is included in the next section of this report.

An additional way to assess the RDHM performance is to compare the model results with another numerical hydrological model. The Basin Characterization Model (BCM) has been developed by the USGS (Flint et al 2015, Flint and Flint 2012) to assess the impact of climate change on stream flows in the Russian and Eel River basins. The BCM was applied using climate model forcings downscaled to a 270-m grid cell resolution to generate daily unimpaired flows. One location where the BCM model outputs could be compared to the RDHM was the Russian River nr Ukiah (USGS 11461000). The flow recession period for June - September for 2011 and 2012 was used for comparison of the RDHM and BCM model results with the USGS gaged flows. Focused RDHM calibration efforts were applied for the 2011 recession period (Figure 48 (a)) and a close correspondence with gaged flows was obtained. Without focused calibration efforts the RDHM correspondence to gaged low flows can be poor as shown for the dry-down period in 2012 (Figure 48(b)).

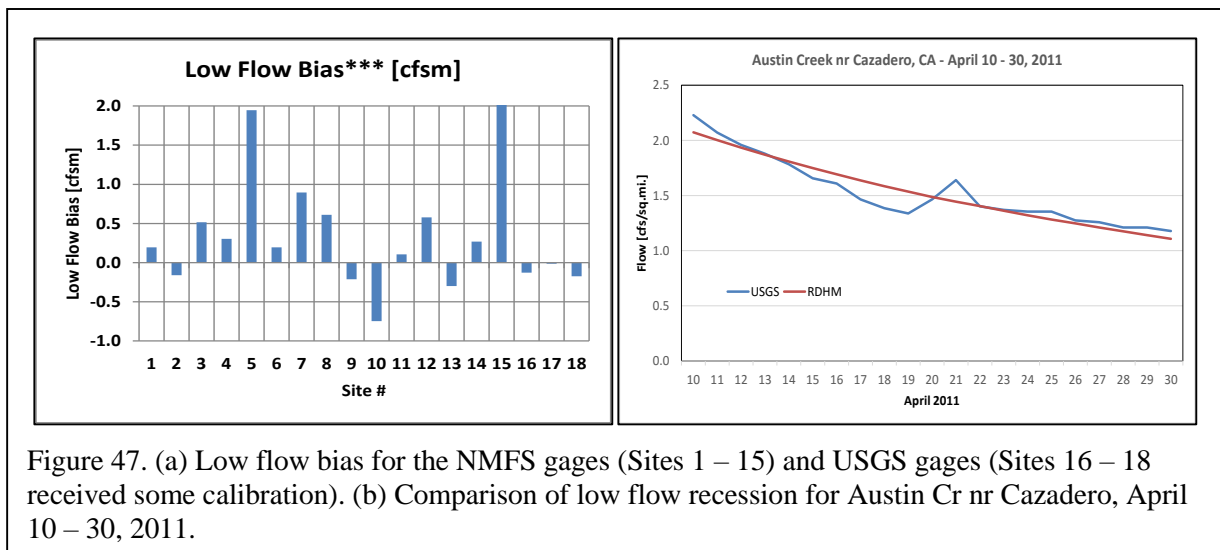


Figure 47. (a) Low flow bias for the NMFS gages (Sites 1 – 15) and USGS gages (Sites 16 – 18 received some calibration). (b) Comparison of low flow recession for Austin Cr nr Cazadero, April 10 – 30, 2011.

Table 12. Low flow verification statistics.

#	NMFS Sites	Low Flow	Low Flow	Low Flow	Low Flow	Low Flow	Low Flow	Total	Rating	Low Flow	Low Flow
		Correl** [%]	NSE**	Bias** [cfs]	Bias** [%]	Bias*** [cfs]	Bias*** [cfsm]	Bias* [cfs]	Bias** [cfs]	Bias** [cfs]	Bias [cfs]
1	Mark West Creek at River Road	92.3%	-0.08	1.77	4.1%	9.7	0.19	91.9	1.8	9.7	0.19
2	Green Valley Creek near Martinelli Road	80.9%	-1.69	-8.29	-63.4%	-6.1	-0.16	9.3	8.3	6.1	0.16
3	Feliz Creek nr Hopland	86.7%	0.65	14.67	25.5%	11.8	0.52	0.3	14.7	11.8	0.52
4	Franz Creek at Chalk Hill Road	95.6%	0.88	-2.70	-4.9%	7.0	0.30	27.8	2.7	7.0	0.30
5	Pena Creek	76.1%	-1.18	25.78	48.8%	24.5	1.95	33.7	25.8	24.5	1.95
6	Dooley Creek	92.9%	-1.62	9.58	69.5%	2.9	0.19	17.5	9.6	2.9	0.19
7	Redwood Creek at HWY 128	91.0%	-0.08	3.75	10.4%	12.5	0.90	17.7	3.7	12.5	0.90
8	Mark West Creek at Calistoga Road	86.2%	0.36	-0.63	-2.5%	8.3	0.61	20.0	0.6	8.3	0.61
9	Atascadero Creek at Mill Station Road	81.7%	0.65	0.45	3.0%	-2.9	-0.21	7.5	0.5	2.9	0.21
10	Sausal Creek at E. Soda Rock Ln	81.2%	0.42	7.99	23.1%	9.4	0.75	0.2	8.0	9.4	0.75
11	York Creek at N. State Street	96.3%	0.32	-2.04	-18.5%	1.2	0.11	29.1	2.0	1.2	0.11
12	McNab Creek	80.6%	-0.14	5.13	42.5%	4.8	0.58	12.8	5.1	4.8	0.58
13	Atascadero Creek at Water Trough Road	91.1%	0.59	-1.33	-12.6%	-1.4	-0.30	4.2	1.3	1.4	0.30
14	Bidwell Creek at Laufenburg Ranch	92.0%	0.26	-3.12	-32.0%	1.2	0.27	5.6	3.1	1.2	0.27
15	Mill Creek below Felta Creek	83.0%	-0.33	25.74	61.5%	15.3	4.38	9.0	25.7	15.3	4.38
16	Santa Rosa Creek at Santa Rosa	88.2%	0.45	-16.40	-27.3%	-7.3	-0.13	30.8	16.4	7.3	0.13
17	Austin Creek nr Casadero	75.8%	0.52	0.90	0.9%	-0.8	-0.01	11.6	0.9	0.8	0.01
18	West Branch Russian River nr Ukiah	87.6%	0.75	-2.50	-3.1%	-1.6	-0.02	6.0	2.5	1.6	0.02
Average		87%	0.04	3.3	7%	4.9	0.6	18.6	7.4	7.2	0.6
StDev		6%	0.79	10.6	34%	8.2	1.1	21.1	8.2	6.2	1.0
Max		96%	0.88	25.8	70%	24.5	4.4	91.9	25.8	24.5	4.4
Min		76%	-1.69	-16.4	-63%	-7.3	-0.3	0.2	0.5	0.8	0.0
Calibration Sites		Average	82%	0.63	-0.80	-1%	-1.21	8.82	1.70	1.21	0.015
		StDev	8%	0.17	2.40	3%	0.55	3.99	1.13	0.55	0.002

* Total series period is 1 Feb 2011 - 30 Apr 2011 when available
** Rating flow series is below upper limit of NFS rating curve
*** Low flow is April 15 - April 30 recession period

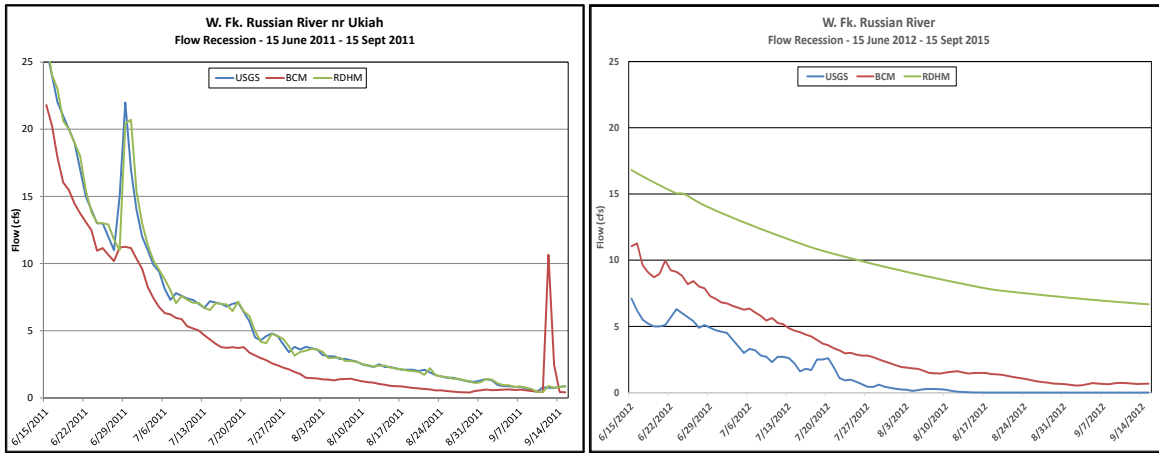


Figure 48. Comparison of RDHM and BCM simulations of daily flows with USGS observed flows at the W.Br. Russian River nr Ukiah gage (a) June 15 – Sept 15, 2011 (calibration period), and (b) June 15 – Sept 15, 2012 (not calibrated).

The CDFs support characterization of the likelihood that RDHM low flow predictions can be expected to be within a given range; or greater or less than a given value. For example, if the RDHM predicts a flow of 20 cfs at a location having drainage area of 100 sq. mi., then (using Curve E - Calibrated) the 95% confidence interval would be 22 cfs to 18 cfs. If Curve D (Best 1/2 of stations) is used the range is 60 cfs to 0 cfs. The likelihood that the flow is zero can also be estimated. Using the same estimated flow of 20 cfs, the likelihood that the flow is zero using The Calibrated curve (D) ($X=-0.04$ cfs, $StDev = 0.178$ cfs; $z = 1.3$) is 9%. Using Curve E, the likelihood of zero is 0%.

4.4 Assessment of Multi-Radar Multi-Sensor Precipitation (MRMS) Products

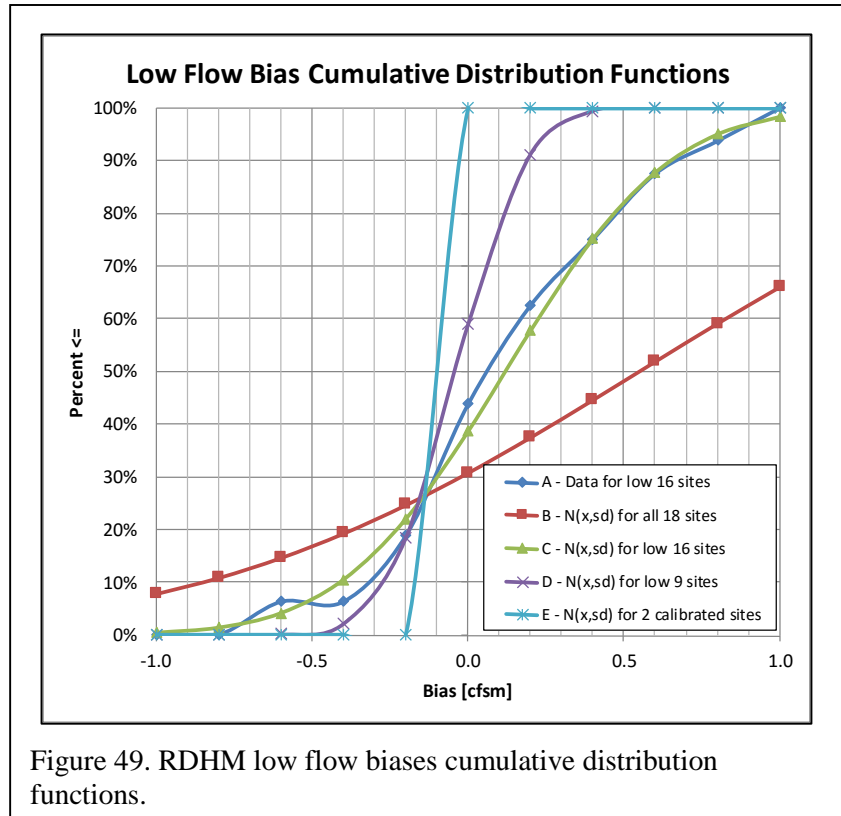
As noted earlier, a companion study (Willie et al 2015) involved the use of radar-rainfall imagery to map precipitation distribution across the basin using the MRMS procedures (see description above). Briefly, data for 2012 and 2014 rainfall events were used to assess KPIX radar calibration relative to NEXRAD (KDAX and KMUX) and the S-Prof/disdrometers at DVS and STR. A combination of radar and rain gauge data were gathered in order to assess the impact of KPIX on QPE in the Russian. The data were used as input to the MRMS and included:

- 4 NEXRAD WSR-88D radars: KBHX, KBBX, KDAX, and KMUX (Level II data files obtained from NCDC).
- KPIX, non-NEXRAD radar, operating at C-band frequency (data obtained from NSSL).
- 61 analysis gauges (used to generate QPE grids) obtained from the California Data Exchange Center (CDEC).
- 10 independent gauges that are a combination of NOAA HMT and HADS gauges.

The MRMS generated a suite of QPE mappings using various combinations of radars and rain gages (Figure 49). These QPE were then applied to the RDHM to determine which method provided the best runoff simulations. Several scenarios were assessed to examine the influence of distance from the radars and locations of rain gages.

Rainfall fields generated by both radar with gauge correction and radar with vertical profile of reflectivity (VPR) & gauge correction (GC) products were evaluated (Figure 51). For the 2012/11/28 event at the Austin Creek station, the VPR-GG correlation product showed the better timing. The impacts of the rain gauge locations for the 2014/12/04 event at the Austin Creek station showed that the “radar with VPR and gauge correction” product is optimal. Addition of VPR correction improves precipitation estimation for the locations farther away from the radar station, especially for moderate events. Radar only products, regardless the absolute precipitation depth, showed marginally better simulation timing.

With the RDHM calibrated, both the “Radar with Gauge Correction” and “Radar with Gauge and VPR Correction” products exhibited the best skill with average Nash–Sutcliffe coefficients (NSCs) 0.84 and 0.86, respectively, for the seven evaluation events (Figure 50). The Radar-Only data produced the worst NSCs. For the sub-watersheds far away from the radar, the quality of the “Radar with VPR and Gauge Correction” products in simulating hydrologic responses became especially apparent.



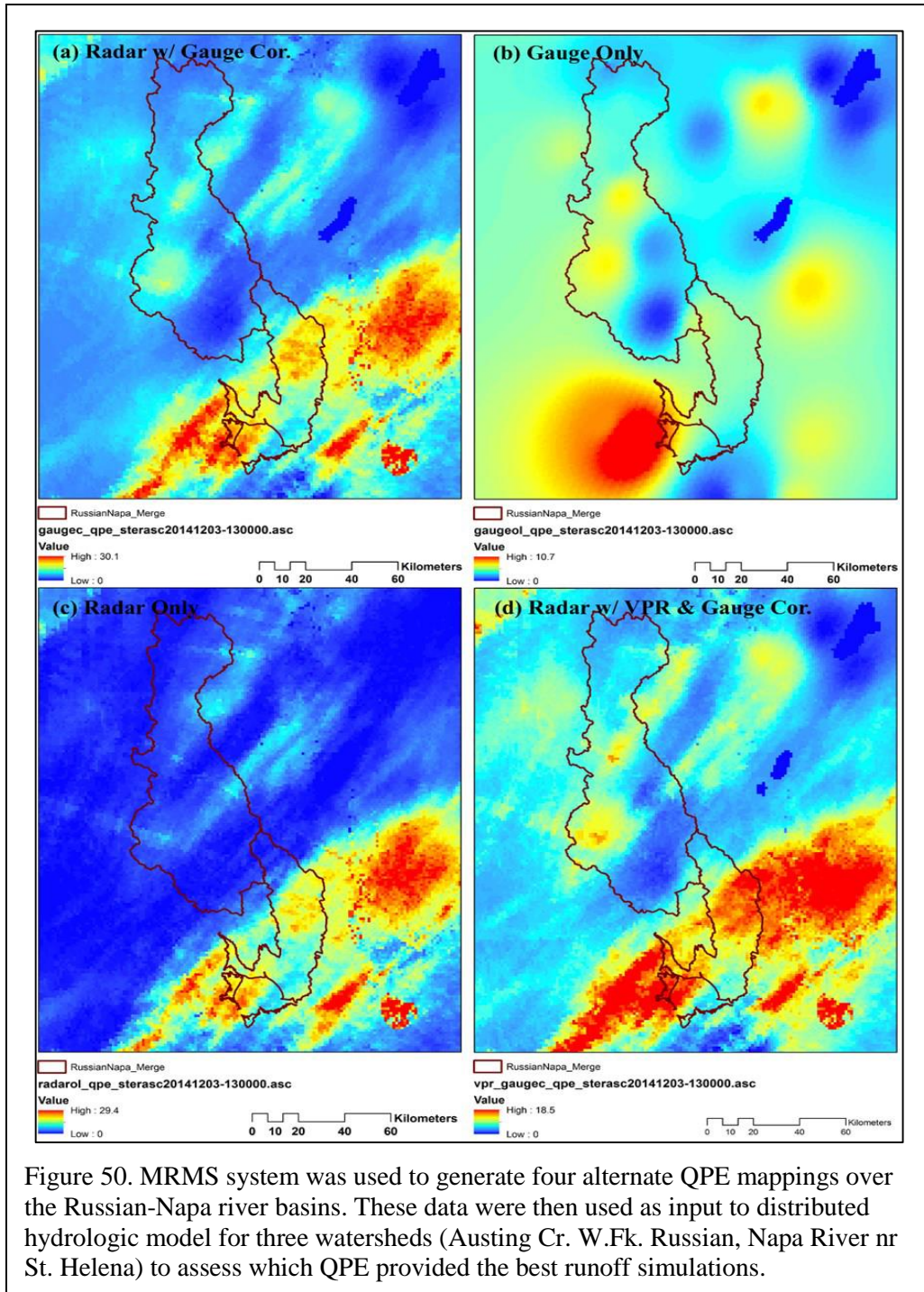


Figure 50. MRMS system was used to generate four alternate QPE mappings over the Russian-Napa river basins. These data were then used as input to distributed hydrologic model for three watersheds (Austing Cr. W.Fk. Russian, Napa River nr St. Helena) to assess which QPE provided the best runoff simulations.

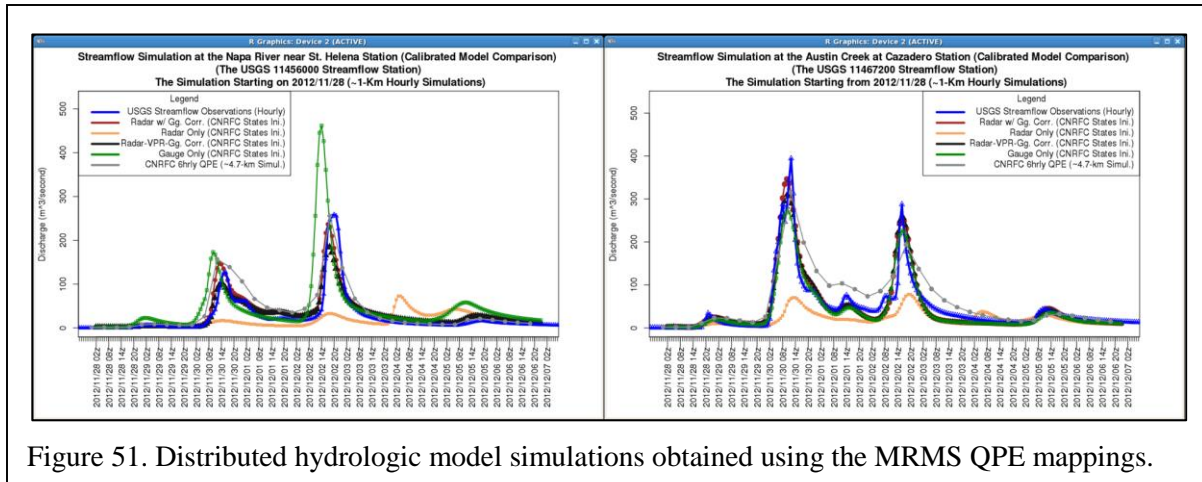


Figure 51. Distributed hydrologic model simulations obtained using the MRMS QPE mappings.

4.5 Comparison of 4 km and 1 km RDHM simulations

Comparing with the models at the HRAP resolution (~4.1-km at the Russian River basin), high-resolution simulations (~1-km) ordinarily result in better discharge simulations (Figure 52). However, there are still differences between 1-HRAP and 1/16 HRAP models. The difference can be minor or moderate depending on the variations of the hydrologic states through the simulation period and the shape of the watershed boundary (i.e. how much difference that a watershed be delineated by the 1-HRAP against 1/16-HRAP connectivity file). For the events dominated by the tension water capacities

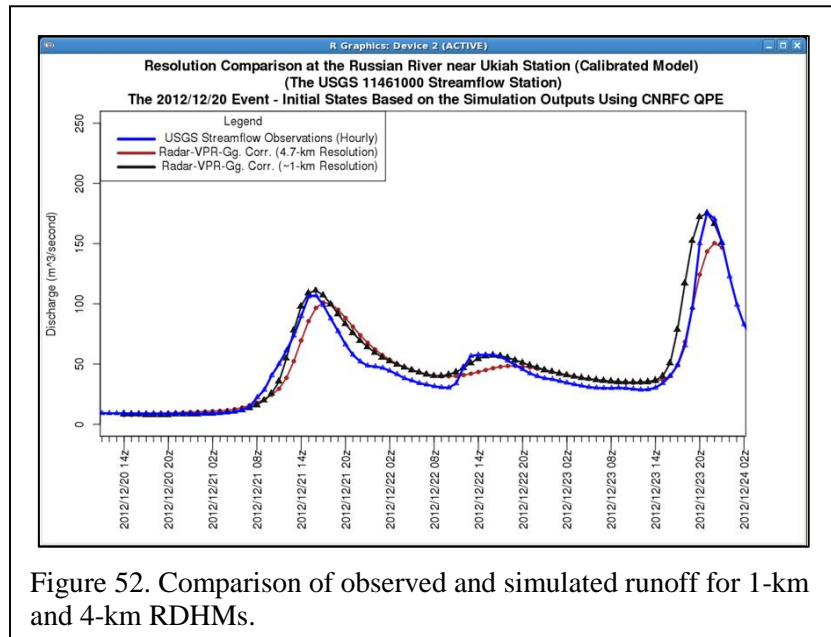


Figure 52. Comparison of observed and simulated runoff for 1-km and 4-km RDHMs.

(UZTWM or LZTWM) and occurred in the watersheds with high saturated hydrologic conductivity (K_s), for instance, the difference of the simulated discharge between both models is significant. For the events dominated by soil types or free water functions, on the other hand, the difference between both of the models become smaller. Generally, 1/16-HRAP models always generate discharge more comparable to the USGS observations than the 1-HRAP models. Thus, a conclusion can be drawn: with flow courses and drainage areas more closely imitating the corresponding features in real world, high resolution simulations can improve discharge estimation. The effect of resolution on hydrograph is especially vibrant for the first peak flow event after longer dry period.

4.6 Comparison of Observed and Simulated Soil Moisture

Soil moisture observations have been compared with soil moisture values simulated using the RDHM (Zamora 2015). The model was run using the default a priori soils and routing parameter estimates and the CNRFC operational 6-h gridded surface air temperature and precipitation forcing fields. Regression

analysis has been used to quantify the differences found between the RDHM simulated soil moisture values and the HMT soil moisture observations during a 394-day simulation. Results of this study suggest that RDHM skill varies by season in the Russian River basin, showing the best skill during early spring, summer, and late summer. The use of RDHM to help identify soil moisture stations with strong observational bias was also addressed.

Koren et al. (2007) showed that soil moisture simulated by SAC-HT had a higher bias than the Mosaic (Mitchell et al. 2004; Koster and Suarez, 1996) or Noah (Ek et al. 2003) Land Surface Models (LSM) when compared with the observations in the Oklahoma Mesonet. SAC-HT performance tended to be weakest in dry basins, and at the lower soil levels. When a climate adjustment to the SAC-HT a priori non-frozen parameters was used, the biases were reduced. Koren et al. speculated that the lack of a root-zone treatment of evapotranspiration in SAC-HT contributed to the bias. Later work completed by Koren et al. (2008) showed that soil moisture observations could be used to improve parameter consistency in watershed calibrations without reducing the accuracy of the outlet hydrograph. Koren et al. also found that the improvements in the SAC-HT simulations were strongest in dry watersheds where there is no strong direct interconnection between basin runoff and soil moisture.

Soil moisture observations from the Oklahoma Mesonet were also used to test the impact of the a priori soil physical parameters on RDHM/SAC-HT simulations of streamflow by Zhang et al. (2012). Zhang et al. concluded that SAC-HT soil moisture simulations that used the U.S. Department of Agriculture National Resources Conservation Service USDA NRCS Soil Survey Geographic database (SSURGO) derived a priori SAC-HT parameters, resulted in the best overall simulations when compared with the observations. Once again OHD investigators found that SAC-HT had difficulty simulating soil moisture in the SAC-HT lower zone. Lee et al. (2011) evaluated the impact of assimilating streamflow and soil moisture observations from the Oklahoma Mesonet, on RDHM/SAC-HT simulations of streamflow and soil moisture. Lee et al. found that assimilating soil moisture observations into RDHM did not significantly improve the streamflow simulations. But that the assimilation of soil moisture helped reduce systematic bias in the soil moisture simulations. Lee et al. speculated that their results could be a result of their implementation of data assimilation (DA), which resulted in a significantly underdetermined inverse problem. They also suggested that structural and parametric errors in hydrological models, observational uncertainty, and soil heterogeneity not represented in the a priori physical parameters could also explain their somewhat counter-intuitive results.

The HMT configuration of SAC-HT output the simulated soil moisture values at depths of 10 and 15 cm. The depths are the same depths used in the HMT soil moisture observing network. The 2-minute soil wetness fraction estimates at each HMT observing location were block averaged over a 6-hour time interval and compared with the RDHM 6-h simulation values. The RDHM values were extracted from the HRAP cell nearest the HMT observing locations. The soil wetness fraction estimates at 10 and 15 cm simulated by SAC-HT were compared with each other during the entire simulation. Very little difference in the soil moisture estimated at those depths was found. This finding is consistent with the idea that both of these physical depths lie in the SAC “upper tank” after the physical soil depths are mapped to the SAC “tanks.” As mentioned earlier, additional probe depths have been added to some of the HMT observing locations after 12 March 2012. In this study the comparison was only carried out between the SAC-HT 15 cm simulation depth and the 15 cm HMT observational depth.

Time series from six of the validation locations are shown in Figure 53. The observed and simulated soil moisture comparison indicates that RDHM reproduces precipitation driven soil moisture increases, and the subsequent infiltration/drydown events. However, it is obvious that a systematic offset exists at most validation points. The offset is large during late spring and summer. It is also very pronounced in the October – January time frame. The large discrepancy found at the WLS observing location (Figure 53 (a)) at the start of the RDHM run is related to the “cold start.” The WLS evaluation point lies in the watershed's uppermost HRAP cell. The delayed response of the RDHM soil state to precipitation during

this time period is directly related to “spin up”, and the course channel routing imposed by 4-km HRAP grid.

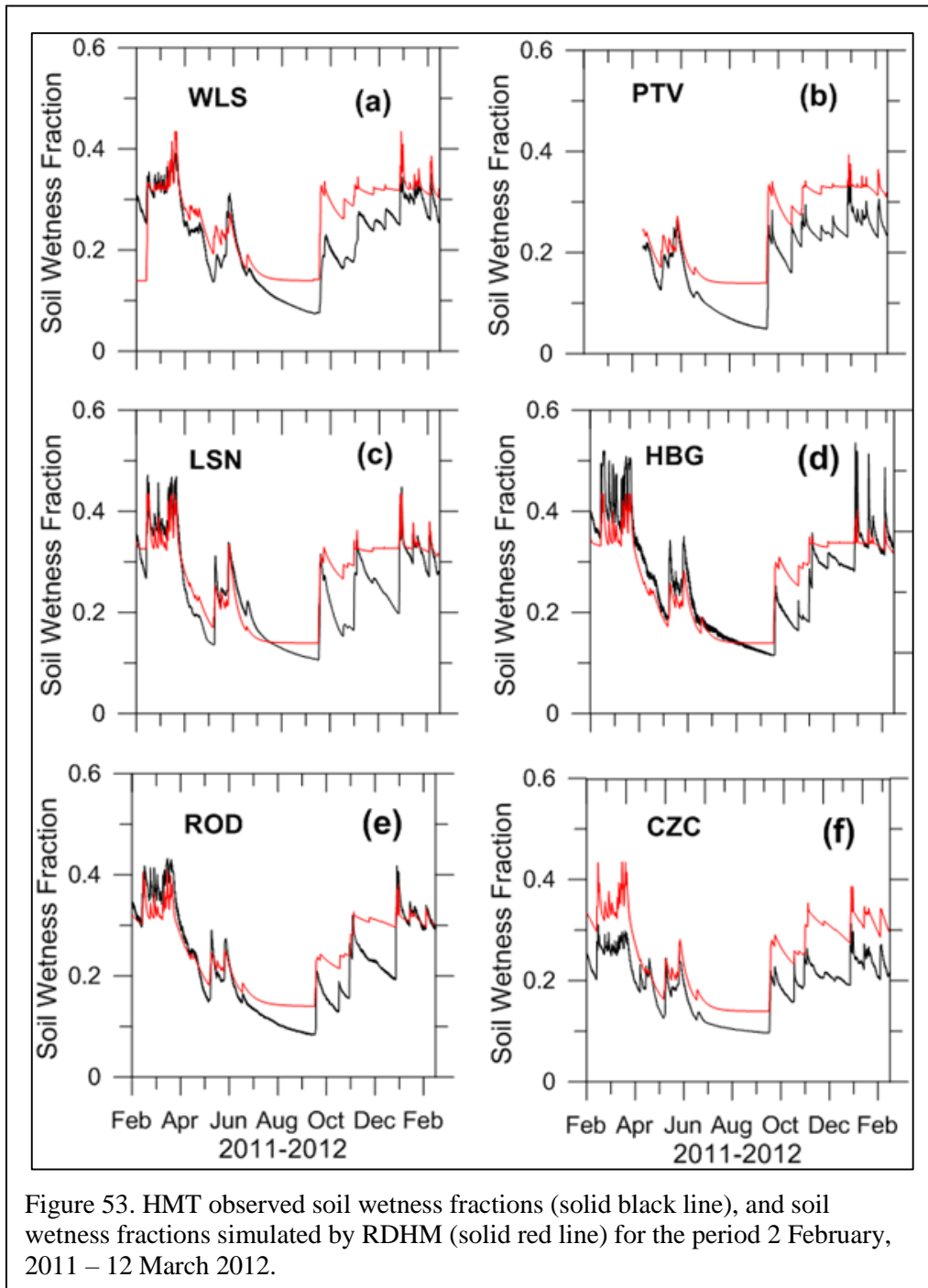


Figure 53. HMT observed soil wetness fractions (solid black line), and soil wetness fractions simulated by RDHM (solid red line) for the period 2 February, 2011 – 12 March 2012.

Another notable feature of the comparison is the way RDHM reproduces the late spring and summer soil dry-down. The observations indicate that in the absence of precipitation, the soils in the upper 15.0 cm of the basin dry to a minimum soil wetness fraction that lies between 0.1 and 0.08 (10.0 – 8.0% VWC). RDHM does not replicate this basin dry-down characteristic. Instead the model reaches the lowest seasonal VWC in early June. After that time the model maintains that value until the first fall/winter season precipitation event.

The correlation between the HMT observations and the RDHM simulated soil wetness simulated values was carried out for each HMT station in the basin for the entire analysis period (Figure 52(b)). The statistics clearly indicate that RDHM can simulate upper zone soil wetness with considerable skill when the entire analysis period is considered. The overall model bias ranges from -0.06 to -0.03 soil wetness fraction. The correlation coefficients range from 0.91 to 0.67. The lowest R2 was found at HLD.

When one compares the mean values of soil wetness fraction from both the simulation and the observations at HLD, there is no indication that the RDHM tendency to overestimate soil moisture differs from any other observational location. However, the time-series (Figure 54) and regression analysis indicate that the model systematically underestimates (~ 10% VWC) and overestimates (~ 10% VWC) soil water content after the initial mid-October rainfall events.

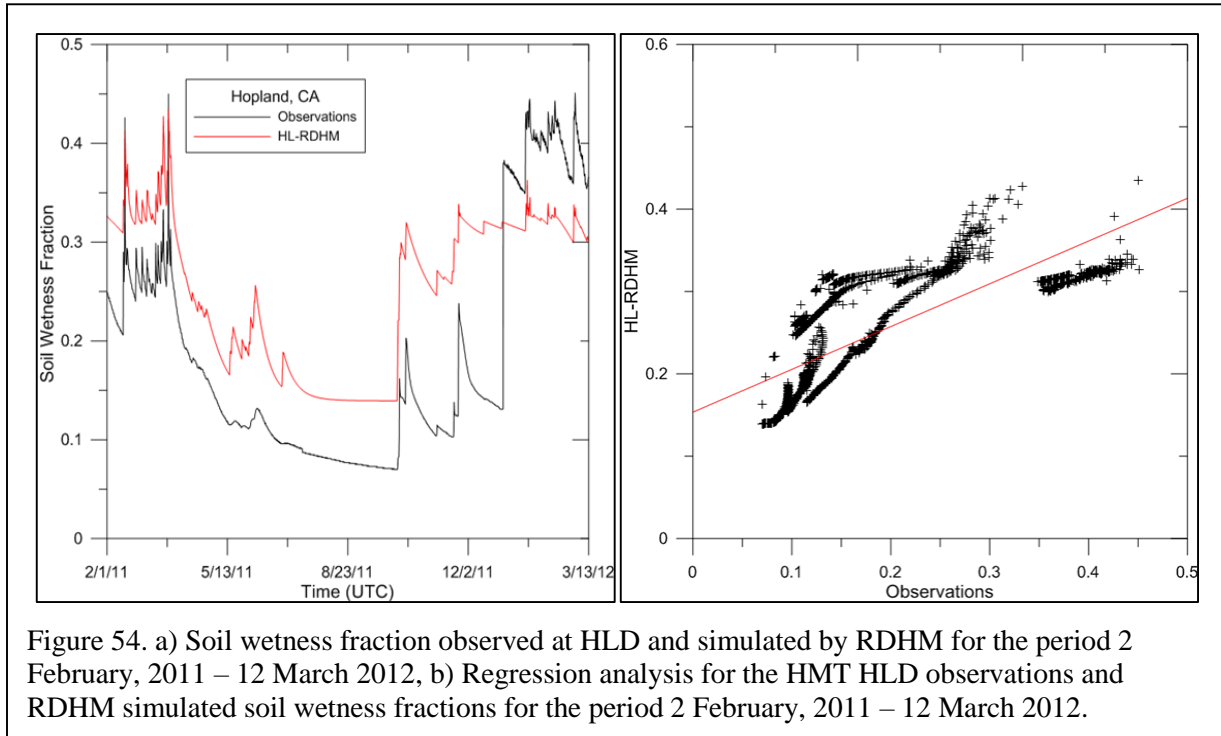
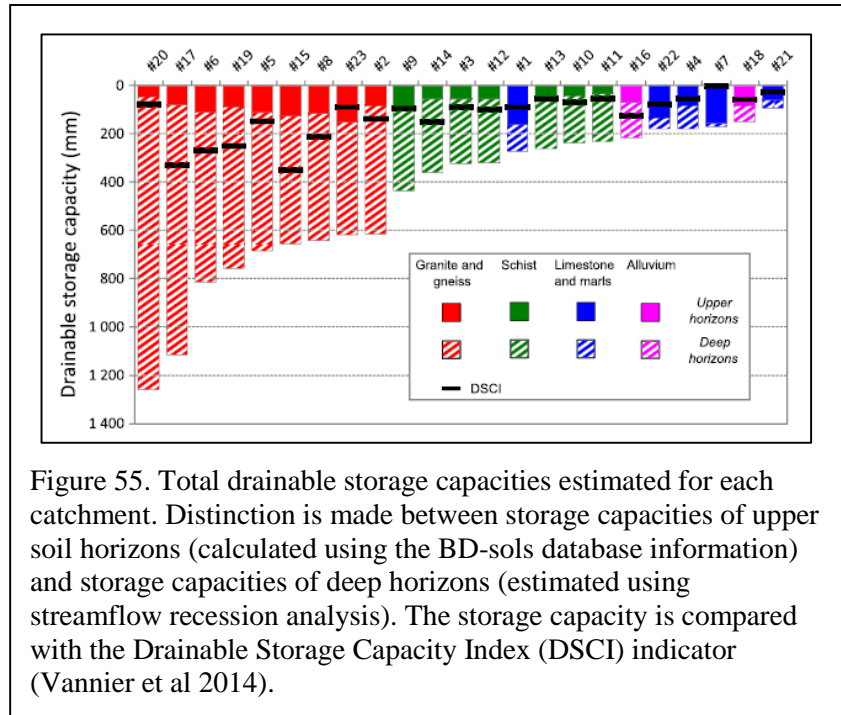


Figure 54. a) Soil wetness fraction observed at HLD and simulated by RDHM for the period 2 February, 2011 – 12 March 2012, b) Regression analysis for the HMT HLD observations and RDHM simulated soil wetness fractions for the period 2 February, 2011 – 12 March 2012.

Consideration of the deeper soil and bedrock influences beyond the shallow soils which can play a major role in subsurface water transfer and storages was addressed by Vannier et al (2014). They used streamflow recession analysis to estimate obtain an estimation of the drainable storage capacity of weathered rock horizons. For the catchments studies, upper soil presents a drainable storage capacity lower than 200 mm, but the whole storage capacity (upper + deep horizons) ranges from 600 to 1200 mm (Figure 54 X). It seems that the Russian-Napa basins have bedrock geologic conditions similar to the watersheds studied by Vannier et al. and that it may be that storage capacities are in the range 600 to 1200 mm. Application of the streamflow recession approach to the Russian-Napa basins is on-going.



5. RDHM APPLICATIONS

Several applications of the DM simulation model have been accomplished to address topics of interest for forecast operations. These include 1) threshold frequency, 2) integration with a water management model, 3) implementation

5.1 Threshold Frequency Application

The RDHM has been developed to include the concept of threshold frequency (TF) which represents flood flows for each grid translated to their equivalent flood frequency, or recurrence interval (Reed et al 2007). It is intended to provide a more understandable representation of the criticality of the flows in terms that forecasters and the general public can better understand. Procedures for estimating the TF values typically involve long term simulations of surface runoff using gridded precipitation data sets. This approach requires extensive data compilation and computer processing which can be difficult and time consuming.

An alternate way to derive the gridded TF estimates was applied using the USGS flood frequency regional regression analysis of basin characteristics (Gotvald et al 2012, Pelle et al 2014). The USGS approach used generalized least squares regression to develop a set of equations for estimating flows with 50-, 20-, 10-, 4-, 2-, 1-, 0.5-, and 0.2-percent annual exceedance probabilities for ungaged basins in California. These equations for the North Coast region of California (Table 13) were applied to each grid of the RDHM model, each of which has a drainage area and mean annual precipitation value based on the PRISM (Daly 1994, <http://www.prism.oregonstate.edu/normals/>).

The regression equations developed by Gotvald were used to validate results produced by HRAP grids in RDHM. Six of the nine USGS gages examined by Gotvald performed well when calculated with the HRAP grids. The poor performance of the other three gages can be attributed to the low resolution of the 4km HRAP grid and PRISMs poor performance at those gages at higher elevations (>2000 feet).

Using the flows calculated for the eight frequency intervals from Gotvald's regression equations for the North Coast, logarithmic equations were fitted for each HRAP grid. From these equations, the frequencies of flows from RDHM were calculated for each HRAP grid (Figure 55(a)). The approach applied is considered a feasible and efficient way to generate the TF values for any location where the USGS regression analyses have been developed.

Simulated flows for each grid output from the RDHM for a moderate flood event in December 2012 were then translated to the corresponding flow frequency to generate a time series of TF for the event. RDHM six-hour output was obtained for each HRAP grid within the Russian River basin and then fitted with a logarithmic equation. From these equations, storm event frequency was determined for each HRAP grid discharge value from December 2, 2012 to December 3, 2012 in six hour increments. Figure 55(b) illustrates the results for the peak flows for this event. Results show that the extreme ends of small tributary flow branches are most at risk for flooding despite their low flow values.

Table 13. USGS regional regression equations for California North Coast Region flood frequencies. Drainage area (mi²) and precipitation (inches) (after Gotvald et al 2012).

Percent annual exceedance probability [%]	Recurrence interval [years]	Regression Equations North Coast (Region 1)
50	2	$1.82(\text{DRNAREA})^{0.904}(\text{PRECIP})^{0.983}$
20	5	$8.11(\text{DRNAREA})^{0.887}(\text{PRECIP})^{0.772}$
10	10	$14.8(\text{DRNAREA})^{0.880}(\text{PRECIP})^{0.696}$
4	25	$26.0(\text{DRNAREA})^{0.874}(\text{PRECIP})^{0.628}$
2	50	$36.3(\text{DRNAREA})^{0.870}(\text{PRECIP})^{0.589}$
1	100	$48.5(\text{DRNAREA})^{0.866}(\text{PRECIP})^{0.556}$
0.5	200	$61.0(\text{DRNAREA})^{0.863}(\text{PRECIP})^{0.531}$
0.2	500	$79.3(\text{DRNAREA})^{0.860}(\text{PRECIP})^{0.503}$

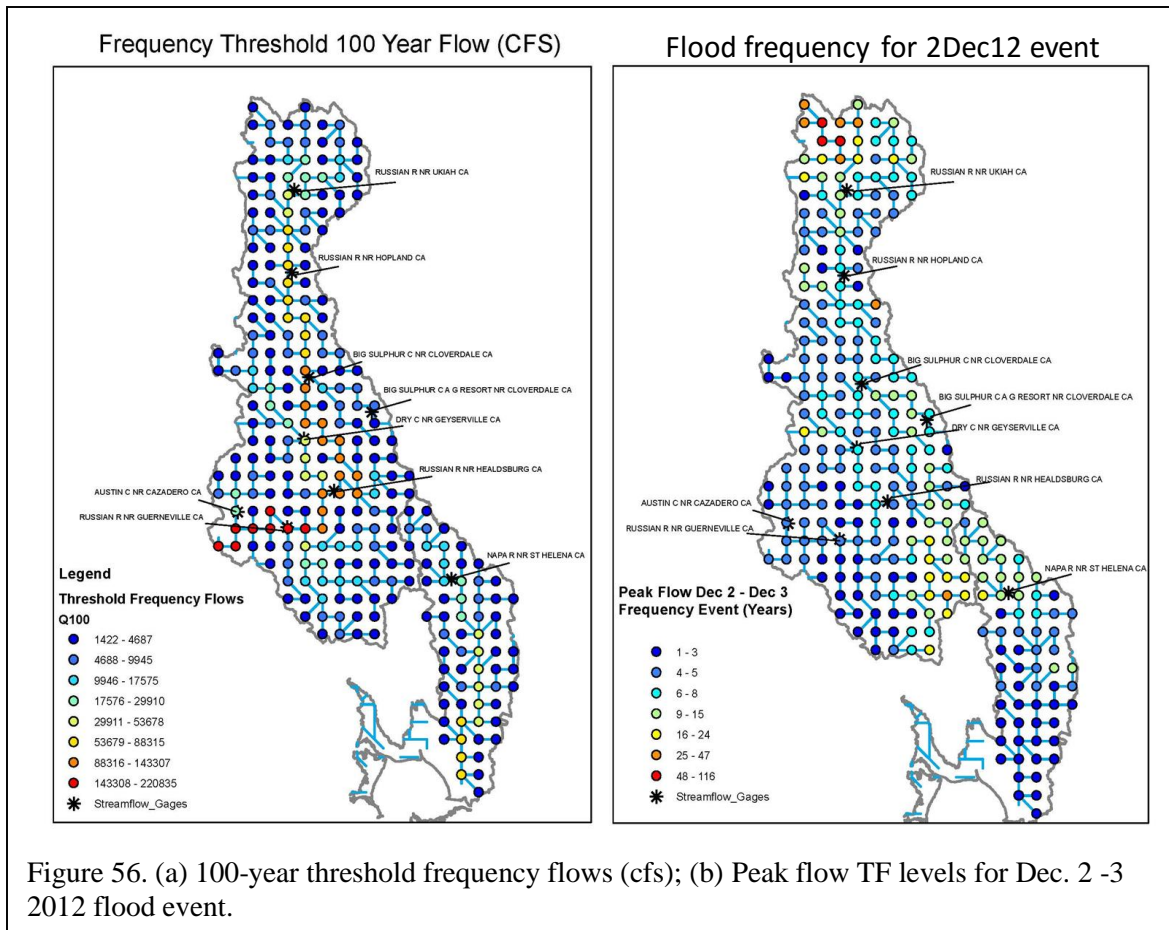


Figure 56. (a) 100-year threshold frequency flows (cfs); (b) Peak flow TF levels for Dec. 2 -3 2012 flood event.

5.2 Fisheries Habitat Assessment

The RDHM simulated flows may provide a basis for assessment of fisheries habitat in the Russian-Napa River basins with particular emphasis on tributaries to the main stem. A primary emphasis is on low flow stream conditions, however, annual hydrologic data are being developed to identify other aspects of water availability and environmental stream flow needs. As formulated, the RDHM represents so-called “natural” or “unimpaired” flows resulting from the watershed landscape and soils, which do not account for water management influences of storage or diversions. The Russian River Tributaries Water Budget modeling (described below) involves integration of the RDHM simulated flows with the ModSim water management model. In this section we describe initial attempts to examine how the RDHM simulated flows might be used to characterize fisheries habitat.

Stream Path and Flow Profiles

Of interest is the flow distribution along the stream trace which can be determined from the RDHM grids. Figure 57 shows a watershed map with the main stem stream path highlighted (blue), and the major tributary Forsythe Creek (yellow). Given the RDHM 1-km grids that lie along the stream path various data can be retrieved to construct a profile. Figure 58 show an elevation profile from the Forsythe Creek headwater down to the junction with the W. Br. and thence down to the gage location (green star). Also shown is the contributing drainage area along the profile. This figure illustrates an advantage of the gridded data structure of the model in that data can be extracted and displayed for any location and time for a watershed of interest. This extraction can be for a point (e.g. the gage location), a profile (as shown), or a 2-D display.

A general purpose functionality has been developed to extract the flows along the stream trace at a selected point in time, or for a selected flow frequency, and to plot these as a flow profile (Figure 59). The flow at the USGS gage at 8 cfs is the flow that is exceeded 60% of the time. The 90% and 10% uncertainty bounds are determined using the Bias (-0.015 cfs) and StDev (0.002 cfs) estimated at the gage for the calibrated RDHM model (described above). The assumption is that the flow uncertainty statistics determined at the gage can be projected upstream to other locations. The Unit Flow profile shows reaches along the profile that are gaining flow relative to other reaches. For example, at about Mile 15 from the Forsythe Creek headwater there is a noticeable drop in the unit flow rate; this is where the W. Br. joins.

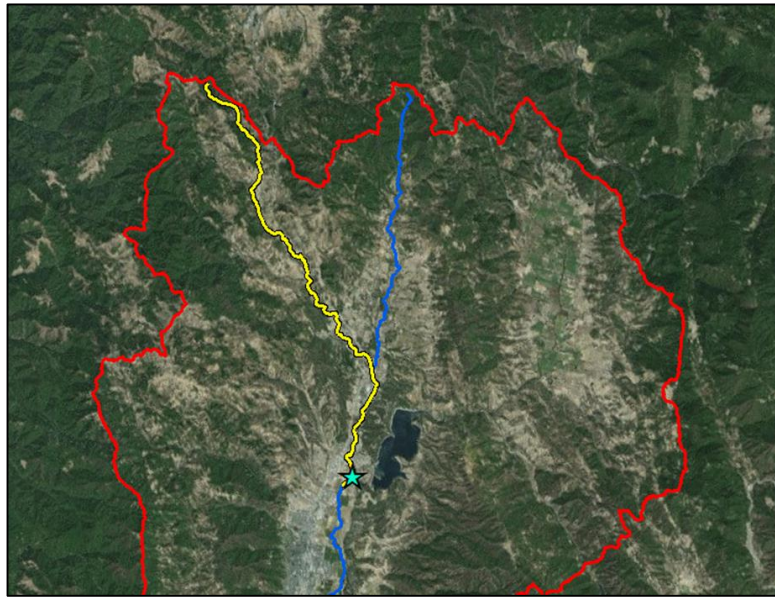


Figure 57. W. Br. Russian River stream trace from the Forsythe Creek headwater (yellow line) down to the junction with the W. Br. (blue line), and thence to the USGS gage near Ukiah (green star).

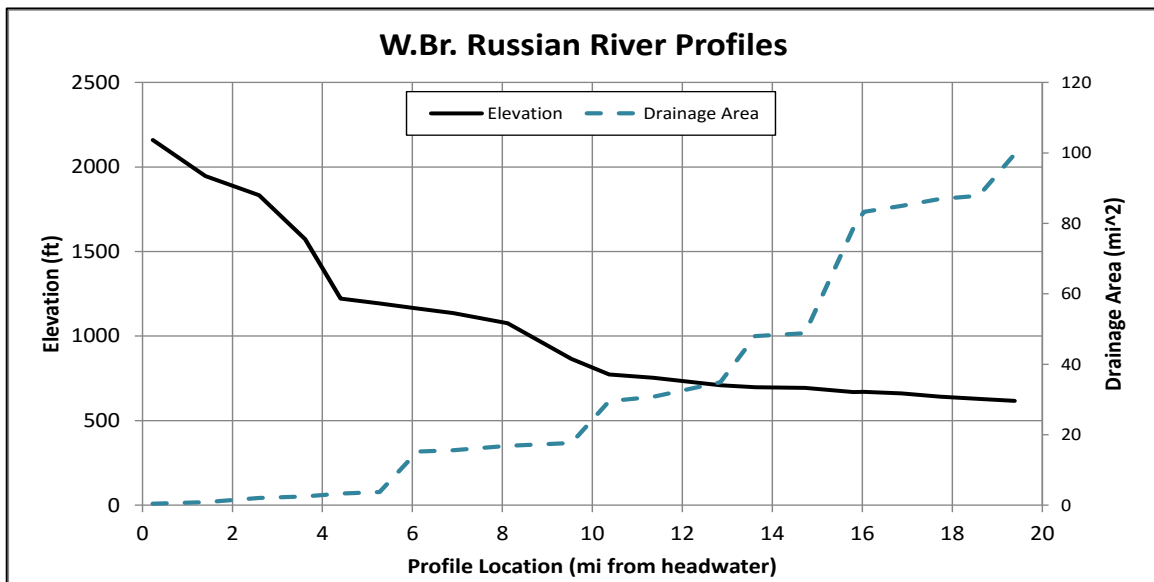


Figure 58. Profile of elevation and drainage area extracted from the RDHM 1-km grids which lie on the stream path.

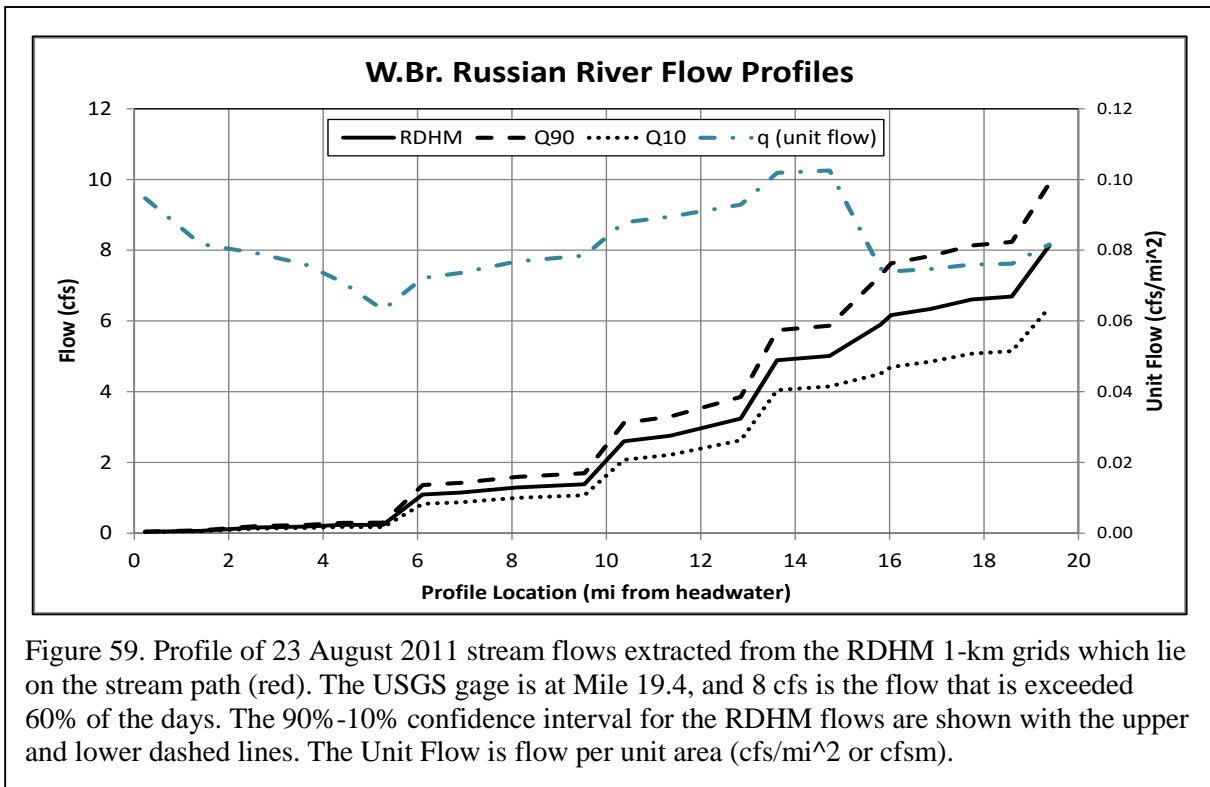


Figure 59. Profile of 23 August 2011 stream flows extracted from the RDHM 1-km grids which lie on the stream path (red). The USGS gage is at Mile 19.4, and 8 cfs is the flow that is exceeded 60% of the days. The 90%-10% confidence interval for the RDHM flows are shown with the upper and lower dashed lines. The Unit Flow is flow per unit area (cfs/mi² or cfs/m).

Assessment of Flows for Fisheries Habitat

A method to characterize fisheries habitat quality, called the Intrinsic Potential Index (IPI), has been developed by the NMFS (Agrawal et al 2005). More recently, the method has been applied by Fuller and Daugherty (pers. comm., Nov. 2015). With the IPI approach, landform, lithology, and hydrology interact to govern movement and deposition of sediment, large wood, and other structural elements along a river network. These broader-scale characteristics and processes thereby control gross channel morphology at the scale of stream segments or reaches, as reflected in the frequency and characteristics of constituent habitat units (e.g., pools, runs, riffles, side-channels, etc.). The IP concept assumes that this hierarchy of organization, structure, and dynamics of physical habitat is reflected in the biological organization of stream communities. In the case of salmonids, the biological response manifests itself as heterogeneity in the distribution, abundance, and productivity of different species and life stages within a stream network. The underlying framework for the IP models assumes that three primary indicators of landform and hydrology - channel gradient, an index of valley width, and mean annual discharge — reasonably constrain channel morphology and hence the potential of a reach to express habitat conditions favorable to a particular salmonid species at some stage of its life. These three characteristics are effectively constant features of the landscape, and thus provide the basis for predicting both potential habitat under historical conditions and the potential for physical processes to recreate suitable habitat if left to operate more or less naturally. Among-species or life-stage differences in habitat affinities are accommodated through species-specific curves relating suitability to the three physical metrics.

Fisheries habitat assessment for W.Br. Russian River based on Intrinsic Potential Index mapping for steelhead. (J. Fuller, pers. comm.; Appendix C). The IPI mapping was conducted along the main stem and tributaries of the W.Br. Russian River watershed. Reach-specific values for each characteristic (i.e., gradient, valley constraint, and mean annual discharge) are converted to habitat suitability scores through functions (“suitability curves”) that convert the value of each variable to a scale of 0-1. The IPI values were tabulated along the stream path illustrated above and plotted on the profile along with the elevation

(Figure 60). This illustrates that a stream profile can be obtained for ecological values, along with physical and hydrological attributes.

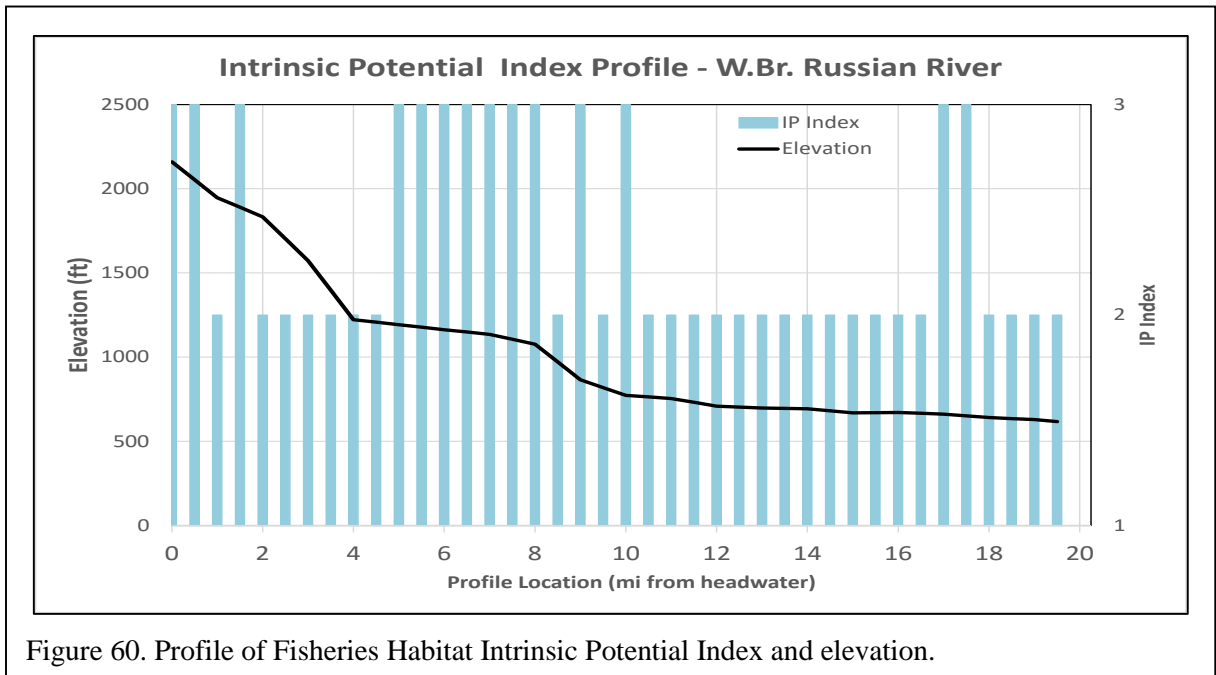


Figure 60. Profile of Fisheries Habitat Intrinsic Potential Index and elevation.

The DHM, like any hydrological model, is not a perfect representation of the hydrological cycle. It requires calibration with observed data to establish that the predictions adequately match what actually occurs. This underscores the importance of flow measurements and continuous gaging. This report highlights the accuracy of the DHM in comparison to gaged flows at NMFS and USGS gaged sites. The NMFS data indicates that when applied without parameter adjustments the DHM adequately represents the general pattern of seasonal flows, but it has limited accuracy for low flows. However, when calibrated to gaged data, such as was done for two USGS gages, the low flow accuracy can be quite good. In addition, the predictive uncertainty of the DHM has been quantified using statistics on Bias and Standard Deviation. This allows the flow predictions to be characterized within confidence intervals (e.g. 90% to 10% envelope). It also allows the likelihood that the flow may be zero or not to be stated.

The assumption that the low flow representation at a gaged location can be extended upstream to interior locations requires validation. Although the DHM represents the dynamics of the hydrological cycle as influenced by terrain, soils and vegetation, and rainfall, it may not adequately represent the dynamics of groundwater interchanges that control low flows along “gaining” and “losing” reaches. The coupling of the DHM with the ModSim water management model provides a means to represent gaining and losing reaches. The magnitude of gains and losses can be handled in the ModSim in a manner similar to human-induced changes to the flows, such as diversions and irrigation return flows. But the location and magnitude of these flow alterations needs to be confirmed by field observations.

5.4 Integration with Water Management Model

To account for water management influences the RDHM generated “natural” flows are being coupled with the MODSIM model to obtain “managed” flows at any location (Fields et al 2015). Together, the coupled natural and managed flow models provide an estimate of the total water budget, allowing researchers and stakeholders together to better understand the relationships between reservoir storage, streamflow, agricultural diversions, and return flows at any location in the basin.

GeoMODSIM is a GIS-based version of the MODSIM generalized river basin management decision support system (DSS) tool (Labadie, 2012; Triana and Labadie 2007; Triana, et al 2010), developed by Dr. John Labadie in the Civil and Environmental Engineering Department at Colorado State University. GeoMODSIM allows the user to efficiently model complex stream networks and to evaluate management strategies with consideration of water rights, agricultural diversions, and environmental flow requirements, while taking advantage of the spatial data base management and modeling tools available in the GIS environment.

Integration of a RDHM for flow data with the stream network structure of the MODSIM river basin management software is a key to developing a fully coupled model of the system that combines MODSIM with RDHM and gridded demand models within GeoMODSIM. Shown here (Figure 61(a)) is the integration of a map layer for the RDHM into the custom ArcMap™ (ESRI, Inc.) interface with GeoMODSIM for providing spatially distributed natural or unregulated inflows generated from quantitative precipitation information (QPI) fields. In addition, we are working to generate vineyard irrigation demands for grape frost and heat protection from a high resolution gridded frost and heat model (Reynolds et al 2014). Integration of the gridded U.S. Geological Survey Modular Ground-Water Flow Model (MODFLOW) into GeoMODSIM has also been accomplished (Triana et al, 2010; Morway et al, 2015).

To demonstrate the potential of a full-scale tributary model, a prototype model was developed for a tributary within the Russian River basin. The selected tributary is characterized by the proximity of vineyards to the stream as well as its classification as critical endangered species habitat. Overall, the tributary watershed encompasses 14.6 square miles, with the stream network model automatically created in GeoMODSIM using NHD-Plus hydrography data readily available from the USGS (Figure 61(b)). GeoMODSIM can be applied to planning the geospatial placement of proposed irrigation ponds, allowing analysis of the best locations for proposed instream and off-stream pond storage.

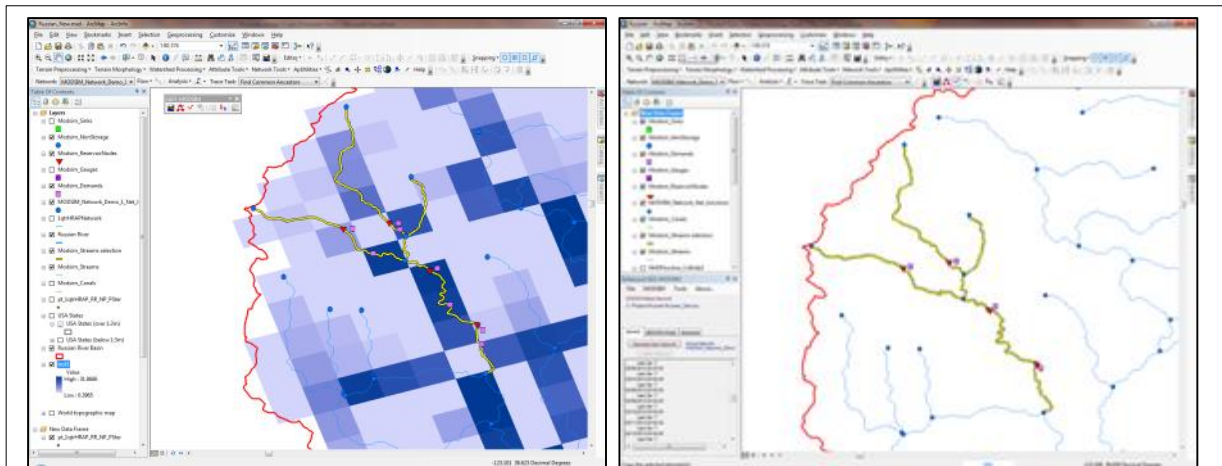


Figure 61. (a). Prototype tributary model in GeoMODSIM coupled with the RDHM for providing watershed inflows to the stream network model of a tributary in the Russian River basin. (b) Prototype tributary GeoMODSIM model showing four agricultural demand nodes.

Recent water management trends in the Russian River basin include increased restrictions on agricultural diversions in order to sustain environmental flows for fisheries. In 2010, the California State Water Resources Control Board (SWRCB) adopted new policies intended to maintain environmental flows for the protection of fishery resources, in particular threatened and endangered anadromous salmonids (SWRCB, 2010). Additionally, in 2011 the SWRCB adopted further restrictions on diversions and groundwater pumping for purposes of frost protection against late-spring frost events (SWRCB, 2011). Although legal proceedings surrounding these restrictions are ongoing, there is increasing

recognition by all stakeholders of the need for better understanding of the effects of agricultural activities on tributary flows and how to improve water management so as to mutually benefit both interests.

Agricultural aspects of the system include demands for both irrigation and frost protection, as well as on-stream and off-stream agricultural ponds for enhancing timely water supply for irrigation as well as maintaining environmental flows. Although irrigation water demands for vineyards are relatively small in terms of total streamflow rates, during the dry season, even small diversions from a stream can be detrimental to environmental flows. In the early spring, vineyards spray irrigate to form a protective layer of ice on the developing grape buds when a frost event is predicted. While there are generally only 5-6 frost events per season, their sporadic nature and the high flow rates required for frost protection can have significant impacts on streamflow.

For this demonstration, environmental flow requirements in the system were approximated based on minimum estimated streamflow rates in the tributary. Future work will focus on developing environmental streamflow requirements based on California State Water Resources Control Board guidelines for minimum flow requirements. For this demonstration, proxy input flows were estimated throughout the system based on scaled streamflow gage data from the main stem Russian River, whereas future work will focus on use of the gridded RDHM model for spatially distributed natural inflow prediction.

The system was modeled based on two scenarios – the historic case and a managed case. The historic scenario does not include any environmental instream flow requirements on the tributaries but does impose irrigation and frost agricultural demands, as well as hypothetical on-stream ponds for supply and diversion. The historic simulation was run in daily time steps over a one-year period, revealing that downstream of the agricultural diversions, instream flows were frequently reduced to zero during periods of peak demand associated with frost events, as well as during extended dry periods that are prevalent during the summer irrigation season (Figure 62(a)). At the same time, most agricultural ponds remained at or near capacity.

Development of the managed scenario starts with the same base assumptions of the historic scenario, but then includes two key modifications. First, instream flow requirements are imposed downstream of each agricultural pond. Second, the on-stream agricultural ponds are modified to include improved operations that allow more flexibility for downstream releases. The results of the managed scenario

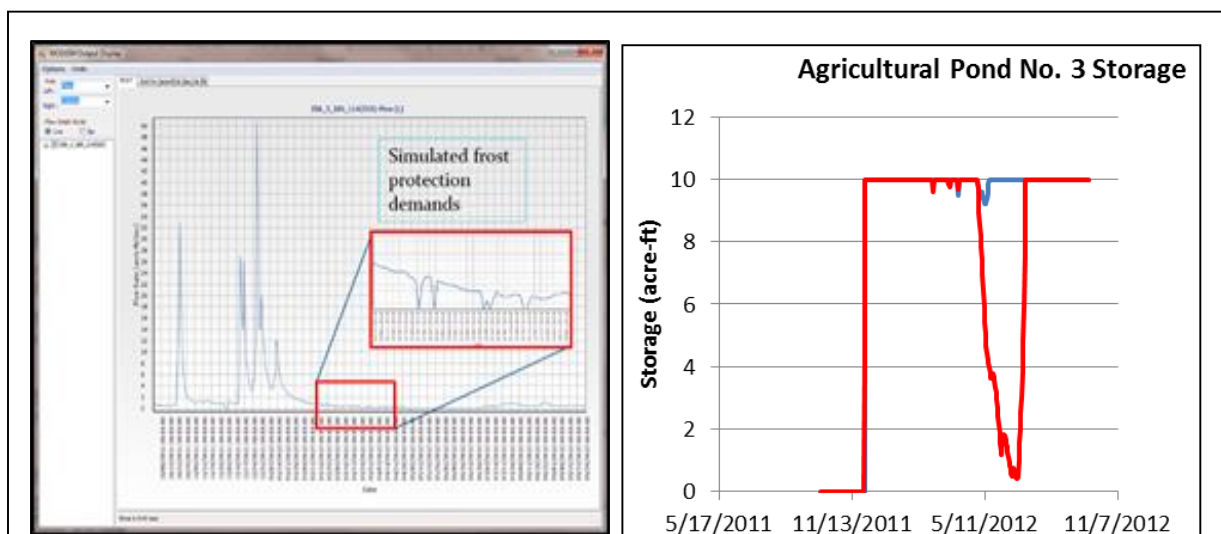


Figure 62. (a) GeoMODSIM output showing the effects of simulated frost demands. (b) GeoMODSIM results demonstrating the benefits of improved pond operation.

demonstrate that with improved operation of the agricultural ponds, the environmental needs of the endangered fish species can be met while satisfying nearly all of the agricultural demands (Figure 62(b)).

5.3 Implementation in CHPS-FEWS

The HMT-West activities have included development and calibration of a distributed hydrologic model, the NWS Office of Hydrologic Development’s (OHD) Research Distributed Hydrologic Model (RDHM), to prototype the distributed approach for flood and other water resources applications (Halgren and Johnson 2015). The HMT-West has applied the RDHM to the Russian River (RR) basin to support assessment of gap-filling weather radars for high resolution precipitation nowcasting and forecasting. The RR RDHM has received attention as a forecast tool to support NWS flash flood operations as well as various water management purposes in the basin, including water supply forecasting and endangered fisheries habitat enhancement.

The objective of this research-to-operations activity is to assess whether a distributed hydrologic modeling approach can provide enhanced hydrologic services for flash flood and other water resources purposes by the NWS and its partner water management agencies.

This project has involved implementing a CHPS-FEWS standalone instance on an ESRL-PSD workstation and integrating the developed Russian River RDHM model (Figure 63). The CHPS-FEWS was set up to ingest gridded precipitation data feeds to force the RDHM model to continuously maintain carryover states. The Russian River RDHM model is now running hourly via automation in CHPS-FEWS on a workstation at ESRL-PSD. Initial states were developed using archived and disaggregated CNRFC QPE beginning in October 2013. Hydrologic forecasts are based on the HRRR dataset and automatic simulation initializes using 48 hour-old states and forecast out to 24 hours.

The ESRL/PSD HMT program has advanced the implementation of RDHM during the past several years. Building off the OHD DMIP2 project (Smith et al 2012), we have implemented the RDHM for the Russian River basin. The RDHM has been used to perform calibration and sensitivity exercises using alternate precipitation fields (CNRFC, MRMS, HRRR) and spatial resolution (HRAP 4.12km and 1/16 HRAP 1.03 km).

Most recently, through collaboration with Riverside Technologies (RTi), we have implemented the Russian River RDHM in the CHPS/FEWS to interface with real-time precipitation feeds (HRRR, CNRFC, MRMS) (Figure 63). Remote login capabilities to the ESRL/PSD/HMT Hydro server have been established for the NWS Weather Forecast Office-Monterey (WFO-MTR), Western Region (WR) and Colorado State University (CSU). These remote logins allow researchers to access the RDHM to perform retrospective model studies of various kinds as well as tracking flood events as they happen (e.g. December 2014). The FEWS workflows automatically trigger updating of the input data and forecast execution based on latest-available observed and forecast precipitation data.

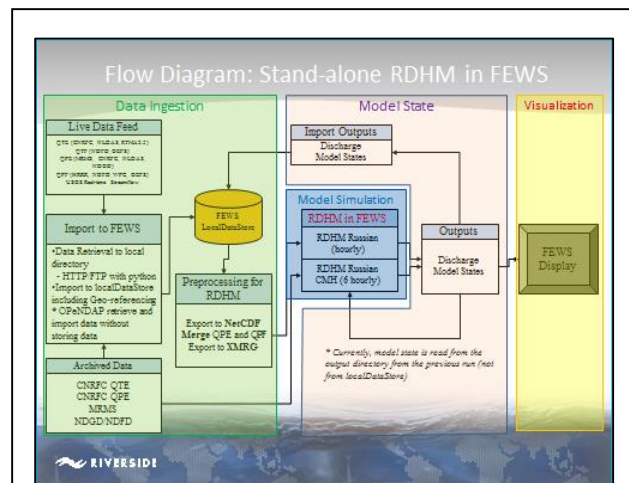


Figure 63. Flow diagram of stand-alone RDHM within FEWS. System involves real-time data ingest and preprocessing for RDHM, establishing model states, and visualization.

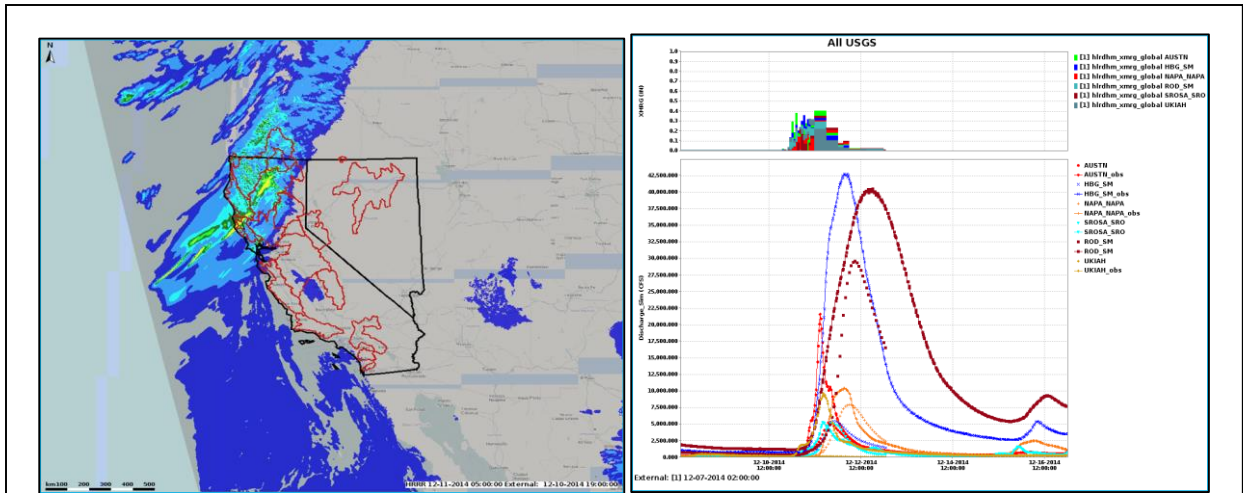


Figure 64. (a) Precipitation fields including HRRR forecasts retrieved and converted to RDHM forcing on-the-fly using FEWS built-in procedures including OPeNDAP. (b) Time series of streamflows are generated in CHS-FEWS at selected grid points in the basin. These can be compared to gaged flows as part of model validation process.

Web-oriented displays of RDHM output have been developed to provide animations of precipitation, flood runoff and soil moisture (Figure 65). These products can be accessed by any interested users and provide a means for extending the RDHM assessment to the wider emergency and water resources management community in the SF Bay region.

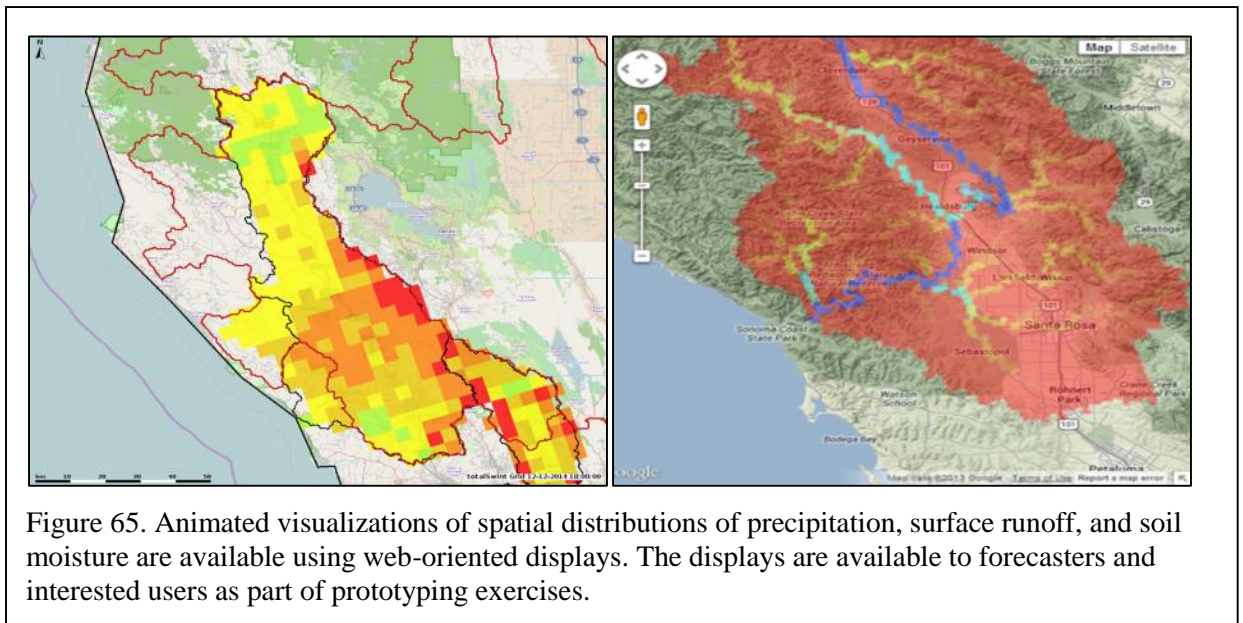


Figure 65. Animated visualizations of spatial distributions of precipitation, surface runoff, and soil moisture are available using web-oriented displays. The displays are available to forecasters and interested users as part of prototyping exercises.

During implementation of CHPS-FEWS and RDHM at ESRL-PSD, there has been ongoing coordination with the NWS forecast operations agencies having operational jurisdiction over the Russian River basin. These include the NWS' WFO-MTR, WR and the CNRFC.

6. CONCLUSIONS AND RECOMMENDATIONS

6.1 Conclusions

A number of conclusions are made based on the research and development accomplished.

Distributed Hydrologic Model Setup

The spatial database established by the NWS National Water Center includes initial definition of RDHM HRAP grids for the entire continental U.S. Access to the data and RDHM setup were accomplished in a straightforward manner without undue effort. The XMRG data format proved awkward to use and convert to other more common grid data formats. The grid structure is consistent in defining the terrain and flow path connectivity between grids and to the stream network. The grid resolution at ~4 km is somewhat coarse in defining RDHM flow paths for small drainage areas. A ~1 km grid (1/16 HRAP) was shown to better address drainage network which correspond to the actual network. Even though a higher grid resolution may not be advantageous given the grid resolution of precipitation forcing, the advantages for flow network representation for small areas carry forward.

Distributed Hydrologic Model Default Parameter Values

The spatial database established by the NWS National Water Center includes initial definition of RDHM parameter values for the HRAP grids for the entire continental U.S. The parameter values were based on generally available CONUS-wide spatial databases for terrain, soils and land use. Initial simulations using the default parameter values seemed to do well in reproducing the general patterns (space and time) and magnitude of surface runoff. Directed manual calibration efforts improved RDHM simulation performance for overall water balance, and estimations of flood peaks and low flows.

Calibration of the RDHM

Calibration of the RDHM can be more daunting than for a lumped model as parameter estimates are required for all grids. The manual procedure can be effective using trial-and-error procedures guided by understanding of model parameter sensitivities and interactions. However, a manual approach to calibration is time consuming, non-objective, and non-reproducible by other modelers. The calibration process employed did result in improved performance of the RDHM in comparison to observed gaged flows, especially for lows which are influenced by deeper subsurface factors not well represented in the base shallow soils data.

Hydrologic Estimation at Grid Locations

Distributed modeling provides higher resolution detail on hydrologic response at ungaged locations which is needed by water managers and the general public. The lumped (or semi-lumped) approaches provide flow estimations only at selected river network locations. The RDHM provides hydrologic response time series at any location within the modeled grid space, including surface runoff, soil moisture and evapotranspiration. Selection of the grid resolution can be based on several factors, including primarily the resolution of the forcing precipitation data (e.g. HRAP), the supporting land surface and soils/bedrock data, and/or a need to provide flow estimates at key locations on the drainage network (e.g. diversion locations, flood impact sites).

RDHM Accuracy - Overall

The RDHM has been shown to provide so-called “natural” surface flow estimates that are reasonably accurate when the precipitation forcings are accurate (e.g. location, timing and intensity), the land surface and subsurface parameters portray the hydrologic response (e.g. soil moisture and evapotranspiration dynamics), and water management influences are minimal.

RDHM Accuracy - Rainfall

The accuracy of the precipitation forcings is a primary source of uncertainty for any lumped or distributed model. In general, the CNRC QPE data was reasonably accurate and provided a good basis for assessing accuracy of the RDHM. However, comparison of the CNRFC QPE rainfall fields to (independent) rain gage readings indicated general underestimation of actual rainfall amounts. This is reflected in RDHM performance statistics for overall water balance and peak flows. The PRISM climatology is monthly and may be inadequate in capturing the precipitation distribution patterns of storms moving through the areas with orographic variation, such as the Cazadero site in the Austin Creek watershed and for relatively short duration storms. Also, the CNRFC QPE is a gauge-only product and therefore heavily relies on the reliability of the gauge data at neighboring stations; when the network is sparse the quality of the gauge interpolation is degraded. There are also some flood events for which the timing is evidently missed. For the RDHM surface flow estimates for small drainage areas having only a few grids are especially sensitive to inaccuracies in rainfall location and intensity. Larger areas allow for smoothing of input precipitation patterns.

For the MRMS application, rainfall fields generated by both radar with gauge correction and radar with VPR & gauge correction products are well estimated in terms of magnitude and timing. The impacts of the rain gauge locations for the 2014/12/04 event at the Austin Creek station showed that the “radar with VPR and gauge correction” product is optimal. Addition of VPR correction improves precipitation estimation for the locations farther away from the radar station, especially for moderate events. This makes sense, given the increasing height of the radar beam and potential for “bright band” contamination as distance from the radar site increases. Radar only products, regardless the absolute precipitation depth, showed marginally better simulation timing.

RDHM Accuracy – Flood Flows

The accuracy of flood flow predictions is considered reasonable in general, but there can be significant inaccuracies associated with three factors, 1) precipitation, 2) initial soil and bedrock moisture conditions, and 3) water management actions. Precipitation accuracy (discussed above) involves the magnitude, timing and location which can be problematic in a basin with highly variable terrain. The largest mis-matches between observed and simulated flood flows are attributed to precipitation inaccuracies. Peak flows generated by the RDHM correlate moderately well with observed discharges although there is a consistent underestimate of the peaks.

Initial soil and bedrock moisture conditions seem to strongly effect simulation accuracies for flood events occurring after prolonged dry periods. These subsurface moisture dynamics may cause the consistent negative volumetric bias whereby the RDHM generates more runoff than observed. Calibration efforts on selected watersheds (esp. Austin CR. W.Br. Russian and Napa R. nr St. Helena) demonstrated improvements in simulation accuracies.

Water management factors of reservoir capture of flood flows and diversions for water supply and irrigation can strongly influence RDHM simulation accuracies. The RDHM does not have capabilities for representing these factors. However, we have initiated an application involving RDHM coupling with a water management model (ModSim) to demonstrate how to address this shortcoming.

RDHM Accuracy – Low Flows

The accuracies of RDHM simulation for low flows were determined using flow records at 15 NMFS gage sites plus 3 USGS gage sites. The NMFS data were not used for calibration and thus provide an independent verification.). Eleven (11) of the 15 NMFS sites have positive biases (73%) indicating that the RDHM consistently underestimates low flows. Noteworthy is that the three calibration sites at USGS gages have average low flow bias of -0.11 cfs; the Austin Creek basin (Site 17) has a low flow bias of -0.01 cfs (equivalent to 0.83 cfs for the 62.8 sq. mi. basin); this basin was the focus of extended calibration efforts and indicates the best correspondence between observed and simulated flows that

might be obtained. Also, low flows are especially sensitive to water management practices for diversions, storage and irrigation return flows.

RDHM Accuracy – Soil and Bedrock Moisture Dynamics

The RDHM demonstrated reasonable performance for representing soil moisture dynamics for moist conditions. However, RDHM performance was not satisfactory for reproducing observed surface runoff levels after prolonged dry periods. It seems that in the Russian-Napa river basins there are factors related to deeper fractured bedrock moisture uptake and drainage phenomenon that are not well represented by the RDHM. Shallow soil moisture monitoring has limited effectiveness in representing these deeper subsurface processes.

Results shown here indicate that “out of the box” RDHM can simulate soil moisture values in the upper soil layers of the Russian river basin with skill. Model skill varies seasonally. The weakest performance was found during the winter season. Overall the model soil moisture values are 2.0 to 6.0% higher than the observations. These findings are in accord with previous research on this topic. The use of an RDHM soil moisture simulation over an entire basin has been used to improve the accuracy of in situ soil moisture observations.

RDHM Accuracy – Water Management Influences

Many sub-watersheds of the Russian-Napa river basins having significant areas are strongly influenced by water management practices of diversions and storage, and irrigation and return flows. RDHM surface runoff estimations are characterized and “natural” flows which do not reflect water management practices. Thus the RDHM estimated flows in stream channels often do not correspond well to observed flows.

RDHM Application - Threshold Frequency Application

The threshold frequency application is intended to provide a more understandable representation of the criticality of the flows in terms that forecasters and the general public can better understand. Generation of the TF levels for each grid in the RDHM was made simpler and faster through use of USGS statistical analyses directed to predicting peak flow frequencies for ungaged watersheds. Results show that the extreme ends of small tributary flow branches are most at risk for flooding despite their low flow values.

RDHM Application – Fisheries Habitat Assessment

Application of the DHM for low flows is being examined to determine its applicability for fisheries habitat assessment and restoration. The DHM provides a capability to represent hydrologic response at a specific site for example a time series of flow variations over a selected period of time. Profiles of watershed physical characteristics (e.g. elevation, slope) and stream flows along a stream path can be displayed. These data can be displayed along with ecological variables as available. Although the RDHM represents the dynamics of the hydrological cycle as influenced by terrain, soils and vegetation, and rainfall, it may not adequately represent the dynamics of groundwater interchanges that control low flows along “gaining” and “losing” reaches.

RDHM Application - Integration with Water Management Model

To account for water management influences the RDHM generated “natural” flows are being coupled with the MODSIM model to obtain “managed” flows at any location. A prototype coupled model was developed for a tributary within the Russian River basin. The selected tributary is characterized by the proximity of vineyards to the stream as well as its classification as critical endangered species habitat. Results of a managed scenario demonstrate that with improved operation of agricultural ponds, the environmental needs of the endangered fish species can be met while satisfying nearly all of the agricultural demands. Although not addressed in this study, it is anticipated that larger reservoir storage and release information could be applied within the water management model and, when coupled with the

RDHM, could provide more accurate simulations of observed streamflow in basins where water management occurs.

RDHM Application - Implementation in CHPS-FEWS

A CHPS-FEWS standalone instance of the Russian-Napa RDHM was implemented on an ESRL-PSD workstation. The CHPS-FEWS was set up to ingest gridded precipitation data feeds to force the RDHM model to continuously maintain carryover states. The Russian River RDHM model is now running hourly via automation in CHPS-FEWS on a workstation at ESRL-PSD. Initial states were developed using archived and disaggregated CNRFC QPE beginning in October 2013. Hydrologic forecasts are based on the HRRR dataset and automatic simulation initializes using 48 hour-old states and forecast out to 24 hours. This application is now available to support assessment of whether a RDHM approach can provide enhanced hydrologic services for flash flood and other water resources purposes by the NWS and its partner water management agencies.

6.2 Recommendations

Distributed Hydrologic Model Setup

The RDHM data management capabilities should be modernized to accommodate more common grid data file formats. While the XMRG file format is efficient in minimizing file size, it is a non-standard format that is difficult to manipulate and does not maintain metadata.

Distributed Hydrologic Model Default Parameter Values

The RDHM database on default parameters should be updated to reflect application experiences in specific watersheds. While the RDHM default database provided reasonable foundation for simulations, modifications of base values as part of the calibration process may be valuable to other users in regions having similar land surface and subsurface characteristics.

Calibration of the RDHM

Automated methods for RDHM calibration should be used, perhaps in combination with manual review, to avoid the large time commitments associated with manual calibration.

RDHM Accuracy – Rainfall

The accuracy of precipitation tracking and forecasting could be improved. Use of multiple sensors, such as the MRMS, could potentially provide better definition of precipitation fields in regions with highly variable terrain having orographic influences.

RDHM Accuracy – Flood Flows

The accuracy of flood flow prediction should be improved through continuing research on precipitation tracking and forecasting, as well as accounting for soil and bedrock moisture dynamics, and water management influences.

RDHM Accuracy – Low Flows

The RDHM capability to represent low flows requires advancement of procedures for soil and bedrock moisture dynamics, as well as accounting for water management influences.

RDHM Accuracy – Soil and Bedrock Moisture Dynamics

The RDHM should be advanced to better establish initial conditions for soil and bedrock moisture, especially after prolonged dry periods. Existing soil moisture observing locations at WLS, PTV, ROD, HBG, HLD, and LSN should be augmented with additional soil probes at depths of 5, 20, 50 and 100 cm.

RDHM Accuracy – Fisheries Habitat Assessment

RDHM calibration for low flows is required to obtain accuracy levels that may support fisheries habitat assessments.

RDHM Accuracy – Water Management Influences

The RDHM should have capabilities to represent reservoir storage and release operations.

NWS RDHM Flash Flood Concept of Operations

Hydrologic modeling is only one component of the overall forecast process – further work is required to ascertain how this could be done to support NWS RFC and WFO operations.

7. REFERENCES

- Agrawal, A., R.S. Schick, E.P. Bjorkstedt, R.G. Szerlong, M.N. Goslin, B.C. Spence, T.H. Williams, and K.M. Burnett. 2005: Predicting the Potential for Historical Coho, Chinook and Steelhead Habitat in Northern California. NOAA Technical Memorandum NOAA-TM-NMFS-SWFSC-379. 34 pgs. June.
- Anderson, E. 2002: Calibration of Conceptual Models for Use in River Forecasting. August. NWS Hydrologic Research Laboratory. <http://www.nws.noaa.gov/oh/hrl/calb/calbmain.htm>
- Anderson, R.M., V.I. Koren, S.M. Reed 2006: Using SSURGO data to improve Sacramento Model a priori parameter estimates. *Journal of Hydrology* 320 (2006) 103–116
- Andrews, E. D., R. C. Antweiler, P. J. Neiman, and F. M. Ralph, 2003: Influence of ENSO on flood frequency along the California coast. *J. Climate*, 17, 337-348.
- Bellon, A., G. Lee, and I. Zawadzki, 2005: Error statistics of VPR corrections in stratiform precipitation. *J. Appl. Meteor.*, 44, 998–1015.
- Bjorkstedt1, E.P., B.C. Spence, J.C. Garza, D.G. Hankin, D. Fuller, W.E. Jones, J.J. Smith, and R.M. Macedo. 2005: An Analysis of Historical Population Structure for Evolutionarily Significant Units of Chinook Salmon, Coho Salmon, And Steelhead in the North-Central California Coast Recovery Domain. NOAA Technical Memorandum NOAA-TM-NMFS-SWFSC-382. 231 pgs October.
- Boyle, DP, HV Gupta, and S. Sorooshian. 2001: Toward improved streamflow forecasts: Value of semidistributed modeling. *Water Resources Research*, Vol. 37, No. 11, Pages 2749-2759, November 2001.
- Burnash, R. J., 1995: The NWS River Forecast System - Catchment modeling. *Computer Models of Watershed Hydrology* V. P. Sing Ed. Water Resources Publications.
- California Department of Water Resources. (DWR), 2003. Crop water use in California. http://www.water.ca.gov/pubs/use/land_and_water_use/crop_water_use_in_california_bulletin_113-4_bulletin_113-4.pdf
- California Water Atlas. 1979: California Office of Planning and Research; California. Dept. of Water Resources http://archive.org/details/The_California_Water_Atlas
- Carpenter, T.M. and K.P. Georgakakos 2006: Intercomparison of lumped versus distributed hydrologic model ensemble simulations on operational forecast scales. *Journal of Hydrology* (2006) 329, 174– 185.
- CNRFC (California-Nevada River Forecast Center (CNFC) 2004: RFC Use of PRISM Data. <http://www.cnrfc.noaa.gov/products/rfcprismuse.pdf>
- Colorado Basin River Forecast Center (CBRFC) 2004: Statistical Analysis of Two Time Series. http://www.cbrfc.noaa.gov/present/rdhm/STAT-Q_User_manual.pdf
- Coplen, T. B., P. J. Neiman, A. B. White, J M. Landwehr, F. M. Ralph, and M. D. Dettinger, 2008: Extreme changes in stable hydrogen isotopes and precipitation characteristics in a landfalling Pacific storm, *Geophys. Res. Lett.*, 35, L21808, doi:10.1029/2008GL035481.
- Cosgrove, Brian A., Overview and Initial Evaluation of the Distributed Hydrologic Model Threshold Frequency (DHM-TF) Flash Flood Forecasting System. NOAA Technical Report NWS 54. March 2012.
- Daly, C., R. P. Neilson, and D. L. Phillips, 1994: A Statistical-Topographic Model for Mapping Climatological Precipitation over Mountainous Terrain. *J. Appl. Meteor.*, 33, 2, 140-158.
- Daly, C., R.P. Neilson, and D.L. Phillips, 1994: A Statistical-Topographic Model for Mapping Climatological Precipitation over Mountainous Terrain. *J. Appl. Meteor.*, 33, 140-158. <http://prism.nacse.org/>

Dettinger, M. D., F. M. Ralph, M. Hughes, T. Das, P. J. Neiman, D. Cox, G. Estes, D. Reynolds, R. Hartman, D. Cayan, and L. Jones, 2012: Design and quantification of an extreme winter storm scenario for emergency preparedness and planning exercises in California, *Nat. Hazards*, 60, 1085-1111.

Dettinger, M.D., Ralph, F.M., Das, T., Neiman, P.J., and Cayan, D., 2011: Atmospheric rivers, floods, and the water resources of California. *Water*, 3 (Special Issue on Managing Water Resources and Development in a Changing Climate), 455-478.

Ek, M. B., K. E. Mitchell, Y. Lin, E. Rogers, P. Grunmann, V. Koren, G. Gayno, and J. D. Tarpley, 2003: Implementation of Noah land surface model advances in the National Centers for Environmental Prediction operational mesoscale Eta model. *J. Geophys. Res.*, 108, D22, 8851.

Fields, C. L. Johnson, J. Labadie. 2015: Tributary-Scale Decision Support System Using Gridded Forecast Data. 2015 American Water Resources Association (AWRA) Annual Conference. Denver, CO. Nov. 19.

Fleming, M. 2012: Determination of a Hydrologic Index for the Russian River Watershed using HEC-ResSim. Report PR-85, US Army Corps of Engineers, Institute for Water Resources, Hydrologic Engineering Center, Davis, CA. 122 pgs. July.
<http://www.hec.usace.army.mil/publications/ProjectReports/PR-85.pdf>

Flint, A. L., L. E. Flint, and M. D. Dettinger, 2008: Modeling soil moisture processes and recharge under a melting snowpack. *Vadose Zone J.*, 7, 350-357.

Flint, L.E. and A.L. Flint 2012: Downscaling future climate scenarios to fine scales for hydrologic and ecological modeling and analysis. *Ecological Processes* 1:2. doi:10.1186/2192-1709-1-2
<http://www.ecologicalprocesses.com/content/1/1/2>.

Flint, L.E., Flint, A.L., Curtis, J.A., Delaney, C., and Mendoza, J., 2015: Provisional simulated unimpaired mean daily streamflow in the Russian River and Upper Eel River Basins, California, under historical and projected future climates: U.S. Geological Survey Data Release, doi.org/10.5066/F71C1TX4

Fulton, R.A. 1998: WSR-88D Polar-to-HRAP Mapping. Technical Memorandum, Hydrologic Research Laboratory, Office of Hydrology, National Weather Service. 33 pgs.
<http://www.nws.noaa.gov/oh/hrl/papers/wsr88d/hrapmap.pdf>

Glaudemans, M. Paul Tilles, B. Lawrence. 2009: Interactive Quality Control and Operational Product Generation of Hourly Multi-Sensor Precipitation Estimates in the NWS. American Meteorological Society Annual Meeting.

Gotvald, A.J., Barth, N.A., Veileux, A.G., and Parrett, Charles, 2012: Methods for determining magnitude and frequency of floods in California, based on data through water year 2006: U.S. Geological Survey Scientific Investigations Report 2012-5113, 38 p., 1 pl., available online at
<http://pubs.usgs.gov/sir/2012/5113/>.

Gourley, J.J. and B.E. Vieux. 2005: A Method for Evaluating the Accuracy of Quantitative Precipitation Estimates from a Hydrologic Modeling Perspective. *Journal Hydrometeorology*, v6, pp 115-133, April.

Halgren, J., L. Johnson, T. Coleman and R. Cifelli. 2015: RDHM-CHPS Research-to-Operations Demonstration, Russian-Napa River Basins, CA. Poster for 6th NOAA Testbed and Operational Proving Ground Workshop. April 14.

Haydon, W. D. 2007. Landslide Potential Evaluation Russian River Watershed, Sonoma and Mendocino Counties, California. California Department of Conservation, California Geological Survey. 37 pgs. July.

Illston, B. G., J. B. Basara, C. A. Fiebrich, K. C. Crawford, E. Hunt, D. K. Fisher, R. Elliott, and K. Humes, 2008: Mesoscale monitoring of soil moisture across a statewide network. *J. Atmos. Ocean. Technol.*, 25, 2, 162-182.

Kennedy/Jenks Consultants. 2007: Santa Rosa IRWP - Discharge Compliance Project, Regional Groundwater – Surface Water Interactions along the Russian River and the Laguna de Santa Rosa. Technical Memorandum I-8, prepared for the City of Santa Rosa. 140 pp. May.

Kingsmill, D. E., P. J. Neiman, F. M. Ralph, and A. B. White, 2006: Synoptic and topographic variability of Northern California precipitation characteristics in landfalling winter storms observed during CALJET. *Mon. Wea. Rev.*, 134, 2072-2094.

Kitzmilller, D, S. Van Cooten, F. Ding, K. Howard, C. Langston, J. Zhang, H. Moser, Y. Zhang, J.J. Gourley, D. Kim, D. Riley. 2011: Evolving Multisensor Precipitation Estimation Methods: Their Impacts on Flow Prediction Using a Distributed Hydrologic Model. *J. Hydrometeorology*, V12, pp 1414-1431. December.

Koren, V. et al. 2006. Evaluation of a grid-based distributed hydrological model over a large area. *IAHS Publ.* 303.

Koren, V. et al. 2008: Use of soil moisture observations to improve parameter consistency in watershed calibration, *J. Phys. Chem. Earth* (2008), doi:10.1016/j.pce.2008.01.003

Koren, V., F. Moreda, and M. Smith, 2008: Use of soil moisture observations to improve parameter consistency in watershed calibration. *Physics and Chemistry of the Earth*, 33, 17-18, 1068-1070.

Koren, V., J. Schaake, K. Mitchell, Q.-Y. Duan, F. Chen, and J. M. Baker, 1999: A parameterization of snowpack and frozen ground intended for NCEP weather and climate models. *J. Geophys. Res.*, 104, 19, 569-585.

Koren, V., M. Smith, Z. Cui, and B. Cosgrove, 2007: Physically-Based Modifications to the Sacramento Soil Moisture Accounting Model: Modeling the Effects of Frozen Ground on the Rainfall-Runoff Process. NOAA Tech. Rep. NWS 52, Office of Hydrologic Development W/OHD 12, 1325 East West Highway, Silver Spring, MD.

Koren, V., M. Smith, Z. Cui, B. Cosgrove, K. Werner, and R. Zamora, 2010: Modification of Sacramento Soil Moisture Accounting Heat Transfer Component (SAC-HT) for Enhanced Evapotranspiration. NOAA Tech. Rep. NWS 53, Office of Hydrologic Development W/OHD 12, 1325 East West Highway, Silver Spring, MD.

Koren, V., S. Reed, M. Smith, Z. Zhang, and D.-J. Seo, 2004: Hydrology laboratory research modeling system (HL-RMS) of the US national weather service. *J. Hydrol.*, 291, 3-4, 297-318.

Koren, V.I., M. Smith, D. Wang, Z. Zhang. 2000: Use of Soil Property Data in the Derivation of Conceptual Rainfall-Runoff Model Parameters, 80th Annual Meeting of the AMS, Long Beach, Ca. January. <http://www.nws.noaa.gov/oh/hrl/distmodel/distmod.htm>.

Ledoux, E., Girard, G., Marsily, G. D., & Deschenes, J. (1989). Spatially distributed modeling: Conceptual approach, coupling surface water and groundwater. In H. J. Morel-Seytoux, *Unsaturated Flow Hydrologic Modeling: Theory and Practice*, NATO Science Series C (pp. 435-454). Kluwer Academic.

Lee, H., D.-J. Seo, and V. Koren: Assimilation of streamflow and in situ soil moisture data into operational distributed hydrologic models: Effects of uncertainties in the data and initial model soil moisture states. *Advances in Water Resources*, 34, 12, 1597-1615.

Lewis, D.L., Harper, J. McGourty, G., Nosera, J., and Sanford, R., 2006. Estimating agricultural water demand and irrigation technology needs: A survey and needs assessment in the Mendocino County Portion of the Russian River, U.C.C.E, U.C Davis, September.

-
- Marcus, L. 2014: Conceptual Model of Streamflow Processes. Personal communication.
- Martner, B. E., S. E. Yuter, A. B. White, S. Y. Matrosov, D.E. Kingsmill, and F. M. Ralph, 2008: Raindrop size distributions and rain characteristics in California coastal rainfall for periods with and without a radar bright band. *J. Hydrometeorol.*, 9, 408-425.
- Matrosov, S. Y., D. E. Kingsmill, B. E. Martner, and F. M. Ralph, 2005: The utility of X-band polarimetric radar for quantitative estimates of rainfall parameters. *J. Hydrometeorol.*, 6, 248-262.
- Matrosov, S.Y., Depolarization estimates from linear H and V measurements with weather radars operating in simultaneous transmission-simultaneous receiving mode, 2004, *J. Atmos. Oceanic Technol.*, 21, 574-583
- Metzger, L.F., Farrar, C.D., Koczot, K.M., and Reichard, E.G. 2006: Geohydrology and Water-Chemistry of the Alexander Valley, Sonoma County, California: U.S. Geological Survey Scientific Investigations Report 2006-5115. In cooperation with the Sonoma County Water Agency.
- Mitchell, K. E., and Coauthors, 2004: The multi-institution North American Land Data Assimilation System (NLDAS): Utilizing multiple GCIP products and partners in a continental distributed hydrological modeling system. *Journal of Geophysical Research: Atmospheres*, 109, D7, D07S90.
- Moreda, F., Koren, V., Zhang, Z., Reed, S., Smith, M., 2006. Parameterization of distributed hydrological models: learning from the experiences of lumped modeling. *Journal of Hydrology* 320, 218–237.
- Moriasi, DN, JG Arnold, MW Va Liew, RL Bingner, RD Hamel, TL Veith 2007: Model Evaluation Guidelines For Systematic Quantification Of Accuracy In Watershed Simulations. *Transactions American Society of Agricultural and Biological Engineers*. Vol. 50(3): 885–900. March.
- Morss, R. E., and F. M. Ralph, 2007: Use of information by National Weather Service Forecasters and emergency managers during the CALJET and PACJET-2001. *Wea. Forecast.*, 22, 539-555.
- National Weather Service (NWS) 2013: NOAA’S National Weather Service Strategic Plan: Building a Weather-Ready Nation. <http://www.nws.noaa.gov/com/weatherreadynation/>. April.
- Neiman, P. J., B. E. Martner, A. B. White, G. A. Wick, F. M. Ralph, D. E. Kingsmill, 2005: Wintertime nonbrightband rain in California and Oregon during CALJET and PACJET: Geographic, interannual, and synoptic variability. *Mon. Wea. Rev.*, 133, 1199-1223.
- Neiman, P. J., F. M. Ralph, A. B. White, D. D. Parrish, J. S. Holloway, and D. L. Bartels, 2006: A multiwinter analysis of channeled flow through a prominent gap along the Northern California coast during CALJET and PACJET. *Mon. Wea. Rev.*, 134, 1815-1841.
- Neiman, P. J., F. M. Ralph, G. A. Wick, J. D. Lundquist and M. D. Dettinger, 2008: Meteorological characteristics and overland precipitation impacts of atmospheric rivers affecting the West Coast of North America based on eight years of SSM/I satellite observations. *J. Hydrometeorol.*, 9, 22-47.
- Neiman, P.J., A.B. White, F.M. Ralph, D.J. Gottas, and S.I. Gutman, 2009: A Water Vapor Flux Tool for Precipitation Forecasting. *U.K. /Journal of Water Management/*, 162, 83-94.
- Neiman, P.J., F.M. Ralph, A.B. White, D.A. Kingsmill, and P.O.G. Persson, 2002: The statistical relationship between upslope flow and rainfall in California’s coastal mountains: Observations during CALJET. *Mon. Wea. Rev.*, 130, 1468 1492.
- Neiman, P.J., P.O.G. Persson, F.M. Ralph, D.P. Jorgensen, A.B. White, and D.A. Kingsmill, 2004: Modification of Fronts and Precipitation by Coastal Blocking during an Intense Landfalling Winter Storm in Southern California: Observations during CALJET. *Mon. Wea. Rev.*, 132, 242 273.

Newman, M., G. N. Kiladis, K. M. Weickman, F. M. Ralph and P.D. Sardeshmukh, 2012: Relative contributions of synoptic and low-frequency eddies to time-mean atmospheric moisture transport, including the role of atmospheric rivers. *J. Climate*, 25, 7341-7361.

Office of Hydrologic Development (OHD) 2009: Hydrology Laboratory-Research Distributed Hydrologic Model (RDHM) User Manual V. 2.4.2. NOAA NWS Hydrology Laboratory. (Last Modified 12/29/09) http://www.cbrfc.noaa.gov/present/rdhm/RDHM_3_0_0_User_Manual.pdf

Pan, F. and C. D. Peters-Lidard, 2008: On the Relationship Between Mean and Variance of Soil Moisture Fields. *JAWRA Journal of the American Water Resources Association*, 44, 1, 235-242.

Pelle, A., G. Tootle, R. Cifelli. 2014: Threshold Frequency Estimation for the Russian-Napa Rivers, CA. Poster at American Geophysical Union Annual Conference. December 15.

Qiao, L., Herrmann, R. B., & Pan, Z. (2012). Parameter uncertainty reduction for SWAT using GRACE, streamflow, and groundwater table data for lower Missouri River basin. *Journal of the American Water Resources Association*, 49(2), 343-358. doi:10.1111/jawr.12021

Ralph, F. M., and Coauthors, 2005: Improving short-term (0-48 h) cool-season quantitative precipitation forecasting: recommendations from a USWRP workshop. *Bull. Amer. Meteor. Soc.*, 86, 11, 1619-1632.

Ralph, F. M., and M. D. Dettinger, 2012: Historical and national perspectives on extreme West Coast precipitation associated with atmospheric rivers during December 2010. *Bull. Amer. Meteor. Soc.*, 93, 783-790.

Ralph, F. M., E. Sukovich, D. Reynolds, M. Dettinger, S. Weagle, W. Clark, P.J. Neiman, 2010: Assessment of extreme quantitative precipitation forecasts and development of regional extreme event thresholds using data from HMT-2006 and COOP observers. *J. Hydrometeorol.*, 11, 1288-1306.

Ralph, F. M., Neiman, P. J., D. E. Kingsmill, P. O. G. Persson, A. B. White, E. T. Strem, E. D. Andrews, and R. C. Antweiler, 2003: The impact of a prominent rain shadow on flooding in California's Santa Cruz mountains: A CALJET case study and sensitivity to the ENSO cycle. *J. Hydrometeorol.*, 4, 1243-1264.

Ralph, F. M., P. J. Neiman, G. A. Wick, S. I. Gutman, M. D. Dettinger, D. R. Cayan, and A. B. White, 2006: Flooding on California's Russian River: Role of atmospheric rivers. *Geophys. Res. Lett.*, 33, L13801, doi:10.1029/2006GL026689.

Ralph, F. M., P. J., Neiman and R. Rotunno, 2005: Dropsonde observations in low-level jets over the Northeastern Pacific Ocean from CALJET-1998 and PACJET-2001: Mean vertical-profile and atmospheric-river characteristics. *Mon. Wea. Rev.*, 133, 889-910.

Ralph, F. M., R. M. Rauber, B. F. Jewett, D. E. Kingsmill, P. Pisano, P. Pugner, R. M. Rasmussen, D. W. Reynolds, T. W. Schlatter, R. E. Stewart and J. S. Waldstreicher, 2005: Improving short-term (0-48 hour) Cool-season quantitative precipitation forecasting: Recommendations from a USWRP Workshop. *Bull. Amer. Meteor. Soc.*, 86, 1619-1632.

Ralph, F. M., T. Coleman, P.J. Neiman, R. Zamora, and M.D. Dettinger, 2012: Observed impacts of duration and seasonality of atmospheric-river landfalls on soil moisture and runoff in coastal northern California. *J. Hydrometeorol.*, (in press Oct 2012).

Ralph, F.M., and M.D. Dettinger, 2011: Storms, Floods and the Science of Atmospheric Rivers. *EOS, Transactions, Amer. Geophys. Union.*, 92, 265-266.

Ralph, F.M., J. Intrieri, D. Andra Jr., S. Boukabara, D. Bright, P. Davidson, B. Entwistle, J. Gaynor, S. Goodman, J. Gwo-Jiing, A. Harless, J. Huang, G. Jedlovec, J. Kain, S. Koch, B. Kuo, J. Levit, S.T. Murillo, L.P. Riishojgaard, T. Schneider, R. Schneider, T. Smith, and S. Weiss, 2012: The emergence of

weather-focused testbeds linking research and forecasting operations. *Bull. Amer. Meteor. Soc.*, (in press Dec 2012).

Ralph, F.M., P.J. Neiman, and G.A. Wick, 2004: Satellite and CALJET aircraft observations of atmospheric rivers over the eastern North-Pacific Ocean during the El Niño winter of 1997/98. *Mon. Wea. Rev.*, 132, 1721-1745.

Rantz, S.E. and T.H. Thompson. 1967: Surface-Water Hydrology of California Coastal Basins Between San Francisco Bay and Eel River. USGS Water-Supply Paper 1851. 65 pgs.
<http://pubs.er.usgs.gov/publication/wsp1851>

Rantz, S.E. and T.H. Thompson. 1967: Surface-Water Hydrology of California Coastal Basins Between San Francisco Bay and Eel River. U.S. Geological Survey Water-Supply Paper 1851. Library of Congress catalog-card No. GS 67-264.

Reed, S. J. Schaake, Z. Zhang. 2007: A distributed hydrologic model and threshold frequency-based method for flash flood forecasting at ungauged locations. *Journal of Hydrology* 337, 402–420.

Reed, S. M., and D.R. Maidment, 1997: Coordinate transformations for Using Nexrad data in GIS-based hydrologic modeling. *J. Hydro. Eng.*, 4, 174-182.

Reed, S.M. and D.R. Maidment. 1995: A GIS Procedure for Merging NEXRAD Precipitation Data and Digital Elevation Models to Determine Rainfall-Runoff Modeling Parameters. CRWR Online Report 95-3, Center for Research in Water Resources, Univer of Texas at Austin. 119 pgs. September.
http://www.ce.utexas.edu/prof/maidment/GISHydro/docs/reports/seann/rep95_3.htm

Ryder, R.A. 1994: Aerobic pond treatment of winery wastewater for vineyard irrigation by drip and spray systems in California, *Actes du Congre`s International sur le Traitement des Effluents Vinicoles*, pp. 67–72.

Schaake, J., A. Henkel, S. Cong. 2004: Application of prism climatologies for hydrologic modeling and forecasting in the western U.S. *Proc. 18th Conf. on Hydrology*, Seattle, WA, Amer. Meteor. Soc., 5.3. [Available online at <http://ams.confex.com/ams/pdfpapers/72159.pdf>.]

Singh, V.P. and D.A. Woolhiser 2002: Mathematical Modeling of Watershed Hydrology. *Journal of Hydrologic Engineering*, Vol. 7, No. 4, July 1, 2002. ©ASCE, ISSN 1084-0699/2002/4-270–292

Smith, M. B., D.-J. Seo, V. I. Koren, S. M. Reed, Z. Zhang, Q. Duan, F. Moreda, and S. Cong, 2004: The distributed model intercomparison project (DMIP): motivation and experiment design. *J. Hydrol.*, 298, 1–4, 4-26.

Smith, M., and Coauthors, 2013: The distributed model intercomparison project – Phase 2: Experiment design and summary results of the western basin experiments. *J. Hydrol.*, 507, 0, 300-329.

Smith, M.B., DP Laurine, VI Koren, , SM Reed, Z Zhang 2003: Hydrologic model calibration in the National Weather Service. In *Calibration of Watershed Models*, Q. Y. Duan, H. V. Gupta, S. Sorooshian, A. N. Rousseau, and R. Turcotte, Eds., AGU, 133-152.

Smith, M.B., V.I. Koren, Z. Zhang, S.M. Reed, J.J. Pan, F. Moreda. 2004: Runoff response to spatial variability in precipitation: an analysis of observed data. *Journal of Hydrology* 298 (2004) 267–286.

Sonoma County Water Agency (SCWA), Beach, R. 1996: *The Russian River: An Assessment of Its Condition And Governmental Oversight*, August 1996.

Sonoma County Water Agency (SCWA). 2004: Final Biological Assessment, Section 3, Environmental Baseline, September.

Sonoma County Water Agency (SCWA). 2012: Russian River Watershed Background: Hydrology.

Spence, B.C., E.P. Bjorkstedt, J.C. Garza, J.J. Smith, D.G. Hankin, D. Fuller, W.E. Jones, R. Macedo, T.H. Williams, E. Mora. 2008: A Framework for Assessing the Viability of Threatened and Endangered Salmon and Steelhead in the North-Central California Coast Recovery Domain. NOAA Technical Memorandum NOAA-TM-NMFS-SWFSC-423. 194 pgs. April.

Spence, B.C., E.P. Bjorkstedt, S. Paddock, L. Nanus. 2012: Updates to Biological Viability Criteria for Threatened Steelhead Populations in the North-Central California Coast Recovery Domain. Report by National Marine Fisheries Service, Southwest Fisheries Science Center, Fisheries Ecology Division. 17 pgs. March.

US Army Corps of Engineers (USACE) San Francisco District. 2004: Water Control Diagram – Coyote Valley Dam – Lake Mendocino, Russian River, California. Attachment A to the Water Control Manual. USACE Sacramento District.

USACE. 1984: "Warm Springs Dam and Lake Sonoma Dry Creek", California Water Control Manual. U.S. Army Corps of Engineers, Sacramento District.

USACE. 1986: "Coyote Valley Dam and Lake Mendocino Russian River", California Water Control Manual. U.S. Army Corps of Engineers, Sacramento District.

USACE. 2003: "Coyote Valley Dam and Lake Mendocino Russian River", California Water Control Manual. U.S. Army Corps of Engineers, Sacramento District.

Vannier, O., I. Braud, and S. Anquetin. 2014: Regional estimation of catchment-scale soil properties by means of streamflow recession analysis for use in distributed hydrological model. *Hydrol. Process.* 28, 6276–6291.

Vignal, B., G. Galli, J. Joss, and U. Germann, 2000: Three methods to determine profiles of reflectivity from volumetric radar data to correct precipitation estimates. *J. Appl. Meteor.*, 39, 1715–1726.

Walls, S.P. 2013: A Geomorphic Typology to Characterize Surface-Groundwater Interactions in the Russian River Basin. MLA Thesis, University of California, Berkeley. 78 pgs.

White, A. B., P. J. Neiman, F. M. Ralph, D. E. Kingsmill, and P. O. G. Persson, 2003: Coastal orographic rainfall processes observed by radar during the California Land-Falling Jets experiment. *J. Hydrometeor.* 4, pp. 264B282.

White, A.N., M.L. Anderson, M.D. Dettinger, F.M. Ralph, A. Hinojosa, D.R. Cayan, R.K. Hartman, D.W. Reynolds, L.E. Johnson, T.L. Schneider, R. Cifelli, Z. Toth, S.I. Gutman, C.W. King, F. Gehrke, P.E. Johnston, C. Walls, D. Mann, D.J. Gottas and T. Coleman, 2012: A 21st century California observing network for monitoring extreme weather events. *J. Atmos. Ocean. Technol.* (submitted Sept. 2012).

Wick, G. A., P.J. Neiman, and F.M. Ralph, 2012: Description and validation of an automated objective technique for identification and characterization of the integrated water vapor signature of atmospheric rivers. *IEEE Trans. Geosci. Remote Sensing*, (in press, 2012).

Willie, D., H. Chen, V. Chandrasekar, R. Cifelli, C. Campbell, D. Reynolds, S. Matrosov, and Y. Zhang, 2015: Evaluation of Multisensor Quantitative Precipitation Estimation in the Russian River Basin. *J. Hydrologic Eng.*, in review

Zamora, R. J., and Coauthors, 2003: Comparing MM5 radiative fluxes with observations gathered during the 1995 and 1999 Nashville southern oxidants studies. *J. Geophys. Res.*, 108, 4050.

Zamora, R. J., F. M. Ralph, E. Clark and T. S. Schneider, 2011: The NOAA Hydrometeorology Testbed Soil Moisture Observing Networks: Design, instrumentation and preliminary results. *J. Atmos. Oceanic Technol.*, 28, 1129-1140, doi: 10.1175/2010JTECHA1465.1.

Zamora, R., C. Hsu, L. Johnson, R. Cifelli, C. Shobe. 2015: Comparing Distributed Hydrological Model Simulations of Soil Moisture with Observations in the Russian River Basin. Paper submitted for publication in *Jour. Hydrometeorology*. September.

Zhang, J., Y. Qi, D. Kingsmill, and K. Howard, 2012: Radar-based quantitative precipitation estimation for the cool season in complex terrain: Case studies from the NOAA Hydrometeorology Testbed. *J. of Hydrometeor.*, 13, 1836-1854.

Zhang, J., V. Koren, S. Reed, M. Smith, Y. Zhang, F. Moreda, and B. Cosgrove, 2012: SAC-SMA a priori parameter differences and their impact on distributed hydrologic model simulations. *J. Hydrol.*, 420-421, 0, 216-227.

Zhang, J., K. Howard, C. Langston, S. Vasiloff, B. Kaney, A. Arthur, S. Van Cooten, K. Kelleher, D. Kitzmiller, F. Ding, D.J. Seo, E. Wells, and C. Dempsey. 2011: National Mosaic and Multi-Sensor QPE (NMQ) System - Description, Results, and Future Plans. *Bulletin American Meteorological Society*. DOI:10.1175/2011BAMS-D-11-00047.1

ABBREVIATIONS AND ACRONYMS

AHPS Advanced Hydrologic Prediction Service
API Antecedent Precipitation Index
AWIPS Advanced Weather Interactive Processing System
CHPS Community Hydrologic Prediction System
CNRFC California-Nevada River Forecast Center
CONUS Conterminous United States
DA Data Assimilation
DEM Digital Elevation Model
DHM Distributed Hydrology Model
DMIP Distributed Model Intercomparison Project
ESP Ensemble Streamflow Prediction
ESRL Earth System Research Laboratory
ET Evapotranspiration
FFG Flash Flood Guidance
GCM Global Climate Model
GEFS Global Ensemble Forecast System
GFS Global Forecast System
GIS Geographical Information System
GLDAS Global Land Data Assimilation System
GLUE Generalized Likelihood Uncertainty Estimation
GOES Geostationary Operational Environmental Satellite
GVF Green Vegetation Fraction
HAS Hydrometeorological Analysis and Support
HEC-HMS US Army Corps of Engineers' Hydrologic Engineering Center Hydrologic
HEFS Hydrologic Ensemble Forecast System
HL Hydrology Laboratory
RDHM Hydrology Lab-Research Distributed Hydrologic Model
HMT Hydrometeorological Testbed
HPC Hydrometeorological Prediction Center
HRAP Hydrologic Rainfall Analysis Project
LIS Land Information System
LSM Land Surface Model
LULC Land Use-Land Cover
MADIS Meteorological Assimilation Data Ingest System
MAP Mean Areal Precipitation
Modeling System
MODFLOW U. S. Geological Survey Modular Ground-Water Model
MODIS Moderate Resolution Imaging Spectroradiometer
NAM North American Mesoscale model
NASA National Atmospheric and Space Administration
NCAR National Center for Atmospheric Research
NCDC National Climate Data Center
NCEP National Centers for Environmental Prediction
NDFD National Digital Forecast Database
NDVI Normalized Difference Vegetation Index
NESDIS National Environmental Satellite Data and Information Service
NEXRAD Next Generation Radar
NLCD National Land Cover Database
NOAA National Oceanic and Atmospheric Administration

NOAA National Oceanic and Atmospheric Administration
NRCS Natural Resource Conservation Service
NS Nash-Sutcliffe efficiency
NSSL National Severe Storms Laboratory
NWP Numerical Weather Prediction
NWS National Weather Service
NWS National Weather Service
NWSRFS National Weather Service River Forecast System
NWSRFS National Weather Service River Forecasting System
OCWS Office of Climate, Water and Weather Services
OHD Office of Hydrologic Development
PDO Pacific Decadal Oscillation
PET Potential Evapotranspiration
QPF Probabilistic QPF
PRISM Precipitation-elevation Regressions on Independent Slopes Model
PSD Physical Sciences Division
QPE Quantitative Precipitation Estimate
QPF Quantitative Precipitation Forecast
QTE Quantitative Temperature Estimate
QTF Quantitative Temperature Forecast
RFC River Forecast Center
RTi Riverside Technology, Inc.
RTMA Real-time Mesoscale Analysis
RTO Research-to-Operations
RUC Rapid Update Cycle
SAC-HT Sacramento Heat-Transfer model
SACSMA Sacramento Soil Moisture Accounting model
SSURGO Soil Survey Geographic database
STATSGO State Soil Geographic database
USACE United States Army Corps of Engineers
USBR United States Bureau of Reclamation
USDA United States Department of Agriculture
USGS United States Geological Survey
WFO Weather Forecast Office
WGRFC West-Gulf River Forecast Center
WR NWS Western Region
WSR 88D Weather Surveillance Radar-1988 Doppler

APPENDIX A. FLOOD FLOW ASSESSMENT STATISTICS

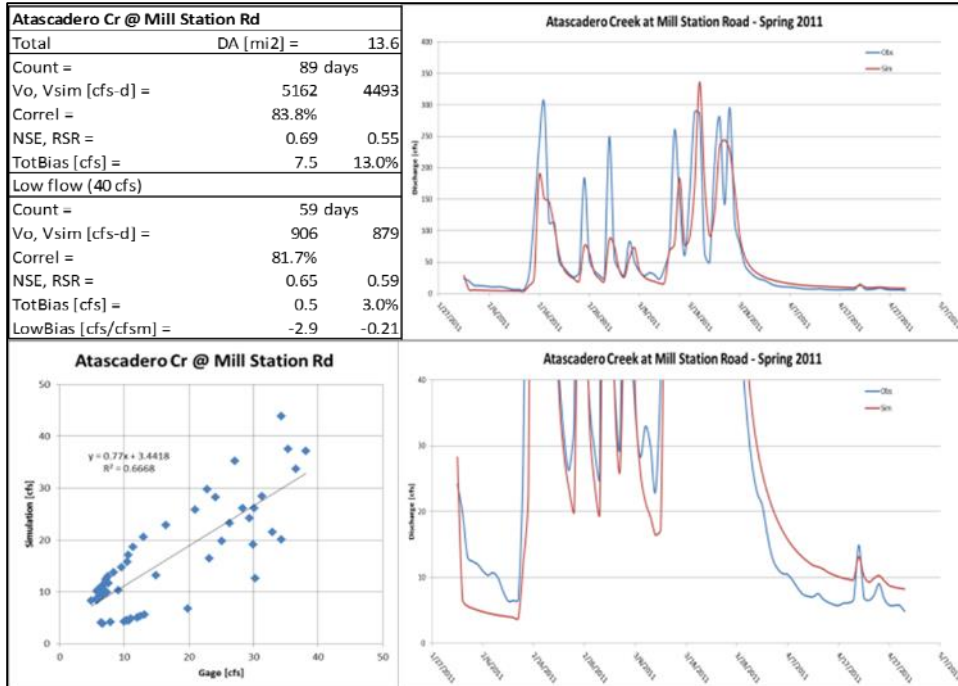
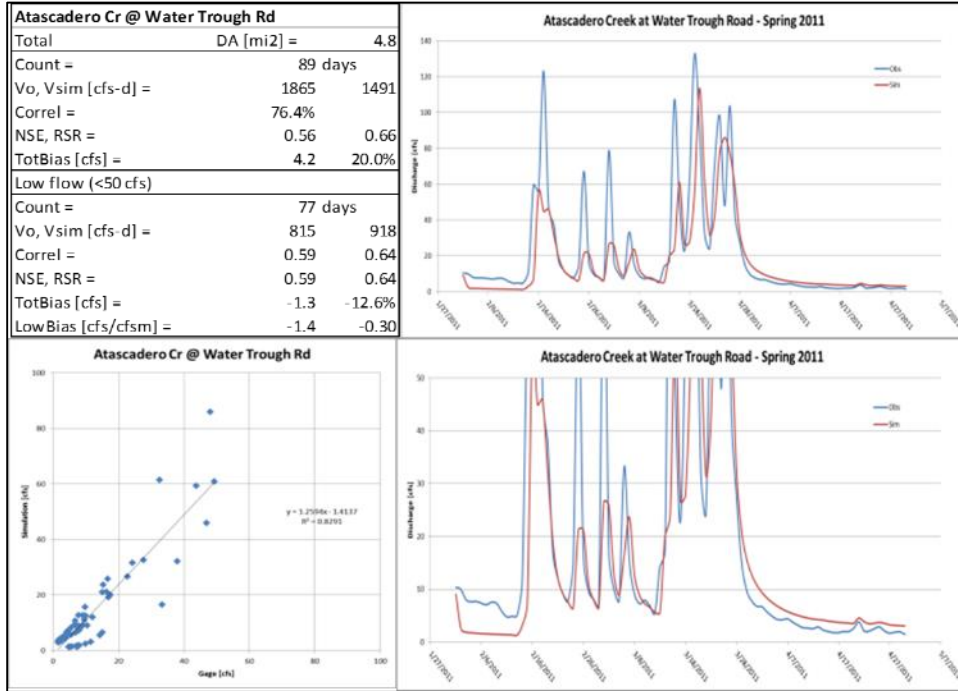
Table A-1. Accuracy statistics at the seven stations for the calibration period.

	Austin Cr			Santa Rosa Cr			Russian R nr Ukiah			E Fk Russian R nr Capella			Napa R nr Napa			Napa R nr St. Helena			Big Sulphur Cr			
	Obs	Sim	Diff [%]	Obs	Sim	Diff [%]	Obs	Sim	Diff [%]	Obs	Sim	Diff [%]	Obs	Sim	Diff [%]	Obs	Sim	Diff [%]	Obs	Sim	Diff [%]	
Drainage area [mi ²]		62.8			57.0			100.0		92.2		218.0		78.8		13.1						
Calibration Period - Feb 2011-Dec 2011																						
Total period statistics																						
RO volume [ft]	2.91	3.16	-8.6	1.26	1.71	-35.7	1.79	2.10	-17.3	2.85	2.08	1.25	1.57	-25.6	1.44	1.64	-13.9	3.58	5.86	-63.7		
Nash-Sutcliffe	0.89			0.77			0.89			0.74		0.88			0.85				-0.13			
Percent bias [%]	-8.5			-27.2			-17.6			27.4		-25.2			-14.4				-62.0			
Flood event statistics																						
16-Feb-11																						
RO volume [ft]	0.37	0.43	-16.2	0.22	0.30	-36.4	0.22	0.24	-9.1	0.21	0.27	-28.6	0.19	0.26	-36.8	0.23	0.29	-26.1	0.57	1.05	-84.2	
Peak Flow [cfs]	4408	4103	6.9	2405	2358	2.0	3212	3326	-3.6	3332	3720	-11.6	5105	5189	-1.6	2706	2798	-3.4	2166	3517	-62.3	
Time to Peak [hrs]	30	36	-6	72	36	36	30	30	0	30	30	0	84	42	42	78	36	42	30	30	0	
Nash-Sutcliffe		0.76			0.31		0.71			0.31			0.33			0.64			0.50			
Percent bias [%]		-17.1			-38.0		-11.3			-31.2		-40.4		-0.67		-25.5			-84.2			
Rmod [Mod. Corre. Coef.]		0.80			0.62		0.72			0.60		0.67		0.79					0.67			
20-Mar-11																						
RO volume [ft]	0.37	0.41	-10.8	0.24	0.23	4.2	0.24	0.25	-4.2	0.29	0.29	0.0	0.26	0.25	3.8	0.31	0.25	19.4	0.53	0.89	-67.9	
Peak Flow [cfs]	3747	4492	-19.9	2959	2771	6.4	3028	2847	6.0	4743	3742	21.1	11523	8997	21.9	5877	4027	31.5	1642	2753	-67.7	
Time to Peak [hrs]	60	60	0	60	60	0	66	66	0	60	60	0	72	66	6	60	60	0	60	60	0	
Nash-Sutcliffe		0.68			0.82		0.87			0.82			0.80			0.78			0.91			
Percent bias [%]		-9.2			4.7		-1.3			-0.7		4.4		4.4		18.1			-68.2			
Rmod [Mod. Corre. Coef.]		0.67			0.83		0.92			0.72		0.73		0.65					0.45			
24-Mar-11																						
RO volume [ft]	0.59	0.51	13.6	0.26	0.28	-7.7	0.40	0.42	-5.0	0.38	0.42	-10.5	0.32	0.33	-3.1	0.32	0.34	-6.3	0.92	1.00	-8.7	
Peak Flow [cfs]	4959	3751	36.6	2373	2569	-8.2	5251	5086	3.1	4029	5768	-43.2	8804	7453	15.3	4041	3653	9.6	1395	3074	-120.3	
Time to Peak [hrs]	48	48	0	48	42	6	48	48	0	48	42	6	54	48	6	48	42	6	90	42	48	
Nash-Sutcliffe		0.67			0.55		0.71			0.42			0.83			0.49			-1.99			
Percent bias [%]		13.4			-8.8		-3.9			-9.4		-3.3		-3.3		-7.3			-9.0			
Rmod [RMSE/StdDev]		0.79			0.68		0.72			0.61		0.88		0.69					0.22			

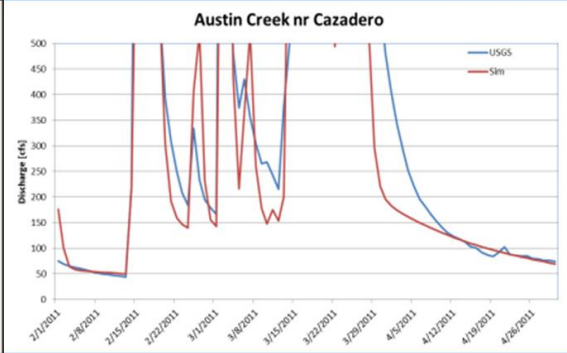
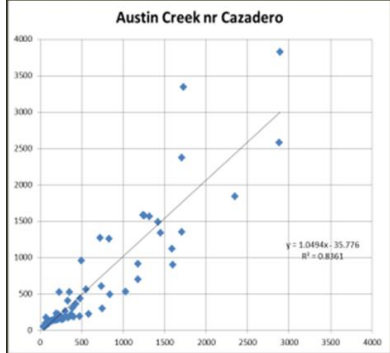
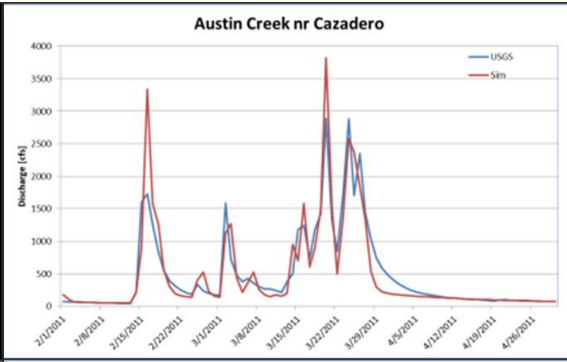
Table A-2. Accuracy statistics at the seven stations for the verification period.

	Austin Cr			Santa Rosa Cr			Russian R nr Ukiah			E FK Russian R nr Capella			Napa R nr Napa			Napa R nr St. Helena			Big Sulphur Cr		
	Obs	Sim	Diff [%]	Obs	Sim	Diff [%]	Obs	Sim	Diff [%]	Obs	Sim	Diff [%]	Obs	Sim	Diff [%]	Obs	Sim	Diff [%]	Obs	Sim	Diff [%]
Drainage area [mi ²]	62.8			57.0			100.0			92.2			218.0			78.8			13.1		
Verification Period - Jan 2012-March 2012																					
Total period statistics																					
RO volume [ft]	0.72	0.75	-4.2	0.32	0.42	-31.3	0.43	0.46	-7.0	0.35	0.49	-40.0	0.25	0.39	-56.0	0.38	0.47	-23.7	1.36	2.07	-52.2
Nash-Sutcliffe	0.90			0.75			0.80			0.65			0.57			0.82			-0.42		
Percent bias			-4.9			-29.4			-7.5			-40.5			-54.1			-19.4			-51.3
Flood event statistics																					
23-Jan-12																					
RO volume [ft]	0.33	0.36	-9.1	0.1	0.19	-90.0	0.20	0.20	0.0	0.14	0.21	-50.0	0.04	0.07	-75.0	0.07	0.12	-71.4	0.23	0.97	-321.7
Peak Flow [cfs]	4374	3812	12.8	1655	2661	-24.5	5041	3378	33.0	3249	2964	8.8	2186	2179	0.3	1943	1679	13.6	796	2969	-272.9
Time to Peak [hrs]	60	66	-6	66	66	0	12	12	0	12	12	0	72	72	0	66	66	0	60	60	0
Nash-Sutcliffe	0.84			0.04			0.75			0.47			-0.07			0.62			-12.04		
Percent bias (%)			-9.3			-84.9			-3.6			-48.7			-106.6			-59.1			-323.2
Rmod (Mod. Corre. Coef.)			0.81			0.63			0.68			0.78			0.86			0.82			0.29
14-Mar-12																					
RO volume [ft]	0.16	0.21	-31.3	0.12	0.18	-50.0	0.09	0.12	-33.3	0.09	0.15	-66.7	0.08	0.14	-75.0	0.13	0.18	-38.5	0.48	0.96	-100.0
Peak Flow [cfs]	2681	2622	26.0	1664	2296	-34.4	1775	2060	-16.0	1681	2248	-33.8	5392	6322	-17.2	3090	3862	-8.8	1777	3216	-151.8
Time to Peak [hrs]	24	30	-6	36	30	6	24	24	-6	24	24	0	42	42	0	36	36	0	30	30	0
Nash-Sutcliffe	0.54			0.45			-0.03			-0.31			0.41			0.69			-3.09		
Percent bias			-36.8			-48.9			-41.5			-66.9			-71.0			-36.0			-101.5
Rmod (=RMSE/\$Dev)			0.72			0.68			0.60			0.61			0.75			0.81			0.37
17-Mar-12																					
RO volume [ft]	0.15	0.14	6.7	0.11	0.12	-9.1	0.10	0.10	0.0	0.08	0.10	-25.0	0.07	0.11	-57.1	0.12	0.13	-8.3	0.32	0.44	-37.5
Peak Flow [cfs]	2179	1586	27.2	1668	1653	0.9	1838	1594	13.3	1415	1570	-11.0	3955	3907	-8.7	2388	2903	3.6	958	1080	-12.7
Time to Peak [hrs]	30	30	0	30	30	0	30	30	0	30	30	0	36	36	0	30	30	0	30	30	0
Nash-Sutcliffe	0.87			0.92			0.92			0.92			0.18			0.91			-0.52		
Percent bias			9.62			-13.61			6.59			-34.51			-59.98			-7.18			-38.93
Rmod (=RMSE/\$Dev)			0.84			0.94			0.95			0.85			0.86			0.90			0.8
28-Mar-12																					
RO volume [ft]	0.35	0.34	2.9	0.07	0.09	-28.6	0.18	0.17	5.6	0.14	0.19	-35.7	0.07	0.09	-28.6	0.10	0.11	-10.0	0.48	0.58	-20.8
Peak Flow [cfs]	6905	5288	23.4	1098	1259	-14.6	5470	3066	43.9	3927	3204	18.4	3319	3448	-3.9	1965	1969	-0.2	1567	2594	-65.5
Time to Peak [hrs]	30	30	0	30	30	0	30	30	0	30	24	6	36	36	42	36	30	6	30	24	6
Nash-Sutcliffe	0.90			0.54			0.78			0.74			0.76			0.85			-0.35		
Percent bias			2.1			-37.8			5.6			-31.4			-32.0			-12.5			-20.5
Rmod (=RMSE/\$Dev)			0.82			0.70			0.62			0.9			0.95			0.91			0.59

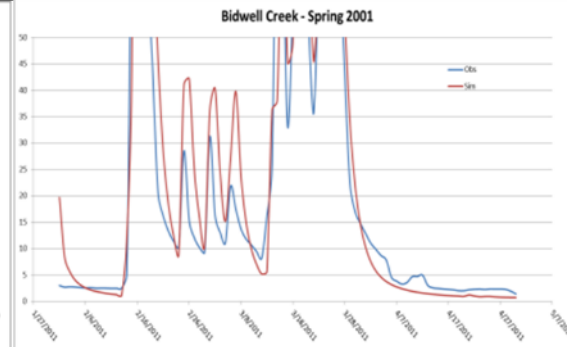
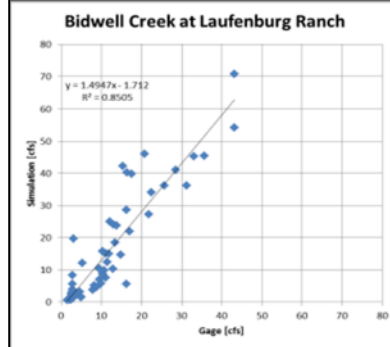
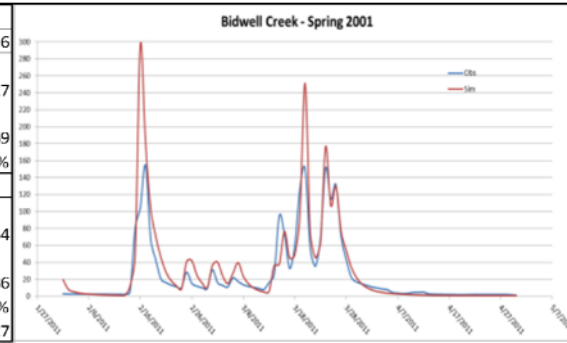
APPENDIX B – LOW FLOW ASSESSMENT STATISTICS



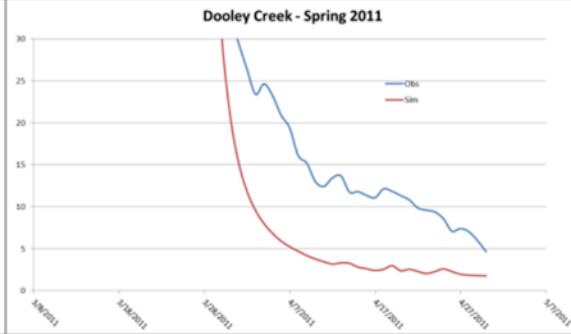
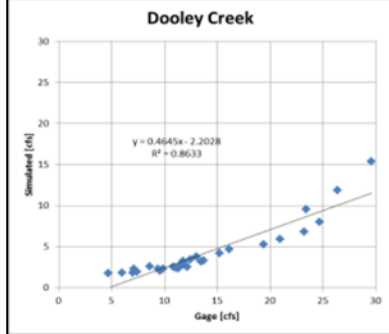
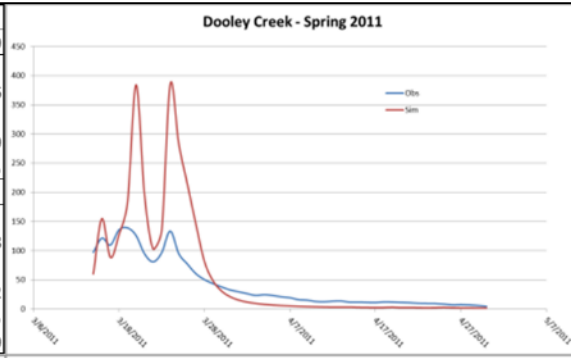
Austin Creek		
Total	DA [mi ²] =	62.8
Count =		89 days
Vo, Vsim [cfs-d]		43494 42457
Correl =		91.4%
NSE, RSR =		0.78 0.47
TotBias [cfs] =		11.6 2.4%
Low Flow (<500 cfs)		
Count =		42 days
Vo, Vsim [cfs-d]		4166 4128
Correl =		75.8%
NSE, RSR =		0.75 0.50
TotBias [cfs] =		0.9 0.9%
LowBias [cfs] =		-0.8 -0.01



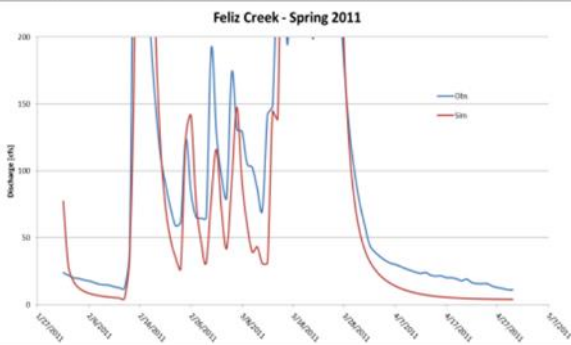
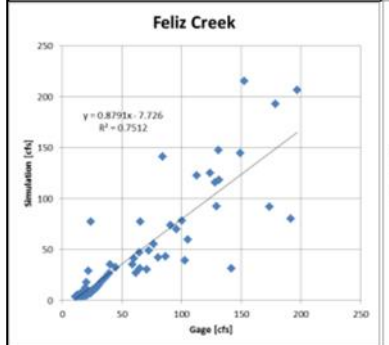
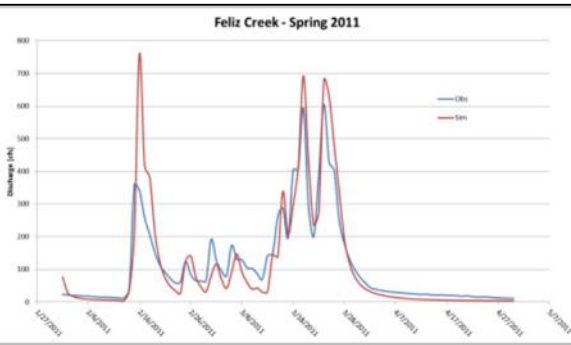
Bidwell Creek		
Total	DA [mi ²] =	4.6
Count =		89 days
Vo, Vsim [cfs-d]		2232 2727
Correl =		88.4%
NSE, RSR =		0.52 0.69
TotBias [cfs] =		-5.6 -22.2%
Low flow (<50 cfs)		
Count =		74 days
Vo, Vsim [cfs-d]		723 954
Correl =		92.0%
NSE, RSR =		0.26 0.86
TotBias [cfs] =		-3.1 -32.0%
LowBias [cfs/cfsm] =		1.2 0.27

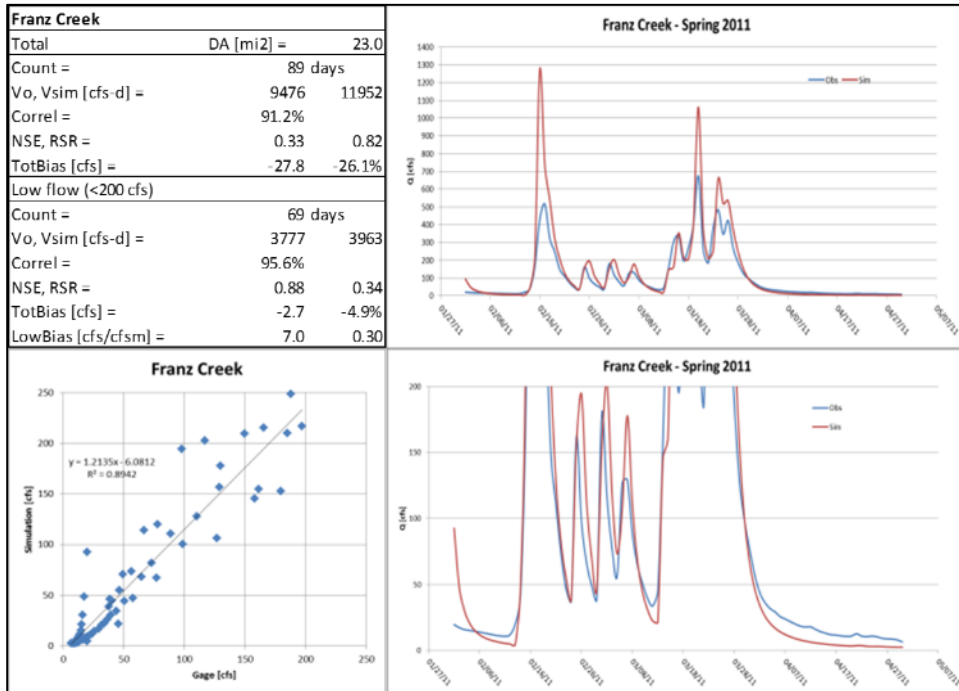
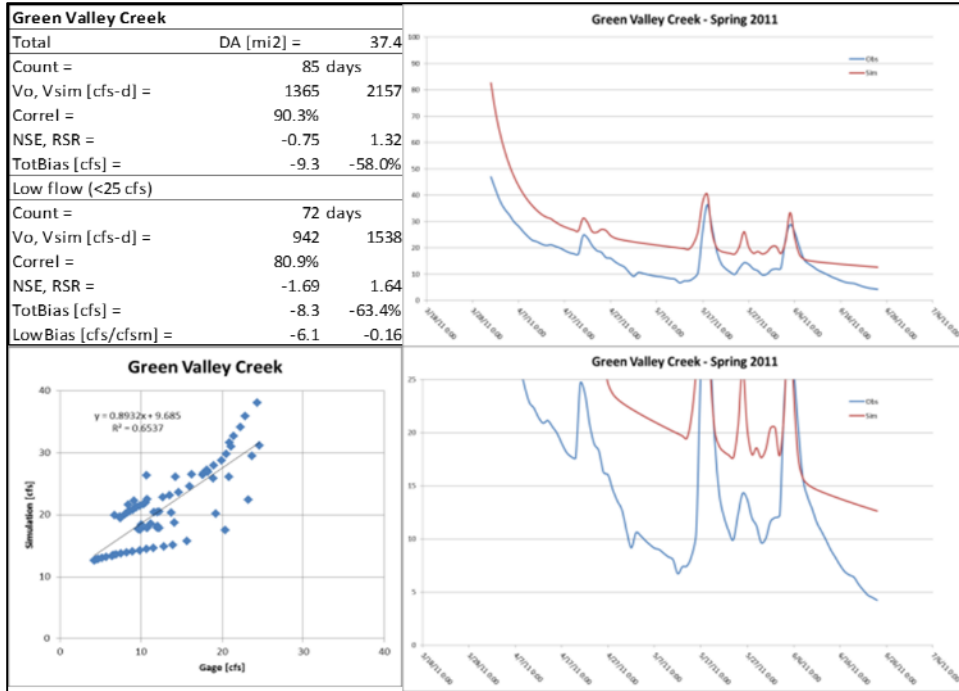


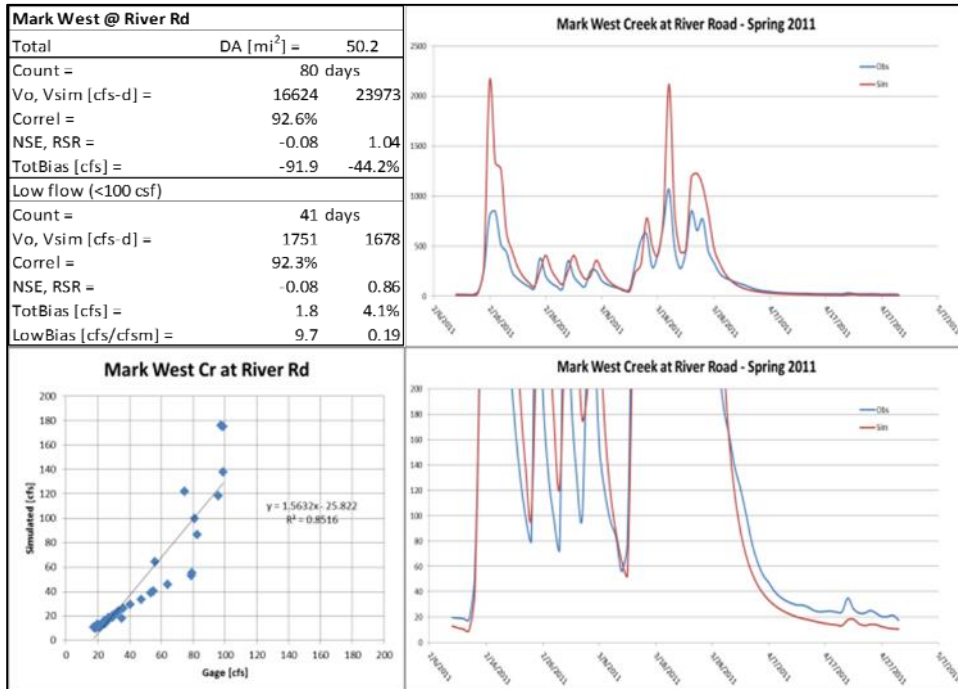
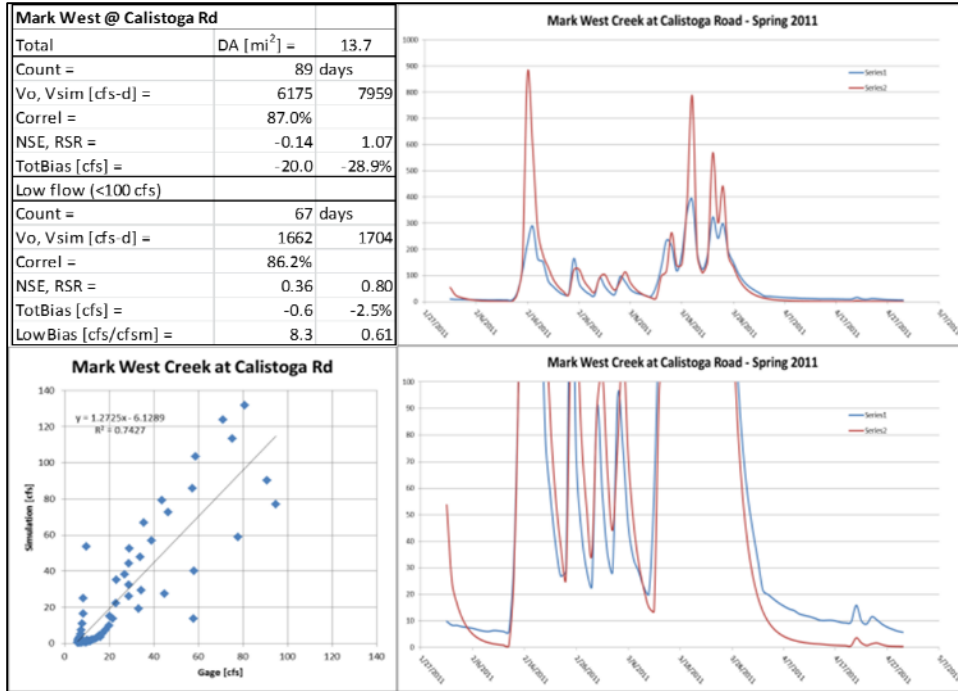
Dooley Creek		
Total	DA [mi2] =	14.9
Count =		47
Vo, Vsim [cfs-d]		1945.39 2766.56
Correl =		85.1%
NSE, RSR =		-1.52 1.59
TotBias [cfs] =		-17.5 -42.2%
Low flow (<30 cfs)		
Count =		30
Vo, Vsim [cfs-d]		413.06 125.78
Correl =		92.9%
NSE, RSR =		-1.62 1.62
TotBias [cfs] =		9.6 69.5%
LowBias [cfs/cfsm] =		2.9 0.19



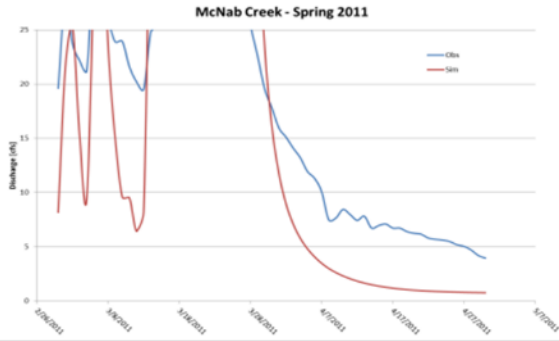
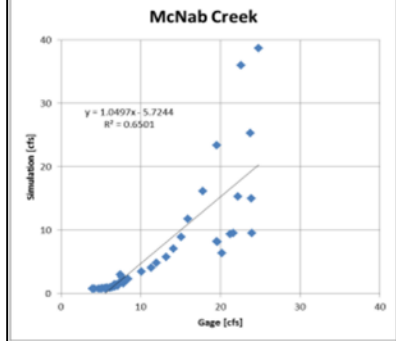
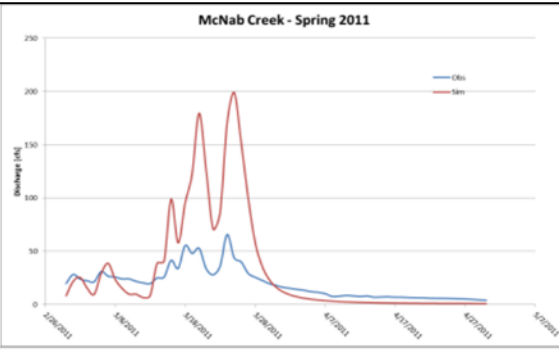
Feliz Creek		
Total	DA [mi2] =	23
Count =		89
Vo, Vsim [cfs-d]		9885.92 9856.32
Correl =		91.8%
NSE, RSR =		0.71 0.54
TotBias [cfs] =		0.3 0.3%
Low flow (<200 cfs)		
Count =		73
Vo, Vsim [cfs-d]		4195.48 3124.40
Correl =		86.7%
NSE, RSR =		0.65 0.59
TotBias [cfs] =		14.7 25.5%
LowBias [cfs/cfsm] =		11.8 0.52



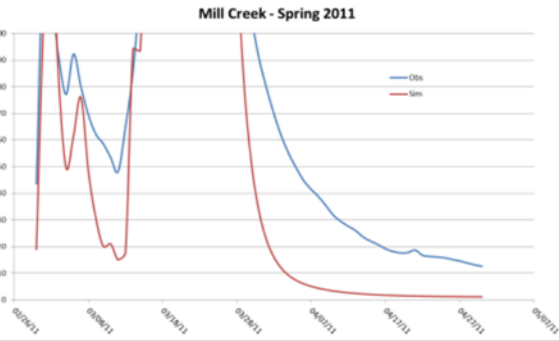
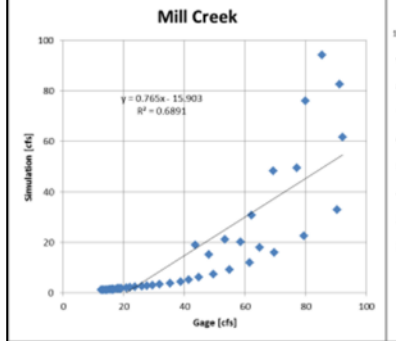
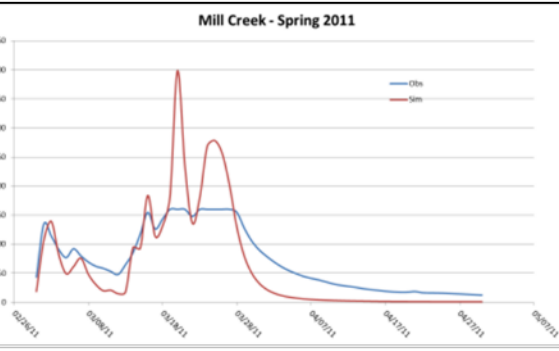




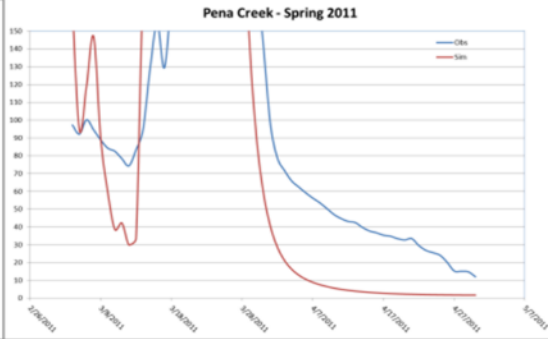
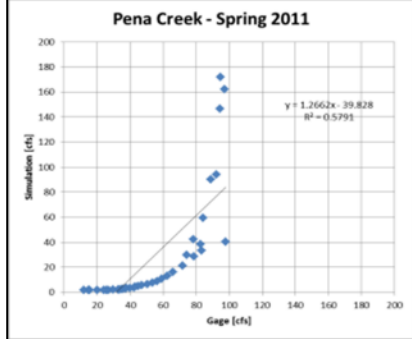
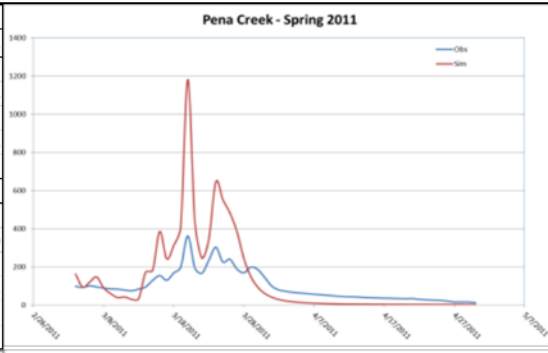
McNab Creek		
Total	DA [mi ²] =	8.3
Count =	61 days	
Vo, Vsim [cfs-d] =	1188 1970	
Correl =	87.7%	
NSE, RSR =	-6.79 2.79	
TotBias [cfs] =	-12.8 -65.9%	
Low flow (<25 cfs)		
Count =	43 days	
Vo, Vsim [cfs-d] =	518 298	
Correl =	80.6%	
NSE, RSR =	-0.14 1.07	
TotBias [cfs] =	5.1 42.5%	
LowBias [cfs/cfsm] =	4.8 0.58	



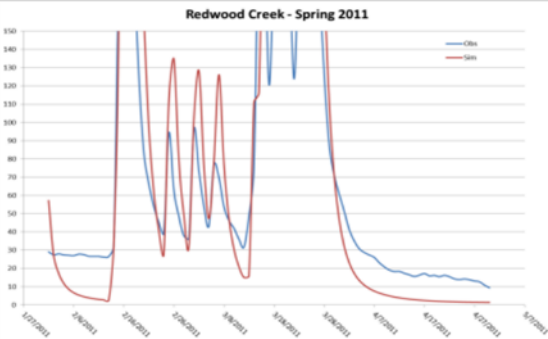
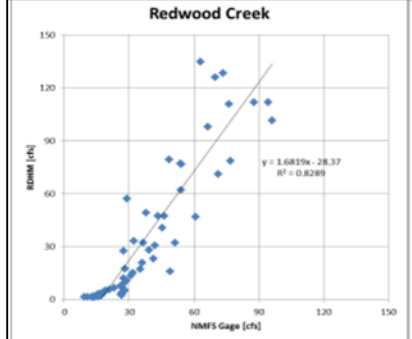
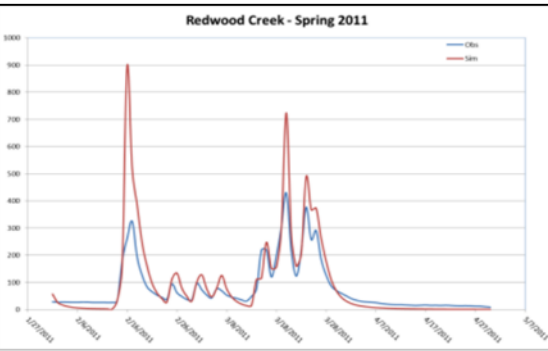
Mill Creek		
Total	DA [mi ²] =	3.5
Count =	61 days	
Vo, Vsim [cfs-d] =	4408 3861	
Correl =	88.6%	
NSE, RSR =	0.13 0.93	
TotBias [cfs] =	9.0 12.4%	
Low flow (<100 cfs)		
Count =	43 days	
Vo, Vsim [cfs-d] =	1800 693	
Correl =	83.0%	
NSE, RSR =	-0.33 1.15	
TotBias [cfs] =	25.7 61.5%	
LowBias [cfs/cfsm] =	15.3 4.38	



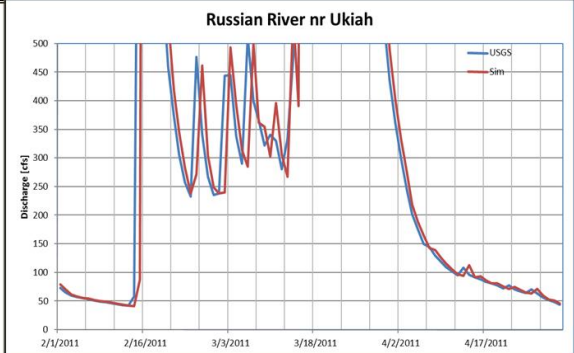
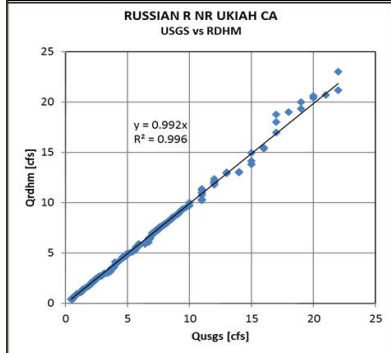
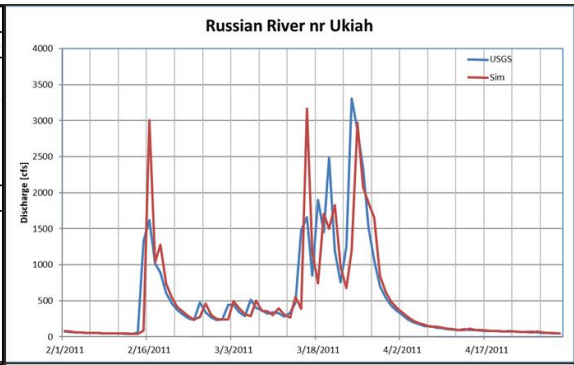
Pena		
Total	DA [mi ²] =	12.6
Count =	58 days	
Vo, Vsim [cfs-d] =	5598	7554
Correl =	91.2%	
NSE, RSR =	-2.8	1.94
TotBias [cfs] =	-33.7	-34.9%
Low flows (<100 cfs)		
Count =	40 days	
Vo, Vsim [cfs-d] =	2111	1080
Correl =	76.1%	
NSE, RSR =	-1.2	1.48
TotBias [cfs] =	25.8	48.8%
LowBias [cfs] =	24.5	1.95



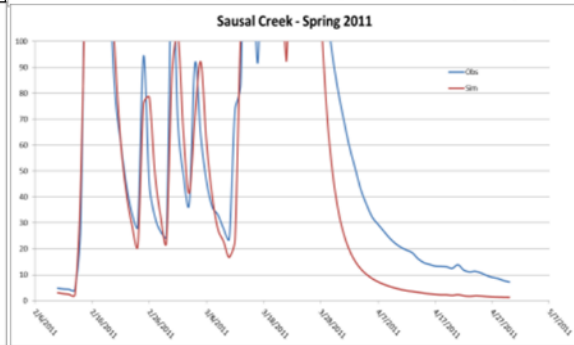
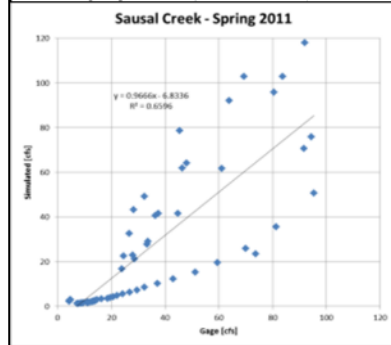
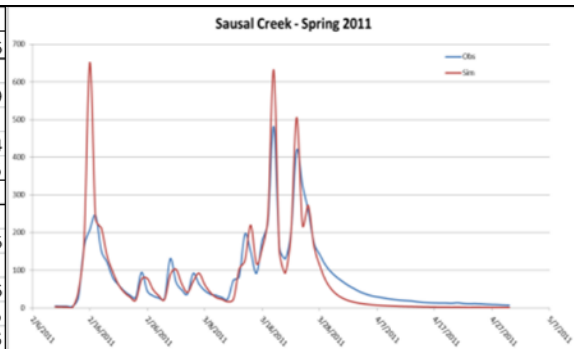
Redwood		
Total	DA [mi ²] =	14.0
Count =	89 days	
Vo, Vsim [cfs-d] =	6903	8480
Correl =	89.8%	
NSE, RSR =	0.08	0.96
TotBias [cfs] =	-17.7	-22.9%
Low flows (<100 cfs)		
Count =	70 days	
Vo, Vsim [cfs-d] =	2528	2266
Correl =	91.0%	
NSE, RSR =	-0.08	1.04
TotBias [cfs] =	3.7	10.4%
LowBias [cfs] =	12.5	0.90



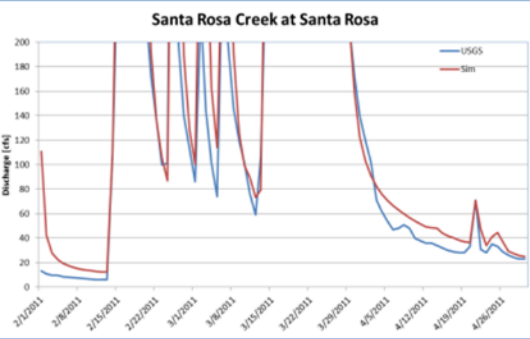
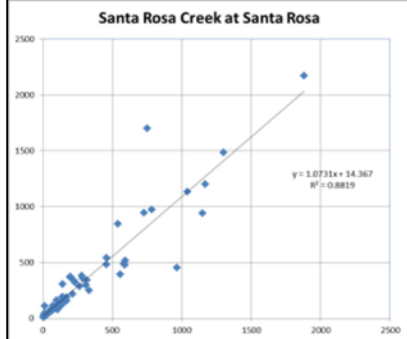
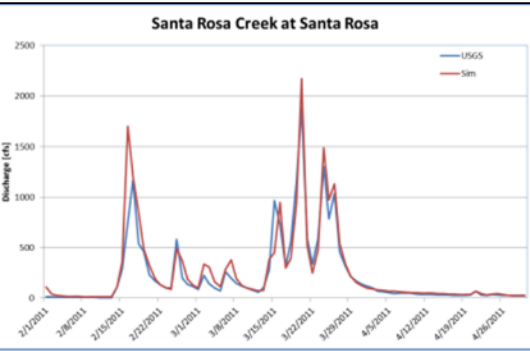
RR nr Ukiah		
Total	DA [mi ²] =	100
Count =		89 days
Vo, Vsim [cfs-d] =	43505	42504
Correl =		80.2%
NSE, RSR	0.60	0.63
TotBias [cfs] =	11.2	2.3%
Low Flow (<500 cfs)		
Count =		67 days
Vo, Vsim [cfs-d] =	12165	12709
Correl =		95.0%
NSE, RSR	0.88	0.34
TotBias [cfs] =	-8.1	-4.5%
LowBias [cfs/cfsm] =	-1.6	-0.02



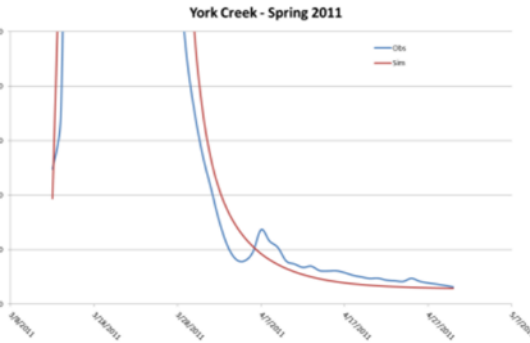
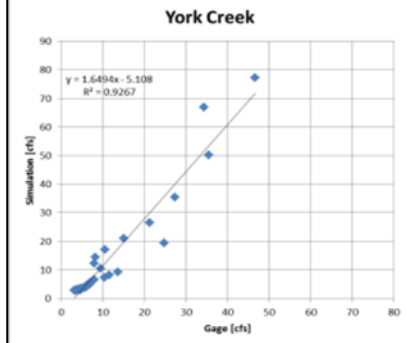
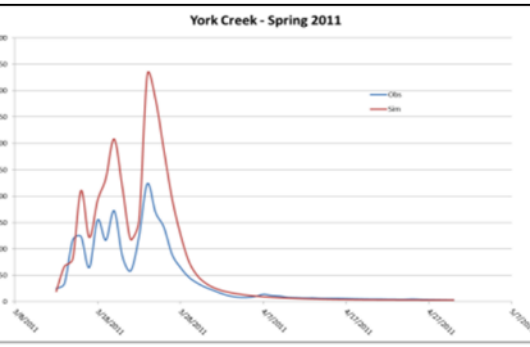
Sausal Creek		
Total	DA [mi ²] =	12.6
Count =		80 days
Vo, Vsim [cfs-d] =	6256	6269
Correl =		89.0%
NSE, RSR =	0.58	0.64
TotBias [cfs] =	-0.2	-0.2%
Low flows (<100 cfs)		
Count =		60 days
Vo, Vsim [cfs-d] =	2076	1596
Correl =		81.2%
NSE, RSR =	0.42	0.76
TotBias [cfs] =	8.0	23.1%
LowBias [cfs] =	-9.4	-0.75



Santa Rosa Creek		
Total	DA [mi2] =	57
Count =	89 days	
Vo, Vsim [cfs-d]	20009	22751
Correl =	93.9%	
NSE, RSR =	0.83	0.41
TotBias [cfs] =	-30.8	-13.7%
Low Flow (<200 cfs)		
Count =	63 days	
Vo, Vsim [cfs-d]	3789	4822
Correl =	88.2%	
NSE, RSR =	0.45	0.74
TotBias [cfs] =	-16.4	-27.3%
LowBias [cfs] =	-7.3	-0.13



York Creek		
Total	DA [mi2] =	11.7
Count =	49 days	
Vo, Vsim [cfs-d]	2088	3514
Correl =	96.1%	
NSE, RSR =	-0.25	1.12
TotBias [cfs] =	-29.1	-68.3%
Low flow (<50 cfs)		
Count =	35 days	
Vo, Vsim [cfs-d]	385	457
Correl =	96.3%	
NSE, RSR =	0.32	0.82
TotBias [cfs] =	-2.0	-18.5%
LowBias [cfs/cfsm] =	1.2	0.11



APPENDIX C. INTRINSIC POTENTIAL FISHERIES HABITAT MAPPING

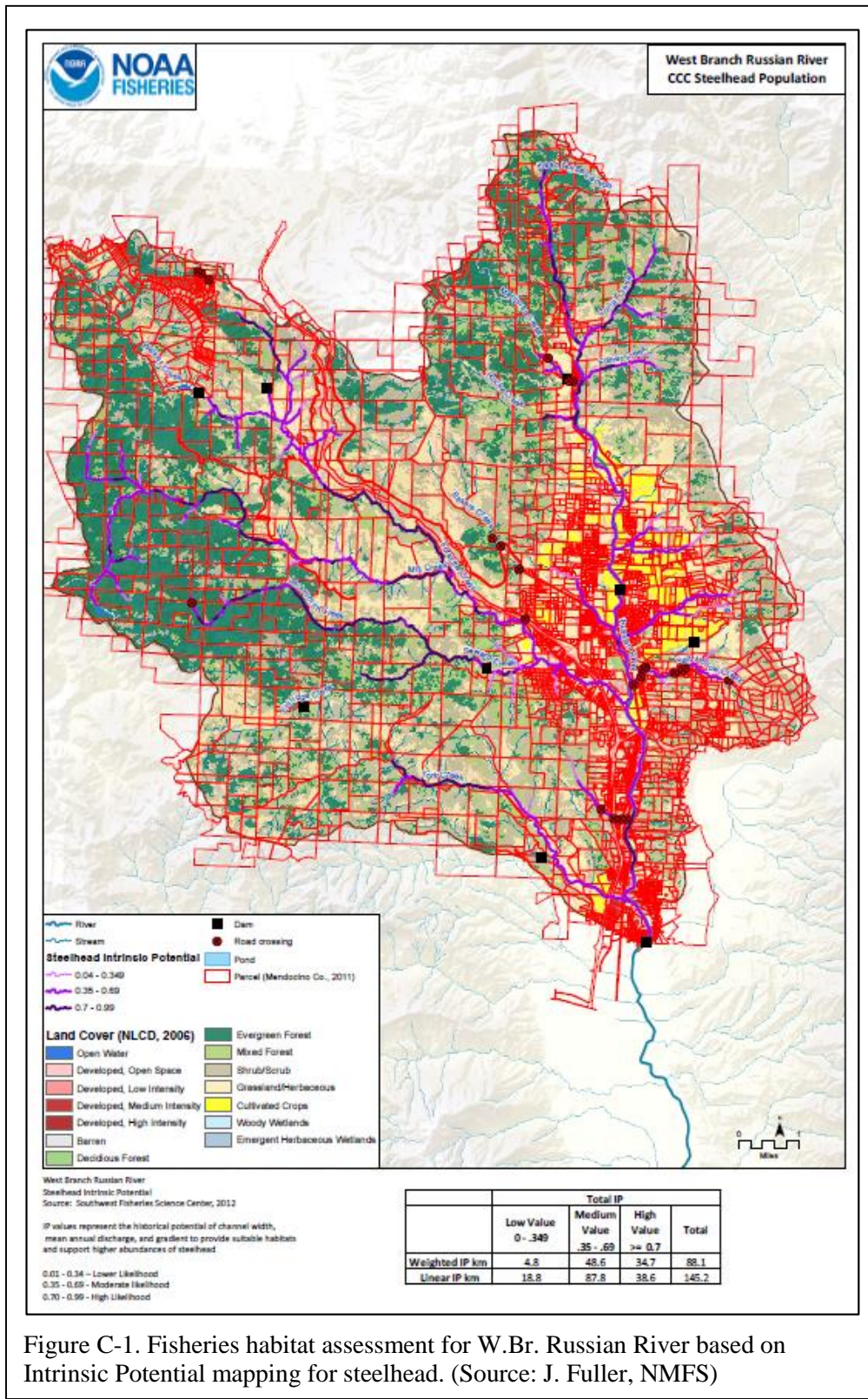


Figure C-1. Fisheries habitat assessment for W.Br. Russian River based on Intrinsic Potential mapping for steelhead. (Source: J. Fuller, NMFS)